

https://dspace.org/

Optimization of the synthesis and performance of bifunctional Co-HZSM-5 catalyst for fischer tropsch synthesis

Mudau, Tsireledzo Lesley

2020-06

https://hdl.handle.net/10539/30089

Downloaded from a DSpace repository. https://dspace.org/

UNIVERSITY OF THE WITWATERSRAND, JOHANNESBURG



Optimization of the Synthesis and Performance of bifunctional Co-HZSM-5 catalyst for Fischer Tropsch synthesis

MSc Dissertation

Prepared by

Tsireledzo Lesley Mudau

551177

Submitted to

A dissertation submitted to the Faculty of Engineering and the Built Environment, University of the Witwatersrand, Johannesburg, in fulfilment of the requirements for the Degree of Master of Science in Engineering.

Supervisor: Prof. Michael Daramola

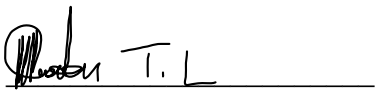
June 2020

Declaration

I, Tsireledzo Lesley Mudau (551177), am a registered student for the degree of Master of Science in Chemical engineering in the academic year of 2020.

I declare that;

- The submitted dissertation is my own unaided work (expect where explicitly indicated) and has not been submitted before for any other degree or examination at any university,
- I am aware that plagiarism (using someone's work pretending is your own) is wrong.
- I have used the required conventions in referencing ideas and findings of others.
- The University of the Witwatersrand is entitled to take disciplinary actions against me if the submitted dissertation in not my unaided work.

Signature of Candidate: 

Date: 24 day of JUNE year 2020

Journal Publications and conference presentations

Journal articles

1. **Mudau T.L**, Daramola M.O; CO conversion to liquid fuel over a bi-functional Co/H-ZSM-5 catalyst for: Effect of support desilication and catalyst promotion. *Applied Catalysis A: General* **(Submitted)**

Conference Proceedings and conferences attended

1. **Mudau T.L**, Daramola M.O; Optimization of the synthesis and Performance of bi-functional Co/H-ZSM-5 catalyst for Fischer-Tropsch synthesis. *International Workshop on Porous Materials and their Applications (IWPMA-2018); Hosted by CISR; Casa Toscana Pretoria, 13-14 September 2019* **(Attendee)**
2. **Mudau T.L**, Daramola M.O; CO conversion to liquid fuel over a bi-functional Co/H-ZSM-5 catalyst for: Effect of support desilication and catalyst promotion. DST-UNESCO National Student Conference; Cape Peninsula University of Technology, Way Bellville Cape Town, 17 September 2018 **(Poster and Oral Presentations)**

Acknowledgements

First and foremost, I give all thanks to the Most High God for making it all work out the best for me. There were times I needed to throw in the towel, but His grace and strength were sufficient for me. I kept believing as the Lord says, “as you have believed, so will it be done for you” and indeed today it is done.

Special thanks to my supervisor Prof. Michael Daramola for your guidance, leadership, support, patience and always checking that everything was going well. Your consistency and outstanding work go unnoticed.

My momma (Mrs. Itani Mudau) and dad (Mr. Tshifhiwa Mudau), I love you, so grateful and blessed to have you. My sisters (Witness and Talifhani Mudau) and nephew (Habalelwi) thank you so much family for your prayers and undying support throughout my academic career. Thank you for always believing in me, encouraging to keep on keeping on and pressing on towards the mark and reaching all the pinnacles of my dreams and goals. Thank you. And how can I forget Mbalikayise Mbele, thank you so much for your prayers and emotional support, her support goes unnoticed.

I thank the National Research Foundation (NRF)/Department of Science and Technology (DST) for your financial support.

My sincere gratitude to my research group: Sustainable Energy and Environmental Research Unit (SEERU) for all the opinions, constructive criticism during presentations and every other thing. I have learnt so much from you and you all have made this work possible today. Thanks.

Last but not least, thanks to Microscopy and Microanalysis Unit (MMU) from the University of the Witwatersrand for providing training for microscopy instruments. To Mr. Bruce Mothibeli, Mr. Motlatsi and Mrs. Janet Smith, thank you for providing with lab equipments and chemicals. To the staff and administrative in the School of Chemical and Metallurgical Engineering, thank you.

Ndaa!!! Ndi a Livhuwa

Table of Contents

Declaration ii

Journal Publications and conference presentations iii

Acknowledgements iv

Table of Figures viii

Table of tables x

List of Abbreviations xi

Abstract xiii

CHAPTER 1 1

Introduction 1

1.1 Motivation and background 1
1.2 Problem statement 4
1.3 Research aim, questions and objective 4
1.4 Scope of the study 5

CHAPTER 2 6

Literature Review 6

2. Fischer-Tropsch Synthesis 6

2.1 Fischer-Tropsch Process 6
2.2 Fischer-Tropsch Chemistry 6
2.3 Fischer-Tropsch catalysis 7
2.3.1 Iron-based catalyst 9
2.3.2 Cobalt-based catalyst 10
2.3.3 Zeolite Support 10
2.3.4 Mechanism of bifunctional Co/H-ZSM-5 catalyst 12
2.4 Fischer-Trospch Reactor Consideration 13
2.4.1 Fluidized bed reactor 14
2.4.2 Slurry bed reactor 14
2.4.3 Fixed bed reactor 15
2.5 Product selectivity & distribution 15
2.6 Fischer-Tropsch Catalyst Synthesis 16
2.6.1 Possible supports of cobalt F-T catalyst 16

2.6.2 Alkaline treatment method 16
2.6.3 Preparation methods of cobalt-supported F-T catalyst 17
2.6.4 Effect of using promoters 18
2.7 Concluding remarks 18
CHAPTER 3 20
Experimental Procedure 20
Synthesis and Characterization of Catalysts 20
3.1 Introduction 20
3.2 Materials and methods 20
3.2.1 Materials 20
3.2.2 Catalyst preparation 20
3.3 Catalyst Characterization Techniques 22
3.3.1 N_2 Physisorption (Brunnat Emmett Teller) analysis 22
3.3.2 Scanning Electron Microscopy (SEM) and Energy Dispersive Spectroscopy (EDS) analysis 22
3.3.3 X-Ray Diffraction (XRD) analysis 23
3.3.4 Fourier Transformed Infrared Spectroscopy (FT-IR) analysis 23
3.3.5 Transmission-Electron Microscopy (TEM) analysis 24
3.3.6 Temperature-Programmed-Reduction (TPR) analysis 24
3.4 Support and cobalt catalyst characterization results 24
3.4.1 N_2 Physisorption (BET surface area) 24
3.4.2 SEM Results 28
3.4.3 XRD Results 29
3.4.4 FT-IR (in ATR) results 31
3.4.5 EDS Results 33
3.4.6 Transmission Electron Microscopy (TEM) Results 34
3.4.7 Temperature Programmed Reduction (TPR) Results 35
3.5 Fisher-Tropsch Synthesis (FTS) studies 37
3.5.1 FTS experimental setup 37
3.5.2 Reactor Design 38
3.5.3 Catalyst Loading and reduction 39
3.5.4 Gas Chromatography & Product analysis 39
3.5.5 Data analysis & calculations 42
3.6 Concluding Remarks 45

CHAPTER 4 ..... **47**

Performance of bi-functional Co/undesilicated-H-ZSM-5 and Co/desilicated-HZSM-5 catalysts during Fischer-Tropsch Synthesis 47

4.1 Introduction 47
4.2 Experimental Operating Conditions 48
4.3 Results and discussion 49
4.4 Concluding remark 55

CHAPTER 5 ..... **57**

Effect of the promoted catalysts during Fischer-Tropsch Synthesis 57

5.1 Introduction 57
5.2 Results and Discussion 58
5.2.1 Characterization of promoted catalyst 58
5.2.2 Performance of Ca-Co/H-ZSM-5 catalysts 60
5.3 Concluding remark 64

CHAPTER 6 ..... **65**

Performance evaluation of the promoted Co/H-ZSM-5 catalyst at low pressure during Fischer-Tropsch Synthesis 65

6.1 Introduction 65
6.2 Experimental Conditions 65
5.3 Results and Discussion 65
6.4 Concluding remark 69

CHAPTER 7 ..... **70**

Conclusion and Recommendations 70

7.1 Conclusions 70
7.2 Recommendations 72

References 73

APPENDICES **81**

Appendix A: Calculations for catalysts 81
Appendix B: Calculations for CO conversion and hydrocarbon selectivity 82
B.1: CO conversion calculation 82
B.2: Hydrocarbon Selectivity calculations 85

Table of Figures

Figure 2-1: An overview of Fischer-Tropsch process 6

Figure 2-2: Formation of zeolites structures, zeolite X &Y, zeolite ZSM-12, zeolite ZSM-5 and zeolite ZSM-22 or Theta-1 (Adapted from Weikamp, (2010), Daramola et al., (2012)) 12

Figure 2-3: Basic building blocks of chemical zeolite structure 12

Figure 2-4: Various Fischer-Tropsch reactor technologies (Adapted from Dancuart & Steyberg, 2007) 13

Figure 2-5: The FTS product distribution as a probability chain growth (α) following ASF model (Adapted from Satterfield et al. 1982). 16

Figure 3-1: Scheme of the alkaline desilication of the zeolite support 21

Figure 3-2: Desilication of the zeolite support (left) and preparation of the Co/H-ZSM-5 catalyst via IWI using the desilicated zeolite 22

Figure 3-3: N_2 adsorption-desorption isotherm 26

Figure 3-4: BJH pore size distribution of H-ZSM-5 support and Co/H-ZSM-5 catalyst 27

Figure 3-5: SEM images of [A] parent ZSM-5, [B] calcined H-ZSM-5, [C] desilicated-H-ZSM-5 and [D] Co/H-ZSM-5, all in 10 000 X magnification 29

Figure 3-6: XRD patterns of standard H-ZSM-5, synthesized H-ZSM-5, desilicated H-ZSM-5 and Co/H-ZSM-5 catalyst. 30

Figure 3-7: FT-IR spectra desilicated and undesilicated-H-ZSM-5 zeolite catalysts. 32

Figure 3-8: The FT-IR spectra [A]: Co/undesilicated H-ZSM-5 before calcination, [B]: Co/desilicated-H-ZSM-5 before calcination, [C]: Co/desilicated-H-ZSM-5 catalyst 32

Figure 3-9: The Energy Dispersive Electroscopy (EDS) analysis results of [A] calcined-ZSM-5, [B] desilicated H-ZSM-5, [C] Co/H-ZSM-5 and [D] Co/desilicated-H-ZSM-5 catalysts 34

Figure 3-10: TEM images of Cobalt-zeolite and Cobalt mesoporous-zeolite catalysts, magnification (X100 nm and X200 nm) 35

Figure 3-11: TPR profile of bi-functional catalyst (Co/H-ZSM-5). 36

Figure 3-12: Fischer-Tropsch experimental setup 38

Figure 3-13: Syngas calibration peaks from TCD 40

Figure 4-1: A change of CO conversion with time every two hours for 48 hours (2 days) over Co/H-ZSM-5 catalysts on FT synthesis 50

Figure 4-2A: Product distribution of both paraffins and olefins over a Co/H-ZSM-5 (un-desilicated) 51

Figure 4-2B: Product distribution of both paraffins and olefins over a Co/H-ZSM-5 (un-desilicated) 52

Figure 4-2C: Product distribution of both paraffins and olefins over a Co/H-ZSM-5 (un-desilicated) 53
Figure 4-2D: Product distribution of both paraffins and olefins over a Co/H-ZSM-5 (un-desilicated) 54
Figure 5-1: XRD patterns of unpromoted Co/H-ZSM-5 catalyst and calcium promoted Co/H-ZSM-5 catalysts. 59
Figure 5-2: The Energy Dispersive Electroscopy (EDS) analysis results of [A] Co/H-ZSM-5 and [B] Ca-Co/undesilicated-H-ZSM-5 catalysts and [C] Ca-Co/desilicated-H-ZSM-5 catalysts 60
Figure 5-3A: Product distribution (olefins and paraffins) on Ca-Co/HZSM-5 catalyst at pressure of 15 bar. 62
Figure 5-3B: Product distribution (olefins and paraffins) on Ca-Co/HZSM-5 catalyst at pressure of 15 bar. 63
Figure 6-1A: Product distribution (olefins and paraffins) on Ca-Co/HZSM-5(55) catalyst at pressure of 8 bar. 67
Figure 6-1B: Product distribution (olefins and paraffins) on Ca-Co/HZSM-5(55) catalyst at pressure of 2 bar. 68
Figure 6-2: Olefin ratio on calcium promoted catalysts at different pressure 69

Table of tables

Table 2-1: Possible costs of catalyst in dollar ($) (Adapted from Dry, 2002) 8

Table 2-2: Comparison between Co-based and Fe-based catalysts over low temperature FTS (Adapted from Luo et al. (2006). 9

Table 3-1: FTIR bands' assignment (Adapted from Coates. 2006). 24

Table 3-2: Textural properties of the ZSM-5, H-ZSM-5 support and Co/H-ZSM-5 catalysts (refer to Table B1-1 from Appendix B)……..25

Table 3-3: Characteristics and operating conditions of GC……..……...41

Table 3-4: Molar response for hydrocarbon products (Adapted from Swinnerton. (1967))…….43

Table 3-4: Characteristics and operating conditions of GC……..……...41

Table 4-1: Summary of experimental conditions for FT synthesis 48

Table 4-2: CO conversions over Co-based catalyst on desilicated H-ZSM-5 supports during FT synthesis 49

Table 4-3: Comparison of CO conversion and average products selectivity between (Sartipi et al., 2014), (Matamela, 2014)) and this study 54

Table 4-4: Olefin ratio, rate of CO consumption and rate of Fischer-Tropsch reaction. 55

Table 5-1: Summary of cobalt crystallite sizes based on XRD 59

Table 5-2: CO conversions over calcium promoted Co/H-ZSM-5 catalyst during FT synthesis 60

Table 5-3: Comparison of % CO conversion and hydrocarbon selectivity of the calcium promoted cobalt-based catalyst in this study with other promoted catalysts in the literature. 64

Table 6-1: Effect of low pressure on CO conversion 66

A1-1: N_2 physisorption data of catalysts 81

List of Abbreviations

AMCSD	American Mineralogists Crystal Structure Database
Ar	Argon
ASF	Anderson-Schultz-Flory
BET	Brunauer-Emmett-Teller
C	Carbon
CH_4	Methane
C_2H_2	Ethylene
Ca	Calcium
Ca $(NO_3)_2.6H_2O$	Calcium Nitrate Hexa-hydrate
CO	Carbon Monoxide
Co	Cobalt metal
Co $(NO_3)_2.6H_2O$	Cobalt (II) Nitrate Hexa-hydrate
Co/H-ZSM-5	Cobalt-zeolite bi-functional catalyst
Co/H-ZSM-5(55)	Cobalt-zeolite bi-functional catalyst desilicated at temperature 55 °C
Ca-Co/H-ZSM-5	Cobalt-zeolite bi-functional catalyst promoted by calcium
CO_2	Carbon dioxide
CTL	Coal to Liquids
EDS	Energy Dispersion Spectroscopy
Fe	Iron metal
FID	Flame Ionization Detector
FT	Fischer-Tropsch
FTIR	Fourier Transmission Infrared
FTS	Fischer-Tropsch Synthesis
GC	Gas Chromatography

gcat	Catalyst weight in grams
GHSV	Gas Hourly Space Velocity
GTL	Gas to Liquid
h	hour
H_2	Hydrogen gas
He	Helium gas
HTFT	High Temperature Fischer-Tropsch Synthesis
H-ZSM-5	Hydrogen form of Zeolite Socony Mobil-5
IZA	International Zeolite Association Database
IWI	Incipient Wetness Impregnation
LTFT	Low Temperature Fischer-Tropsch System
Ni	Nickel-metal
PFR	Plug-Flow-Reactor
SEM	Scanning Electron Microscopy
Si/Al	Aluminum to Silicon Ratio
TCD	Thermal Conductivity Detector
TEM	Transmission Electron Microscopy
TPR	Temperature Programmed Reduction
WGS	Water Gas Shift
wt.%	Weight percentage
WTL	Waste to Liquids
X_{CO}	Carbon monoxide Conversion
XRD	X-Ray Diffraction
ZSM-5	Zeolite Socony Mobil-5

Abstract

To date, the production of liquid fuels is mainly from crude oil via conventional refining processes. The depleting and increasing demand in crude oil motivated the world in discovering an alternative technology for energy production, Fischer-Tropsch synthesis (FTS). FTS process involves the use of synthetic gas (gasified from coal or carbonaceous materials) to produce liquid fuel (hydrocarbons-HCs). Amongst other benefits, FTS can be operated at low temperature Fischer-Tropsch (LTFT) process where the most preferred FT catalyst to be applied is cobalt-based catalyst. The other advantages associated with the use of Co-based catalyst are its activity, stability, lifespan and hindrance of the formation of water and carbon dioxide during FT process.

The main challenge associated with Co-based catalyst on FT synthesis has been the product selectivity control. Usually, the FT catalysts obey the Anderson-Schulz-Flory (ASF) product distribution model, which limits the selectivity of the most desired products, known as gasoline-range hydrocarbons (GRHs) (C_5 - C_{11}). Researchers have discovered that combining FT cobalt catalyst with zeolite into bi-functional catalyst improve the selectivity to GRHs. Zeolite assists in hydrocracking of heavier hydrocarbons due to its microporous nature. However, mesoporous zeolite improves the catalytic performance in FTS. Promotion of the FT cobalt catalyst is also believed to bring some changes in catalytic performance. But there is no report on the promotion of Co-based catalyst on mesoporous zeolite (H-ZSM-5) support during Fischer-Tropsch synthesis (FTS).

The aim of this study was to optimize the performance of bi-functional catalyst (Co/H-ZSM-5) via desilication of H-ZSM-5 zeolite support and calcium Co-based catalyst promotion for Fischer-Tropsch synthesis. A desilication method was performed via alkaline treatment using 0.2M NaOH aqueous solution at 40°C, 55°C and 70°C for 2 h to remove silica from the original ZSM-5 zeolite (Si/A*l* = 40). The desilicated and un-desilicated H-ZSM-5 supports were employed in 10 wt.% of Co in the preparation of the bi-functional catalyst (Co/H-ZSM-5) via incipient wetness impregnation (IWI) method. Four bi-functional catalysts were synthesized individually with active cobalt metal supported on H-ZSM-5 zeolites treated at three temperature values (40°C, 55°C & 70°C) and one on un-treated H-ZSM-5. The prepared bi-functional catalysts were dried at 120 °C for 12 h and then calcined at 550°C for 2 h to achieve the final products, Co/H-ZSM-5 catalysts. These catalysts were characterized and tested on FT process for the production of hydrocarbons. The characterization was done using the following

techniques; scanning electron microscopy (SEM) coupled with Energy Dispersion Spectroscopy (EDS) to study the surface morphology and elemental composition of the catalysts, Nitrogen Physisorption at 77K to determine surface area, pore size, and pore volume and adsorptive properties of catalysts, Fourier Transform Infrared Spectroscopy (FTIR) study chemistry of the catalysts, X-Ray Diffraction (XRD) for crystallinity and structure of catalysts, Transmission Electron Microscopy (TEM) for dispersion of the cobalt metal and Temperature-Programmed Reduction(TPR) for reducibility of the catalysts.

The best performing catalyst (found to be Co/H-ZSM-5(55)) during FT process was further promoted by 2.0 wt.% calcium metal. Co/H-ZSM-5 catalyst was also calcium promoted for comparison's sake. Calcium promoted catalysts were also characterized and evaluated on FTS. For characterization, XRD and EDS were used to check whether Ca was successfully deposited and Ca content on Co-cased catalysts. In total, six catalysts were synthesized and named as follows; Co/H-ZSM-5, Co/H-ZSM-5(40), Co/H-ZSM-5(55), Co/H-ZSM-5(70), Ca-Co/H-ZSM-5 and Ca-Co/H-ZSM-5(55) catalysts, where the value inside the brackets indicates the temperature during desilication of H-ZSM-5.

The textural property of the desilicated H-ZSM-5 obtained through N_2 Physisorption experiments at 77 K shows an enhancement textural property of the catalyst. Desilication method increased the surface area of the original support from 391.81 m^2/g to 419.75 m^2/g, pore size from 5.27 nm to 8.09 nm and the pore volume slightly increased by 20.35%. EDS showed a decrease in silicon content from 50.78 % to 43.13 % after the desilication of H-ZSM-5 zeolite, which led to Si/A*l* molar ratio of 26. For the Co/H-ZSM-5 catalysts, the XRD patterns indicated that cobalt metal was successfully impregnated on H-ZSM-5. Promotion of the Co/H-ZSM-5 catalyst increased the cobalt crystallite sizes from 13.7 nm to 17.0 nm based on XRD results.

The effect of desilication of H-ZSM-5 on the catalytic performance of the Co-catalysts was evaluated in FTS under the same process conditions; temperature (250°C), pressure (15 bar), flow rate (1200 gas hourly space velocity), H_2/CO syngas ratio (2.5) and catalyst weight (0.5g). The analysis of FT results was based on the CO conversion and product selectivity (olefins and paraffins). Prior to the effect of desilication, Co/H-ZSM-5 catalyst resulted in 49.7 % CO conversion, 47.8 % selectivity to methane and 8.8 % selectivity to C_{5+}. Therefore, the use of mesoporous-H-ZSM-5 as a support to Co-based catalyst decreased methane selectivity, enhanced the CO conversion and C_{5+} selectivity. The CO conversion and C_{5+} selectivity

depended on the temperature used during desilication method by NaOH aqueous solution for mesoporous-H-ZSM-5 preparation. Based on the optimum NaOH temperature of 55°C, the mesoporous-H-ZSM-5 on Co-catalyst increased the rate of CO consumption which led to CO conversion of 84.2 %. In addition, C_{5+} selectivity increased to 47.9%, being more selective to olefin than paraffin (obtained C_5 olefin ratio of 7.7).

The influence of calcium promotion to Co-based catalysts maintained its activity, high CO conversion and C_{5+} selectivity. Regarding Ca-Co/H-ZSM-5 and Ca-Co/H-ZSM-5(55) catalysts, CO conversion increased to 50.2% and 90.9 % respectively. On Ca-Co/H-ZSM-5(55) catalyst, selectivity to C_{6+} hydrocarbons were 8.6 % olefin and 34.5 % paraffin compared to 19.9 % olefin and 7.5 % paraffin of Co/H-ZSM-5(55) catalyst. This explains that calcium promoter was more favorable to longer hydrocarbons of paraffins than olefins due to the second reaction of shorter alkenes into saturated HCs.

At low pressure condition (8 bar and 2 bar) but similar other process conditions, CO conversion decreased to 47.7 and 17.4 % caused by decrease in partial pressures of CO. But lowering the amount of pressure kept selectivity to paraffins more than olefins due to calcium promoter, Ca/H-ZSM-5(55). It was concluded that the mesoporosity of the H-ZSM-5 and calcium promotion on the Co-based catalyst played a significant role in overcoming the over-hydrocracking of hydrocarbons and promote the re-adsorption of smaller olefin hydrocarbons into gasoline-range hydrocarbons, respectively.

CHAPTER 1

Introduction

1.1 Motivation and background

Over the years, there has been a rapid growing demand of liquid fuels. This demand is a consequent result of high energy consumption by ever-increasing population. Nada (2011) mentioned that the demand for transport fuels has drastically increased in the past few decades due to vehicles increasing at an alarming rate. The demand for transportation fuels continually rise because of deficient and diminishing of fossil fuel sources. The world energy business depends more on crude oil price to produce liquid fuels. About 90% of all transportation fuels come from crude oil (Falola & Genova., 2005). However, these transportation fuels produced from crude oil (conventional fuels) pose adverse environmental threats such as carbon dioxide (CO_2) emission. Therefore, it has become the world biggest challenge to find alternative and more sustainable energy sources (Daniell et al.,2012). Among other possible alternative processes, Fischer-Tropsch Synthesis (FTS) is the most attractive route for the production of clean fuels at economically feasible cost.

Fischer-Tropsch synthesis (FTS) is a catalytic reaction which converts syngas (predominantly CO and H_2) from derived resources like coal, natural gas and renewable biomass to clean hydrocarbons (liquid fuels) and other chemicals (Lu, 2011). Historically, the first Fischer-Tropsch (FT) process was developed in 1925 by two Germany scientists, Franz Fischer and Hans Trospch aiming to convert coal to liquid fuels. The current focus is on coal to liquids (CTL) and gas to liquids (GTL) as the economical processes. In 1955, South African Coal Oil and Gas Cooperation (SASOL) commercial operated their first FT plant based on coal to liquid fuels (Lualdi, 2012). Up to now, Sasol uses coal derived synthesis gas to produce liquid fuels. Although the current focus for FT process is on CTL and GTL, the conversion of biomass to liquids (BTL) and waste to liquids (WTL) can also be considered. For instance, biomass feedstocks must be derived from sources which do not compete with environmental use for food production or put the environment in danger of deforestation to promote sustainable development (Daniell et al., 2012). In order to be more considerate with the environment, some disposed waste materials can play a role in the production of syngas. Illegal disposal of these waste materials such as municipal waste, industrial packaging and waste tyres pose a major environmental and health risk conditions, particularly waste tyres (Muzenda & Popa., 2015). It is important to discover and implement the effective waste tyre management policies.

According to Muzenda & Popa (2015) about 1.4 billion tyres are sold worldwide each year. In South Africa, approximately 11 million tyres are currently sold, and 275 000 tonnes of these tyres become waste (Muzenda & Popa., 2015). Apart from recycling and re-use of waste tyres, researchers reported that waste tyres can be gasified to harness syngas (carbon monoxide and hydrogen gases) for the production of fuel. Waste tyres are naturally carbon containing sources therefore, through pyrolysis and gasification, syngas is produced which can be used in FTS. Gasification process is the conversion of feedstock (carbon containing sources) to carbon monoxide and hydrogen-rich synthesis gas under the use of oxygen, air or steam (Daniell et al., 2012).

FTS produces several hydrocarbons mainly paraffins and olefins arranged in a product distribution based on the type of catalyst and industrial process used (Dagle et al., 2014). The commonly industrially used catalysts for FT process are Cobalt (Co) and Iron (Fe). These catalysts can be applied on two industrially processes: low-temperature Fischer Tropsch (LTFT) and high-temperature Fischer Tropsch (HTFT) (Sartipi et al., 2013). Either Cobalt (Co) or Iron (Fe) can be applied on low-temperature FT but Co-based catalysts are more preferred to Fe-based catalysts at LTFT (Dancuart & Steynberg, 2007). The cobalt-based catalyst is employed in the FTS reaction for the production of hydrocarbons, mainly paraffins and olefins. In the industry, hydrocracking and isomerization are employed as the second step for isoparaffins (gasoline) after FTS catalytic reaction.

In recent years, many studies have been dedicated on developing effective FTS catalysts which can combine both syngas reaction and hydrocracking and/or isomerization for desired products (gasoline). Interestingly, zeolite was found to be the most useful hydrocracking and isomerization catalyst because of its acidity (Dry, 2002). However, zeolite is naturally microporous which limits reactants to access the catalytically active acid sites. Consequently, many studies in literature focused on the improvement of zeolite performance by synthesizing micro/mesoporous zeolite material, scientifically called hierarchical zeolite. The synthesis of this hierarchical zeolite is believed to increase the accessibility to active sites of zeolites. The synthesis of this hierarchical zeolite can be done either by following non-templating or templating approaches (Zhou et al., 2011). Templating method uses templates such as carbon nanotubes, carbon nanoparticles, carbon nano-fiber, carbon aerogels, polymer aerogels and calcium carbonate (Xing et al., 2016a). For instance, Janssen et al. (2003) successfully generated mesoporous zeolites using carbon nanofibers. However, the process of synthesizing

mesoporous zeolite by templating with carbon sources can be very challenging with high cost of materials particularly carbon nanotubes.

Recently, a few studies have focused on synthesizing mesoporous zeolite by non-templating method particularly dealumination or desilication. Ogura et al. (2001) reported that dealumination treatment in acidic medium generates meso-porosity in zeolite and enhances the catalytic activity but leads to zeolite framework structural change. The removal of Al ions from zeolite framework deforms the structure of zeolite since aluminium is more reactive acid medium compared to silicon. Alternatively, desilication method using alkaline medium can help preserve the structure and meso-porosity of zeolite (Yoo et al., 2012); (Müller et al., 2000). In order to prove the preservation of zeolite framework, Ogura et al. (2001) investigated and found that ZSM-5 zeolite treated with NaOH has no effect on the structure of zeolite , thereby preserving both structural shape and the catalytic activity of the catalyst. In the same view, Groen, et al., (2004) conducted a further investigation and optimization of ZSM-5 using NaOH and considered influence of temperature and time on the treatment. The authors concluded that the best optimal treatment conditions were NaOH concentration of 0.2M for 30 minutes at 338K. A major emphasis of their work was mainly on the optimization mesoporosity and structure of ZSM-5. Abelló et al. (2009) presented the comparison results of ZSM-5 prepared via desilication by tetra-alkylammonium hydroxide (TPAOH) and sodium hydroxide (NaOH) aqueous solutions at the optimal condition reported by Groen et al. (2004). Results of Abelló et al. (2009) indicated that organic hydroxides have low reactivity compared to inorganic sodium hydroxide with a faster desilication by NaOH compared to TPAOH. Based on previous studies, Sartipi et al., (2014) studied the performance of combination of hierarchical H-ZSM-5 and Co-based FT catalyst on FTS. The authors reported that the introduction of hierarchical ZSM-5 on cobalt FT catalyst via incipient wetness impregnation (IWI) method enhanced catalyst activity and catalytic performance in term of CO conversion and selectivity to gasoline (C_5 - C_{11}) from syngas during FT reaction.

Furthermore, Daramola et al. (2017) investigated the catalytic activity of a bifunctional Co/H-ZSM-5 catalyst (without desilicating the support) at low pressure and temperature. The authors reported that CO conversion decreased and high production of methane and C_2 hydrocarbon were produced as both pressure and temperature decreased. It is noteworthy to mention that previous researchers did not consider the effect of NaOH concentration or temperature treatment on desilication and catalyst promotion on the hierarchical catalyst. This study intends

to investigate these variables to enhance further the activity of the catalyst and products selectivity during FTS.

1.2 Problem statement

The industrial Fischer-Tropsch process involves two steps for the production of the liquid fuels. The first step involves the catalytic reaction of syngas to hydrocarbons whereas the hydrocracking and isomerization take place during the second step for the production of the desired products, isoparaffins (gasoline). The issue with two steps FT process is the high energy consumption and high costs for Fischer-Tropsch production facilities. The conversion to gasoline and diesel is also limited by the Anderson-Schulz Flory (ASF) distribution law. A possible solution to these problems is the use of bi-functional catalyst on a single step process. The primary difference between two-steps and single step is that the bi-functional catalyst performs both the FTS reaction and hydrocracking/isomerization of long hydrocarbons.

Lately, most attempts have been focused on the development of effective FTS catalyst which performs both syngas reaction and hydrocracking/isomerization in one closed system. However, the challenge has been on the use of zeolite for hydrocracking purposes. Zeolite is naturally a microporous material which possibly cause over-hydrocracking of hydrocarbons. Desilication method and other methods are being used to create the mesoporosity in zeolite. The use of this mesoporous zeolite combined with FT catalyst (known as bi-functional catalyst) was found to produce desired gasoline range hydrocarbons (GHRs). Although, it produces desired GHRs, the optimization and synthesis of bi-functional catalyst as well catalyst promotion could be instrumental in maximizing the CO conversion and selectivity of the products.

1.3 Research aim, questions and objective

The thesis aims to optimize the performance of bi-functional Co/H-ZSM-5 catalyst by desilication of H-ZSM-5 zeolite making it mesoporous, followed by employing incipient wetness impregnation (IWI) method. Thereafter, promote the catalyst to improve its activity.

From the preceding, the following general research questions are posed for this project:

(i) Can desilication enhance the performance of a bi-functional Co/H-ZSM-5 catalyst prepared via incipient wetness impregnation (IWI) method during FT reaction?
(ii) What will be the effect of catalyst promotion on the reactivity of Co/H-ZSM-5 catalyst prepared in (i) during FT reaction?

(iii) What will be the performance of the best performing catalyst in (ii) when operated at a very low pressure (<15 bar) during F-T reaction?

The following are the project objectives to answer the above research questions:

(i) Synthesize and investigate the influence of desilication on Co/H-ZSM-5 catalyst prepared via incipient wetness impregnation (IWI) method on the performance of the catalyst during FTS.
(ii) To investigate the effect of three different promoters on the reactivity of Co/H-ZSM-5 catalyst during FT synthesis process.
(iii) To evaluate the performance of the best performing promoted bi-functional Co/H-ZSM-5 catalyst in (ii) when operated at low pressure condition during FT reaction.

1.4 Scope of the study

Chapter 1 outlines the motivation and background of the bifunctional catalyst for the Fischer-Tropsch synthesis, problem statement, research aim, questions and objectives.

Chapter 2 provides the relevant literature of the Fischer-Tropsch synthesis. It provides motivation through the detailed explanation method for the preparation of the bifunctional catalysts. It also covers the FT reactor consideration, the type of catalysts and the products selectivity.

Chapter 3 presents catalyst characterization techniques as well as Fischer-Trospch experiment procedure (reactor design, reduction and loading of the catalyst). It also covers how FT data is analysed from the Gas Chromatography, calculation methods of results.

Chapter 4 describes the synthesis and characterization of catalyst, giving the materials and methods used for the preparation of the catalysts. It also discusses the catalyst characterization results.

Chapter 5 discusses the performance results of the bi-functional catalysts, and comparison of results between un-desilicated and desilicated catalyst as well as to literature.

Chapter 6 discusses FT obtained results of the effect of the promoted catalysts

Chapter 7 discusses the performance evaluation obtained results under low pressure FT operation of promoted catalysts.

Chapter 8 draws the conclusion based on all obtained results and recommendations for the future work.

CHAPTER 2

Literature Review

2. Fischer-Tropsch Synthesis

Literature is entailed to discuss the topic of Fischer-Tropsch synthesis process, FT chemistry, catalysts and promoters involved, FT reactors consideration, various methods for catalysts preparation and products of the FTS.

2.1 Fischer-Tropsch Process

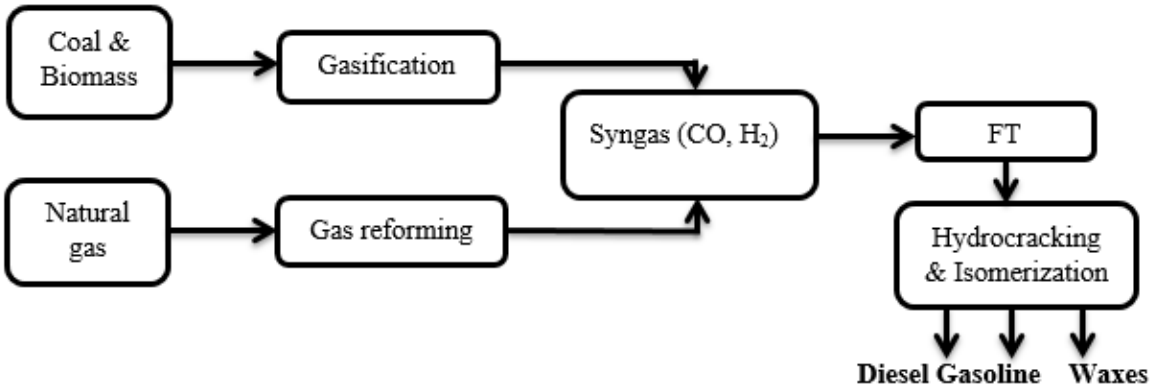


Figure 2-1: An overview of Fischer-Tropsch process

2.2 Fischer-Tropsch Chemistry

Fischer-Tropsch process is the conversion of synthesis gas into variety of hydrocarbons. FT reaction is exothermic and requires heat removal during reaction to avoid catalyst deactivation (Dry, 2002). There are series of chemical reactions which take place during FTS, both desirable and undesirable reactions. The following are the reactions (equation 2.1 to 2.5) of Fischer-Tropsch Synthesis.

Main reactions

Paraffins: $nCO + (2n + 1)H_2 \rightarrow C_nH_{2n+2} + nH_2O$ [2.1]

Olefins: $nCO + 2nH_2 \rightarrow C_nH_{2n} + nH_2O$ [2.2]

Water gas shift reaction: $CO + H_2O \leftrightarrow CO_2 + H_2$ [2.3]

Side reactions

Alcohols: $nCO + 2nH_2 \rightarrow C_nH_{2n+1}OH + (n-1)H_2O$ [2.4]

Boudouard reaction: $2CO \rightarrow C + CO_2$ [2.5]

‘n’ represents the number of carbons.

Generally, Fischer-Tropsch Synthesis reaction predominantly produces paraffins and olefins as represented by main reactions [2.1] and [2.2] depending on the type of catalyst used. Synthesis gas with high H_2/CO ratios and strong hydrogenation of catalyst yields paraffins and low H_2/CO rations and weak hydrogenation of catalyst yields olefins. From main reactions [2.1] and [2.2], water (H_2O) formation is also a primary product. However, water is an undesirable product in FTS which affects the syngas conversion, selectivity of hydrocarbons and the stability of a catalyst (Dalai & Davis., 2008).

The produced water by main reactions is useful during the water gas shift (WGS) reaction [2.3]. WGS (reaction 2.3) is favorable under the use of iron catalyst. This reaction is negligible over cobalt or ruthenium catalyst. During WGS, H_2O reacts with CO to form CO_2 and H_2. The formed hydrogen from WGS is used to make up for the deficient of H_2 in the syngas since iron catalyst is employed on low H_2/CO from coal gasification (Dry, 2002). Alcohols [2.4] can be produced in lesser amount under the precipitated iron catalyst (Yang et al. 2004). Reaction 2.5 is a possible side reaction during FTS. The CO_2 product in reaction 2.3 & 2.5 is produced in abundance under High Temperature FT which can cause catalyst deactivation (Dry, 2002). According to FT research, olefins [2.2] can possibly re-adsorb to produce branched hydrocarbons.

2.3 Fischer-Tropsch catalysis

FT synthesis is essentially a catalytic reaction. The choice of catalyst is crucial in FTS since it has a strong influence on the product distribution. FT products mainly depend on three catalyst properties, namely; activity, lifetime and product selectivity (Bukur et al., 2005). Once the catalyst is deactivated, the selectivity of the products will be highly affected.

Various catalysts for Fischer-Tropsch synthesis have been studied. The most common FT catalysts are transition metals in group 8 to 10 due to their strong and dissociative adsorption of CO and H_2 (Biloen & Sachtler, 1981); (Sun et al., 2017). Iron (Fe), Nickel (Ni), Cobalt (Co) and Ruthenium (Ru) are the only metals with sufficient activity for FT catalysis. Fe metal was the first catalyst used by Franz Fischer and Hanz Tropsch in 1925 during their FTS discovery. However, Fe-based catalysts are commonly used because they are least expensive (see Table 2.1) as compared to the other active metals. The cost comparison of these active metals is shown in Table 2-1

Table 2-1: Possible costs of catalyst in dollar ($) (Adapted from Dry, 2002)

Metal	Relative cost
Iron	1
Nickel	250
Cobalt	1000
Ruthenium	50 000

Reactivity

Among these metals, the Ru-based catalyst is the most active metal which produces high molecular weight hydrocarbons at low temperature (Schultz, 1999). However, Ru metal is very expensive, and its low availability limits its industrial use for FT process (Schultz, 1999). The industrial use of Ni-based catalyst produces high molecular weight hydrocarbons at low temperature due to sufficient reactivity. Disadvantages of Ni-based catalyst are the high methane selectivity and undesirable formation of Nickel Carbonyls compound (highly toxic) which result in loss of activity during reaction under excessive pressure (De Klerk & Furimsky, 2010).

For the above reasons, Iron-based and Cobalt-based catalysts remain the only ones for industrial application. Several studies and research have been focused on Fe and Co catalytic performance for FT synthesis. Luo et al. (2006) tabulated the comparison of both Co-based and Fe-based catalysts based on low temperature Fischer Tropsch (LTFT) as given on the following Table 2-2. A further detailed review of Co-based and Fe-based catalysts is discussed on the following sub-sections.

Table 2-2: Comparison between Co-based and Fe-based catalysts over low temperature FTS (Adapted from Luo et al. (2006).

Properties	Co-based catalyst	Fe-based catalyst
H_2/CO Ratio for feed	2+	0.5 – 2.5
Activity	High	Low
Temperature	Very low	Low to High
Water Gas Shift (WGS) Activity	Very low/ negligible	High
Chain Growth Probability (α)	High	Low
Olefin Selectivity	Low	High
Stability, lifetime	Long	Short
Cost	Expensive	Cheap

2.3.1 Iron-based catalyst

Iron-based catalysts are considered attractive for industrial use not only because they are inexpensive, but they are also flexible and suitable for both low temperature Fischer Tropsch (LTFT) and high temperature Fischer Trospch (HTFT). Both these two FT operating regimes are designed to target selective hydrocarbons or products (Li., 2001). In other words, the choice of LTFT process or HTFT process depends on the products intended to be produced. High temperature FT process on Fe-based catalyst is used to produce gasoline, olefins and linear hydrocarbons (Akhtar et al., 2006). The temperature range for HTFT process is 300°C to 350°C. Low temperature on either Fe-based or Co-based catalyst is used to produce wax (see Table 2.1).

Generally, the production of hydrocarbons under iron-based FT requires lower molar ratio of hydrogen to carbon monoxide (see Table 2-2). Low H_2/CO means CO-rich. The synthesis gas with low H_2/CO are derived from coal or biomass which promotes water gas shift (WGS) reaction, thus make the use of Iron-based catalyst attractive (Schulz, 1999). Water-gas shift (WGS) reaction (reaction 2.3) is the reaction of water (from FTS) and carbon monoxide (CO) to form hydrogen (H_2) and carbon dioxide (CO_2). H_2, a product from WGS, provides FT process with additional hydrogen. The insufficient of hydrogen from coal or biomass with the use of Fe-based catalyst is associated with lower conversion (Lögdberg, 2007).

The preparation of LTFT iron-based catalyst is by the precipitation from iron nitrate solutions promoted with copper/ potassium and bound with silica (SiO_2) or aluminum oxide (Al_2O_3) (Schulz., 1999). For HTFT, the iron-based catalyst is prepared by fusing magnetite consisting of small amounts of promoters (Van Der Laan & Beenackers, 1999). The main disadvantage of iron is its sudden deactivation due to oxidation and coke deposition (Sartipi et al, 2014). However, the advantages of iron catalyst are as follows:

- Iron is the least expensive metal to use.
- It promotes water-gas shift reaction
- It has higher selectivity for olefinic products (Sartipi et al., 2014).

2.3.2 Cobalt-based catalyst

Cobalt based catalysts are the most commonly used catalysts for Fischer Trospch Synthesis. They are only used under low temperature conditions known as LTFT process. Several researchers have investigated activity and selectivity of cobalt catalyst. Based on research and literature, cobalt catalysts possess high activity and selectivity for the formation of mainly straight-chain hydrocarbons known as heavy waxy product (Schulz, 1999). This heavy waxy product (long hydrocarbons) can be broken down to diesel fuel during hydrocracking stage. Unlike with iron catalyst, water-gas shift (WGS) activity is very low or negligible.

Cobalt catalyst is considered the only useful catalyst for synthesis gas with high H_2/CO derived from natural gas, with H_2:CO ratio of at least 2 (Luo et al., 2006). The Co-based catalyst is more active than Fe-based catalyst but inactive for WGS reaction due to H_2-rich syngas. De Klerk & Furimsky. (2010) noted during their research that Co-based LTFT catalysts give a higher conversion and practically proved for its longer catalyst life. The advantages of Co-based catalyst for LTFT are that it is more easily prepared, more robust, cheap and more resistant to Sulphur poisoning (De Klerk & Furimsky, 2010). However, Cobalt is more expensive than Iron (refer to Table 2-2).

2.3.3 Zeolite Support

Zeolites are inorganic materials that can be used for molecular seperations, as catalysts in hydrocarbon processing, chemical sensors or as absorbants. In 1987, Society et al reported about zeolite membranes. Ever since, various researchers focused on the zeolite membranes applications and the improvement of their quality. Their synthesis and applications had been reported in various literature reviews [Caro & Noack, (2008); Daramola et al. (2010); Bowen et al. (2004) and van Koningsveld et al. (1990)]. One of the application of zeolites as powders

or pellets is on inert support to prepare membranes. The International Zeolite Association (IZA) categorizes zeolite membranes with an identification code of three capital letters. According to literature, about 14 zeolite materials including AFI (Chiou et al., 1996) , ANA (Nishiyama et al., 1996), ATN (Washmon-Kriel & Balkus, 2000), BEA (Vu A. Tuan et al., 2002), CHA (Kalipcilar et al., 2002), DON (Muñoz & Balkus, 1999), FAU (Li et al., 2002), FER (Nishiyama et al., 1996), GIS (Dong & Lin, 1998), LTA (Hedlund et al., 1997), MEL (Tuan et al., 2001), MFI (Hedlund et al., 2002), MOR (Navajas et al., 2002) and OFF (Tanaka et al., 2001) have been prepared as membranes. From Figure 2-2, ZSM-5 and Silicalite-1 are classified as MFI structure whereas Faujasite or Zeolites (X and Y) are FAU.

Zeolites are three-dimentional framework structures made from aluminosilicates. This framework zeolite structures are built by Si and Al tetrahedral units (known as $TO_{4/2}$, where T= Al or Si). This three dimensional structure (TO_4) is formulated by linking the tetrahedra units with oxygen atom. The single three dimensional structures can be linked together (see Figure 2-3) to form a structure called secondary building units (Maghsoudi, 2016). Examples of SBUs are (SBUs)(Sodalite unit and Pentasil unit) (see Figure 2-2). van Koningsveld et al. (1990) discussed the layers, sizes of pentasil unit. These SBUs join together to form a long, regular zeolite framework structure with channels and cages between them. The chemical formula of zeolite is $A_{y/m}^{m+}$ $[(SiO_2)_x.(AlO_2)_y].zH_2O$, with A representing cation (normally group I and II) with charge m, x and y define the Si/Al ratio (Weitkamp, 2010).

Figure 2-2 shows the building structure of zeolite from tetrahedral units, secondary building units to zeolites and also shows pore dimensions. From $TO_{4/2}$, T-atoms are situated the vertices and T-O-T bonds represents a single line. For example, a building unit containing 12 T-O-T bonds forms a pentasil unit (also represented in Figure 2-3). When 24 tetrahedral units are combined together, they form a sodalite unit as represented in Figure 2-2. These sodalite units connect together via hexagonal faces to form a secondary building units called Faujasite. Furthermore, zeolites from SBUs have different pores depending of oxygen atoms creating a ring. For instance, there are small, medium and large-pore zeolites made up of 8-member rings, 10-member rings and 12-member rings respectively (Corma et al., 2003).

This study focused on the use of ZSM-5 zeolite which was classified a 10-member rings with pore sizes of about 0.57 nm as represented in Figure 2-2. Pore sizes for other zeolite types are also specified in Figure 2-2.

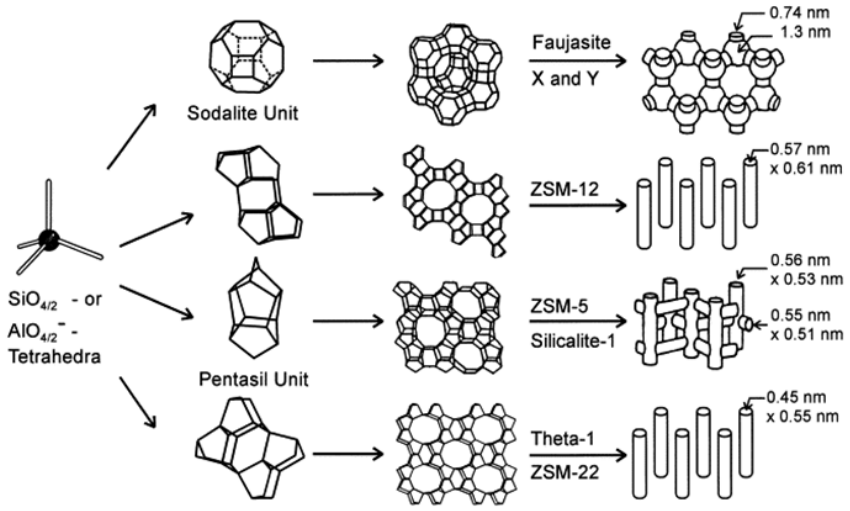


Figure 2-2: Formation of zeolites structures, zeolite X &Y, zeolite ZSM-12, zeolite ZSM-5 and zeolite ZSM-22 or Theta-1 (Adapted from Weikamp, (2010), Daramola et al., (2012))

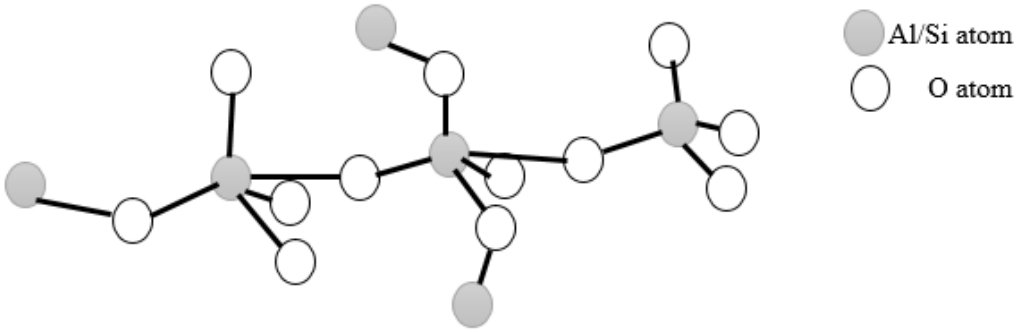


Figure 2-3: Basic building blocks of chemical zeolite structure

2.2.4 Mechanism of bifunctional Co/H-ZSM-5 catalyst

(From Daramola, 2015)

- Mass transfer of syngas (CO & H_2) from the bulk fluid to the external surface of the Co/H-ZSM-5 catalyst pellet
- Diffusion of syngas (CO & H_2) into the cobalt oxide nanoparticles of Co/H-ZSM-5 catalyst pellet
- Adsorption of syngas onto the cobalt oxide surface
- Surface reaction of syngas (CO & H_2) to form the normal hydrocarbons
- Desorption normal hydrocarbons from the cobalt oxide surface
- Diffusion & hydrocracking of normal hydrocarbons from the cobalt oxide nanoparticles of Co/H-ZSM-5 catalyst pellet

- Mass transfer of branched/short hydrocarbons from the Co/H-ZSM-5 catalyst to the bulk fluid.

2.4 Fischer-Trospch Reactor Consideration

The reactor type (together with catalyst) also has a major influence on the FTS product distribution. FTS reaction takes place in three various main catalytic and commercial reactors depicted by Figure 2-4: fluidized reactor, tubular fixed bed reactor and slurry phase reactor (Dry, 2002).

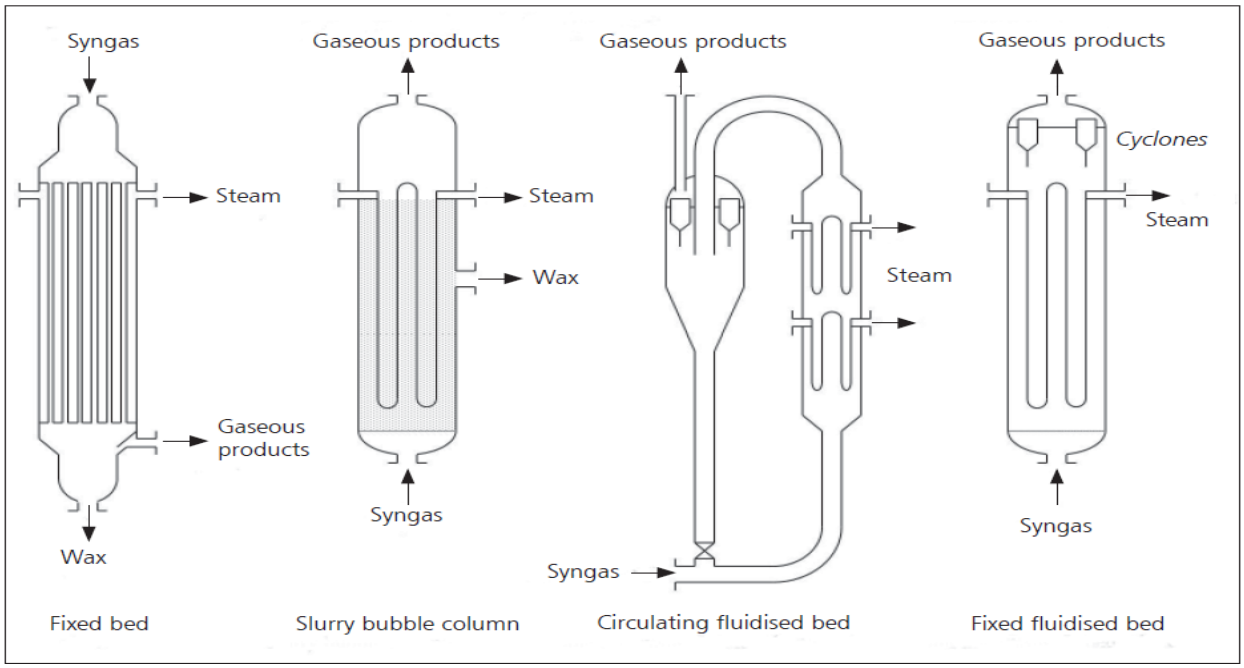


Figure 2-4: Various Fischer-Tropsch reactor technologies (Adapted from Dancuart & Steyberg, 2007)

The FT reaction is of high and exothermic nature. The focus of FT reactor design is to achieve rapid removal of heat of reaction and temperature control (Lee, 2011). Failure or inadequate heat removal leads to the excess methane formation, high carbon deposition (Equation 2.5) and catalyst deactivation due to sintering (Lee, 2011). In FT process, sintering is the main cause of catalyst deactivation. Therefore, the application of all three reactors (Figure 2-4) is designed for rapid heat removal. Fluidized bed reactors (fixed & circulating) are applied at high-temperature FT process (~ 340°C) to produce low molecular weight olefinic hydrocarbons and gasoline under the use of Iron-based catalyst (Lee, 2011). With the aim of producing high molecular weight or long-chain hydrocarbons, both Fixed-bed and slurry reactors are suitable

application for low-temperature FT process (200 – 240°C) with the use of cobalt or iron-based catalyst (Schulz & Claeys, 1999).

2.4.1 Fluidized bed reactor

Fluidized bed reactors are called two-phase reactors since they only involve gas and solid phases. Generally, there are only two types of fluidized reactors, circulating fluidized bed (CFB) and fixed fluidized bed (FFB) as represented in Figure 2-4. Both CFB and FFB have high heat transfer coefficients which are significant for the removal of large amount of heat from the reactors to control reactor temperature (Dancuart & Steynberg, 2007). However, the main difference between the two types of fluidized reactors is about catalyst position. In the FFB, the catalyst bed remains stationary and the syngas pass through the bed upwardly (Figure 2-4) while in CFB the catalyst is entrained with the fast moving gas stream (Figure 2-4) (Lee, 2011).The Kellogg Company introduced the use of FFB which was later applied in respective Sasol plants Secunda, and Sasolburg in 1956 (Schulz & Claeys, 1999). Sasol improved the operation of CFB reactor recently named Sasol Synthol reactor. In South Africa, Sasol Secunda operated 16 advanced reactors of CFB form with a 330 000 ton per annum capacity each (Schulz, 1999). In CFB reactor, reaction heat is removed by the two cooling zones in the riser (see Figure 2-4) (Lee, 2011). The use of CFB reactor is later replaced by the FFB reactor because of its simplicity, low construction cost, easy to operate, little attrition and back mixing and catalyst replacement (Lee, 2011). The vertical cooling tubes immersed inside the FFB is used to remove heat of reaction (see Figure 2-4) (Lee, 2011).

2.4.2 Slurry bed reactor

Slurry bed reactor is in a form of three phase operation system where gas is passed through the suspension of fine catalyst in a liquid with low vapour pressure (Kim et al., 2013). A three-phase system involves the reaction of gas phase (syngas) reactant in the presence of solid phase catalyst for the production of liquid phase products (linear paraffins). Slurry bed reactor (three phase) is more attractive because of its advantages relative to other reactors (particularly fixed bed reactor) uniform temperature, efficient heat & external mass transfer, lower catalyst consumption, lower cost, ease on-line catalyst adjustment and gaseous and wax removed separately(see Figure 2-4) (Dry, 2002).Good temperature control leads to excellent and high conversion of syngas gas to products. However, if syngas contains any form of poison, it then affects the whole catalyst inside the slurry reactor. Slurry bed reactor operates at low-temperature FTS conditions for both co-based and Fe-based catalysts. In fact, Sasol has been

successfully operating a commercial-scale slurry reactor (5 m diameter & 22 m in height) since 1993 (Vosoughi et al., 2017).

2.4.3 Fixed bed reactor

According to literature, **fixed bed reactor** has been used for many years and contains numbers of tubes filled with Fe-based catalyst immersed in boiling water removal of heat (Kim et al., 2013). An example of fixed bed reactor is called ARGE Sasol, Sasolburg South Africa. Sasol originally designed a FBR (ARGE reactor) with shell containing 2050 tubes with 5 cm diameter tube and 12 m high filled with catalyst where the removal of heat is by means of high-pressure steam (Kim et al., 2013). Fixed bed reactor operates at low temperature FTS conditions. The operation of FBR is opposite that of SBR where syngas is introduced from the top (see Figure 2-4). The temperature control can be achieved by introducing high gas velocities and gas recycling (Hu et al., 2012). The FBR advantages are high catalyst load, long catalyst life with little or no poisons and little attrition & back mixing (Satterfield et al. (1982); Daramola et al. (2017)). However, the major problems of FBR are high pressure drop, difficult with on-line catalyst changing and high cost (Satterfield et al., 1982).

2.5 Product selectivity & distribution

FT reaction gives various products spectrum as represented by Figure 2-5. The formation of this product spectrum is described as polymerization kinetic model. ASF model is the commonly known method to explain the product distribution from FTS. From this ASF model, a chain growth probability (α) determines the length of the carbon molecule from carbon atoms C_{n-1} to molecule of carbon atoms C_n (Udaya et al., 1990). ASF kinetic model equation [2.6] is represented below:

$$W_n/_n = (1-\alpha)^2 \alpha^{n-1} \qquad [2.6]$$

Where W_n is the weight fraction of hydrocarbons with carbon number n and α is the chain growth probability.

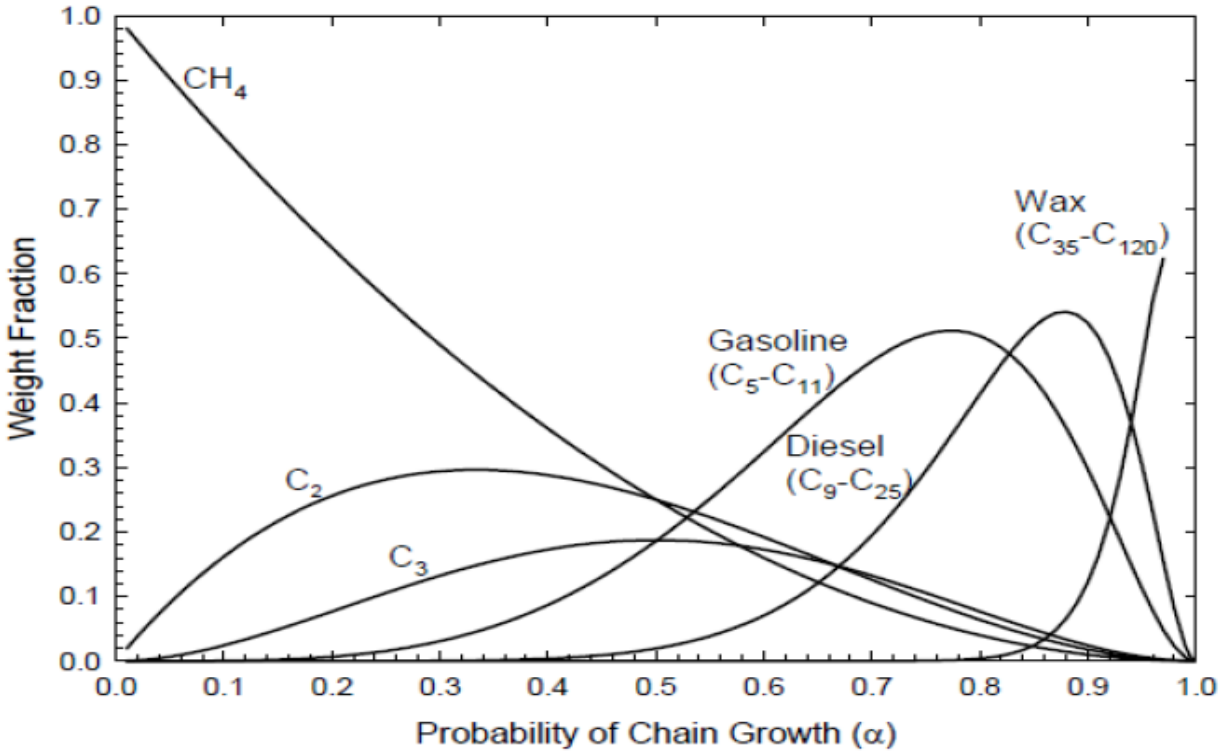


Figure 2-5: The FTS product distribution as a probability chain growth (α) following ASF model (Adapted from Satterfield et al. 1982).

2.6 Fischer-Tropsch Catalyst Synthesis

2.6.1 Possible supports of cobalt F-T catalyst

Bi-functional catalyst is the combination of metallic component and oxide supports or acidic sites (Gayubo et al., 2014). Several studies have been used oxide supports include silica (SiO_2), alumina (Al_2O_3), titania (TiO_2) and zeolite. Numerous reports proved that SiO_2 support was more active than the other oxide supports (Mirzaei et al. (2006); Guo et al., (2013)). However, the application of H-ZSM-5 zeolite due to its acidic site enhances selectivity and products quality during FT process. Sartipi et al., (2013) study detailed that cobalt supported on H-ZSM-5 zeolite is very effective for the direct production of liquid fuel.

This research entails on synthesis of cobalt supported on H-ZSM-5 zeolite as the bi-functional catalyst for F-T synthesis.

2.6.2 Alkaline treatment method

Groen et al. (2004) prepared desilicated-H-ZSM-5 zeolite using alkali-treatment method. Desilication of H-ZSM-5 was carried out by mixing and stirring 330 mg of parent zeolite in 10 ml of 0.2M NaOH solutions and allowed to mix at temperature range of 308 to 358K for a period of 150 to 120 min. After mixing, zeolite solution was cooled down using an ice bath.

Zeolite powder was then filtered from solution and washed until the pH reaches neutral. Zeolite powder was dried at 373K for 12 hours. To introduce H-form on the zeolite, zeolite powder was mixed with 0.1M NH_4NO_3 solution followed by filtration to remove Na^+ ion from the solution. Therefore, NH_4-ZSM-5 was dried and calcined at 373K for 12 h and at 823K for 5 h the respectively.

2.6.3 Preparation methods of cobalt-supported F-T catalyst

Incipient wetness impregnation (IWI) method

Eschemann et al. (2014) prepared Co supported on TiO_2 by incipient wetness impregnation (IWI) method. An aqueous solution of Co $(NO_3)_2.6H_2O$ was impregnated by the TiO_2 support material. Subsequently, the mixed solution was dried overnight at 60 °C followed by calcination at 350 °C for 2 h at temperature at 2°C/min.

Sartipi et al. (2013) applied incipient wetness impregnation (IWI) method with aqueous solution of Co $(NO_3)_2.6H_2O$ where both parent H-ZSM-5 and mesoH-ZSM-5 employed as supports separately. Ammonium form of zeolite (ZSM-5) were calcined at 550 °C and dried to form parent H-ZSM-5 and thereafter used desilication approach to form mesoH-ZSM-5. After impregnation, the samples were kept at room temperature inside a desiccator overnight then dried at 120 °C for 12 h and subsequently calcined at 400°C for 2 h thereafter Co/parent H-ZSM-5 and Co/mesoH-ZSM-5 catalysts formed loaded with 10 wt.% of cobalt metal.

Co-precipitation method

Atashi et al. (2010) prepared cobalt-manganese sample using co-precipitation method. An aqueous solutions of Co $(NO_3)_2.6H_2O$ and Mn $(NO_3)_2.4H_2O$ were pre-mixed inside the round bottomed flask with a condenser and heated at 70°C. A dropwise addition of aqueous Na_2CO_3 to the mixed nitrate solution was done during stirring at constant temperature of 70°C until pH 8 was reached. The precipitate was allowed to cool for 4 h. Thereafter, it was filtered and washed with distilled water for several times. Subsequently, the precipitate was dried in an oven at 120°C for 16 h and calcined in a furnace at 500°C for 16 h to form catalyst. TiO_2 supported catalyst was also done following the same procedure.

Mirzaei et al., (2006) conducted an experiment using co-precipitation method. The method was as follows, an aqueous solutions of Co $(NO_3)_2.6H_2O$ and $Fe(NO_3)_3.9H_2O$ were pre-mixed and heated at 70°C inside the round bottomed flask fitted with a condenser. During the stirring of

mixed nitrate solution at constant temperature, an aqueous Na_2CO_3 was added until pH 7 was reached. The precipitate was left to cool down for 4 h. Thereafter, the precipitate was washed several times with warm distilled water to remove Na^+. The resulting precipitate was dried in an oven at 110°C for 18 h and subsequently calcined in a furnace at 600°C for 6 h to form final catalyst. Different supports such as TiO_2, SiO_2 and Al_2O_3 were also added separately in the mixed nitrate solutions. SiO_2 support was promoted with various alkali metals (Li, K, Rb and Mg) in the form of $LiNO_3$, KNO_3, $RbNO_3$ and $MgNO_3$ solution separately. The resulting precipitates were also dried in an oven at 110°C for 18 h and subsequently calcined in a furnace at 600°C for 6 h to form final catalyst with support and promoter.

In this research incipient wetness impregnation (IWI) method will be applied. Ammonium form of zeolite (ZSM-5) is to be calcined and desilicated to form H-ZSM-5 and follow Sartipi, et al. (2013) and Groen et al. (2004) incipient wetness impregnation (IWI) method cobalt (II) nitrate solution.

2.6.4 Effect of using promoters

The addition of noble or alkali promoters improve the reducibility and selectivity of the catalyst. Among noble promoters (Ru, Re or Pt), studies proved ruthenium promoter to be of higher reducibility compare to other noble metals (Martínez et al., 2003). Alkali promoters include Li, K, Rb, Ca and Mg was studied (Mirzaei et al., 2006). Potassium promoter was found to be more active and selective compare to other alkali promoters.

2.7 Concluding remarks

An overview of Fischer-Tropsh synthesis, its chemistry, catalysis, reaction system has been presented. Various methods for preparing bifunctional catalyst was also discussed. Number of researchers focused on the development of mesoporous zeolite with few reports on the optimization of the bifunctional catalysts and no reports on promotion of the catalysts on the mesoporous zeolite. Therefore, optimizing the bifunctional catalyst to produce mesoporous zeolite from different temperature of alkaline solution as well as promotion of the catalyst could be useful to develop a highly active of catalyst. This dissertation will provide results discussion based on the following statements;

(i) Synthesize and investigate the influence of desilication on Co/H-ZSM-5 catalyst prepared via incipient wetness impregnation (IWI) method on the performance of the catalyst during FTS.

(ii) To investigate the effect of three different promoters on the reactivity of Co/H-ZSM-5 catalyst during FT synthesis process.

(iii) To evaluate the performance of the best performing promoted bi-functional Co/H-ZSM-5 catalyst in (ii) when operated at low pressure condition during FT reaction.

CHAPTER 3

Experimental Procedure

Synthesis and Characterization of Catalysts

3.1 Introduction

This chapter discuss the materials used for catalyst preparation, catalyst preparation and characterization results of the catalysts from N_2 Physisorption (Brunnat Emmett Teller), Scanning Electron Microscopy (SEM) and Energy Dispersive Spectroscopy (EDS), X-Ray Diffraction (XRD), Fourier Transformed Infrared Spectroscopy (FT-IR), Transmission-Electron Microscopy (TEM) and Temperature-Programmed-Reduction (TPR). The chapter includes the discussion of Fischer-Tropsch experimental setup, reactor design, catalyst reduction and products calculations in terms of conversion and selectivity.

3.2 Materials and methods

3.2.1 Materials

Ammonium form of Zeolite Socony-Mobil-5 (ZSM-5) used in this study was purchased from Zeolyst (with Si/A*l* = 40). Sodium hydroxide (NaOH) and ammonium nitrate (NH_4NO_3) solutions were purchased from Sigma-Aldrich. Deionized water with resistivity of 18.2 MΩ was prepared in house. Cobalt (II) nitrate hexahydrate ($Co(NO_3)_2.6H_2O$) was purchased from Sigma-Aldrich used as a cobalt source. Syngas (composition: 20% CO, 50% H_2 & 30% N_2), Argon (Ar), Hydrogen (H_2), Nitrogen (N_2), Air and calibration gas (consists of N_2, H_2, CO, CO_2, CH_4, C_2H_6 & C_2H_4) were purchased from Afrox (pty) SA and used for Fischer-Tropsch Synthesis reaction.

3.2.2 Catalyst preparation

Synthesis of un-desilicated catalyst

Ammonium form of Zeolite Socony-Mobil-5 (ZSM-5) was calcined at 550°C for 5 h and therefore dried overnight at 120°C for 2 h to form H-ZSM-5. Thereafter, the catalyst was prepared using H-ZSM-5 as a support loaded into 10 wt.% of Co, using incipient wetness impregnation (IWI) with aqueous cobalt nitrate solution as a cobalt source. The impregnated sample was kept at room temperature overnight, dried at 120°C for 12 h and therefore calcined 400°C for 2 h. The final product is called Co/H-ZSM-5 catalyst.

Synthesis of desilicated catalyst

The hierarchical mesoporous H-ZSM-5 was prepared using 0.2M NaOH aqueous solution known as desilication method analogous to that of Sartipi et al.(Sartipi, Parashar, Valero-

Romero, et al., 2013) and Groen et al. (Groen et al., 2004) The H-ZSM-5 was added into three separate 0.2M NaOH aqueous solutions (volume $_{\text{base solution}}$/ weight $_{\text{H-ZSM-5}}$ = 8.0 $cm^3 g^{-1}$) vessel heated to 40°C, 55°C and 70°C individually inside the oil bath and each vigorously stirred for 1 hour. Immediately after heating, the suspensions were cooled down to room temperature, then the solid fine particles were filtered by centrifuge followed by washing with deionized water until pH reached neutral. The subsequent solid samples were dried at 373 K then dissolved into 1M NH_4NO_3 aqueous solution to convert alkaline treated into H-form of zeolite. Therefore, samples were filtrated to remove Na^+ ions followed calcination at 550°C for 5 h. The samples obtained are known as hierarchical mesoporous H-ZSM-5. Incipient wetness impregnation (IWI) similar to synthesis of un-desilicated catalyst was followed to produce 3 final products called Co/H-ZSM-5 (desilicated at 40°C), Co/H-ZSM-5 (desilicated at 55°C) and Co/H-ZSM-5 (desilicated at 70°C) catalysts. Figure 3-1 shows the schematic illustration of alkaline desilication of zeolite support and Figure 3-2 depicts the pictures of the desilication of the support and preparation of the catalyst.

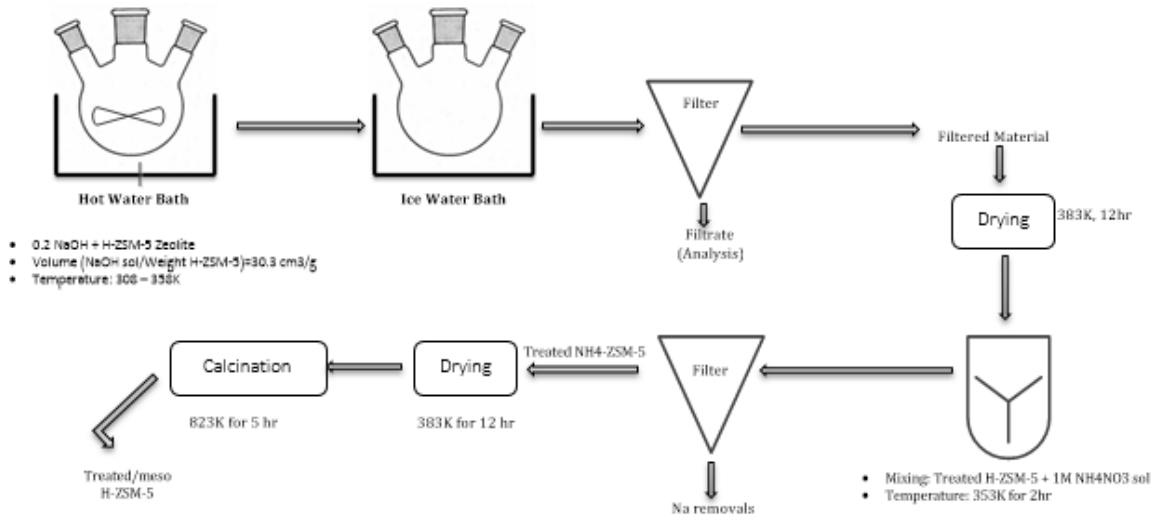


Figure 3-1: Scheme of the alkaline desilication of the zeolite support



Figure 3-2: Desilication of the zeolite support (left) and preparation of the Co/H-ZSM-5 catalyst via IWI using the desilicated zeolite

Promotion of catalyst

The Co/H-ZSM-5 catalyst that displays the best F-T performance in terms of conversion and selectivity was subsequently promoted with calcium metal. The promoter was added during IWI method in the form of Calcium nitrate Ca $(NO_3)_2$ solution by 2.0 wt.% of total. Thereafter, the promoted catalysts were dried and calcined at the same conditions as in **synthesis of un-desilicated catalyst**

3.3 Catalyst Characterization Techniques

3.3.1 N_2 Physisorption (Brunnat Emmett Teller) analysis

N_2 physisorption was performed using Micromeritics TriStar 3000 V6.05 A. instrument using nitrogen temperature at 77K to study surface area, pore size and pore volume of samples. N_2 adsorption-desorption isotherms were used for t-plot method to study between microporosity and mesoporosity. The adsorption branch of the isotherm used to plot BJH model to study mesopore size distribution (Barrett et al. 1951).

3.3.2 Scanning Electron Microscopy (SEM) and Energy Dispersive Spectroscopy (EDS) analysis

SEM was used to study the surface morphology of ZSM-5, H-ZSM-5, Co/H-ZSM-5 and promoted CO/H-ZSM-5. The samples were fixed unto aluminium stubs using carbon conductive tape. The samples were initially coated with a layer of gold-palladium (Au-Pd) to

avoid charge on the specimen surface and degradation. The analysis was done using Carl Zeiss Sigma scanning electron microscope coupled with Oxford X-act Energy Dispersive Spectroscopy (EDS) detector. SEM displayed microscopic images of samples while EDS recorded the elemental compositions in samples. This technique works by striking the sample on the surface using electron beam selectively emit electrons of each element according to its energy level.

3.3.3 X-Ray Diffraction (XRD) analysis

The zeolites (ZSM-5, H-ZSM-5) and bi-functional catalysts (Co/H-ZSM-5) samples were analysed using Bruker D2 phaser generated at 30 kV and 10 mA Lynxeye detector. The diffraction patterns read in 2θ region from 5° to 90° moving with step of 0.027° using Cu-Kα radiation (λ= 1.789 Å). XRD patterns of zeolites obtained were analysed using International Zeolite Association (IZA) database (Baerlocher et al., 2007) and the American Mineralogists Crystal Structure Database (AMCSD) (Downs & Hall-Wallace, 2003). The average particles sizes d was calculated according Scherrer equation [3.1]

$$d = \frac{k\lambda}{\beta cos\theta} \qquad \text{(Dias \& Assaf, 2003; Wang et al., 2013)} \qquad [3.1]$$

Where d is the Co_3O_4 crystalline size (nm), k is the geometrical coefficient constant which is 0.9, λ is the radiation wavelength X-ray (λ= 0.789 nm), β is the width in radians at the half height diffraction peak (known as FWHM stands for full-width at half minimum) and θ is the half of diffraction angle in radians. Since tetra-oxide of cobalt (Co_3O_4) was reduced to Cobalt (Co) metal, therefore the Co_3O_4 particle size was converted to cobalt metal particle size calculated using the formula [3.2]

$$d(Co^0) = 0.75d(Co_3O_4) \qquad \text{(Dias \& Assaf, 2003)} \qquad [3.2]$$

3.3.4 Fourier Transformed Infrared Spectroscopy (FT-IR) analysis

Zeolite materials known as alumno-silicate contain organics such as silicone which can be analysed using FTIR. FTIR analysis was performed to measure the acidity of zeolite materials.

The chemistry of parent and desilicated zeolite samples were evaluated using a PerkinElmer Frontier Fourier transform infrared spectrometer (PerkinElmer, USA) equipped with attenuated total reflectance (ATR) mode. This ATR diamond plate was equipped with internal reflection element at 45 °C angle of incidence. The obtained spectra read from a frequency range of 400 to 4000 cm^{-1} with a resolution of 4 cm^{-1}.

Table 3-1: FTIR bands' assignment (Adapted from Coates. 2006).

Group frequency (cm^{-1})	Functional group/assignment
1560 – 1540/1380 - 1350	Aliphatic nitro compounds
1555 – 1485/1355 - 1320	Aromatic nitro compounds
1640 – 1620/ 1285 - 1270	Organic nitrates
1350 - 1250	Organic phosphates (P=O stretch)
1050 - 990	Aliphatic phosphates (P-O-C stretch)
1995 – 1075/1055 - 1020	Organic siloxane or silicone (Si - O – Si)
1110 - 1080	Organic siloxane or silicone (Si – O –C)
3570 - 3200	Hydroxyl group (-OH)

3.3.5 Transmission-Electron Microscopy (TEM) analysis

Temperature-Electron Microscopy (TEM) was used to study the cobalt metal dispersion within H-ZSM-5 and the internal structure morphology. The TEM investigations were carried out in a JEOL 100S spirit 120 kV equipment. The samples were ultra-sonicated in methanol prior analysis. About 0.1 – 0.5 mg sample was dropped in a copper grid and placed the TEM chamber for analysis.

3.3.6 Temperature-Programmed-Reduction (TPR) analysis

Temperature-Programmed-Reduction (TPR) was applied to evaluate the reducibility of the Co/H-ZSM-5 catalyst. This analysis was carried out using AutoChem II 2920 V3.05 rich in hydrogen. The analysis was done using the following condition; flow rate of 30 ml/ min, temperature range 20 °C – 90 °C with temperature ramp of 8 °C/ min using H_2/Ar ratio of 5%, adopted from Wang et al. (2000) and Daramola et al. (2017).

3.4 Support and cobalt catalyst characterization results

3.4.1 N_2 Physisorption (BET surface area)

The structural properties showing both BET surface area, pore volume and pore diameter of ZSM-5, H-ZSM-5 and Co/H-ZSM-5 catalysts analysed by N_2 physisorption are summarized

in Table 3-2. The pore size distribution (PSD) of these samples determine whether particles are micropores and mesoporous. Particles of the pore size between 0.4 – 2 nm are considered microporous while between 4 – 50 nm are considered mesoporous (Che & Vedrine., 2012). The order of the BET surface area increases from ZSM-5 to un-desilicated H-ZSM-5 then to desilicated H-ZSM-5. The zeolite surface area of ZSM-5, un-desilicated H-ZSM-5 and desilicated H-ZSM-5 are 340.47, 391.08 and 419.74 m^2/g respectively. The increase in BET surface area from un-desilicated H-ZSM-5 (391.08 m^2/g) to desilicated H-ZSM-5 (419.74 m^2/g), microspore volume reduction from 0.12 m^3/g to 0.09 m^3/g and pore diameter increases from 5.27 nm to 8.81 nm is the results of mesopores creation on zeolite due to silica removal through desilication method. Sartipi et al. (2013) reported an increase in BET surface area from 52 m^2/g H-ZSM-5 to 309 m^2/g meso-HZSM-5. The relation from H-ZSM-5 zeolite to Cobalt (from Table 3-2) indicates that Co was successfully loaded on the zeolite support via IWI because of the reduction in BET surface area from un-desilicated -H-ZSM-5 to Co/un-desili-H-ZSM-5 (from 391.08 m^2/g to 289.68 m^2/g), pore volume (0.12 m^3/g to 0.08 m^3/g) and so is the case from desilicated-H-ZSM-5 to Co/desilicated-HZSM-5 catalyst. The total volume of H-ZSM-5 was expected to increase after the treatment of H-ZSM-5 zeolite by the NaOH which known as desilication method.

Table 3-2: Textural properties of the ZSM-5, H-ZSM-5 support and Co/H-ZSM-5 catalysts (refer to Table B1-1 from Appendix B).

Catalyst	BET Surface area (m^2/g)	Microspore pore volume (m^3/g)	Pore diameter (nm)	Si/Al ratio
ZSM-5	340.4731	0.110717	5.9217	47
H-ZSM-5 (un-desil)	391.0832	0.120918	5.2705	48
Co/H-ZSM-5(un-desil)	289.6838	0.083906	6.0706	n/a
H-ZSM-5 (desilicated)	419.7451	0.096307	8.8087	26
Co/H-ZSM-5 (desil)	209.5149	0.046374	13.3103	n/a

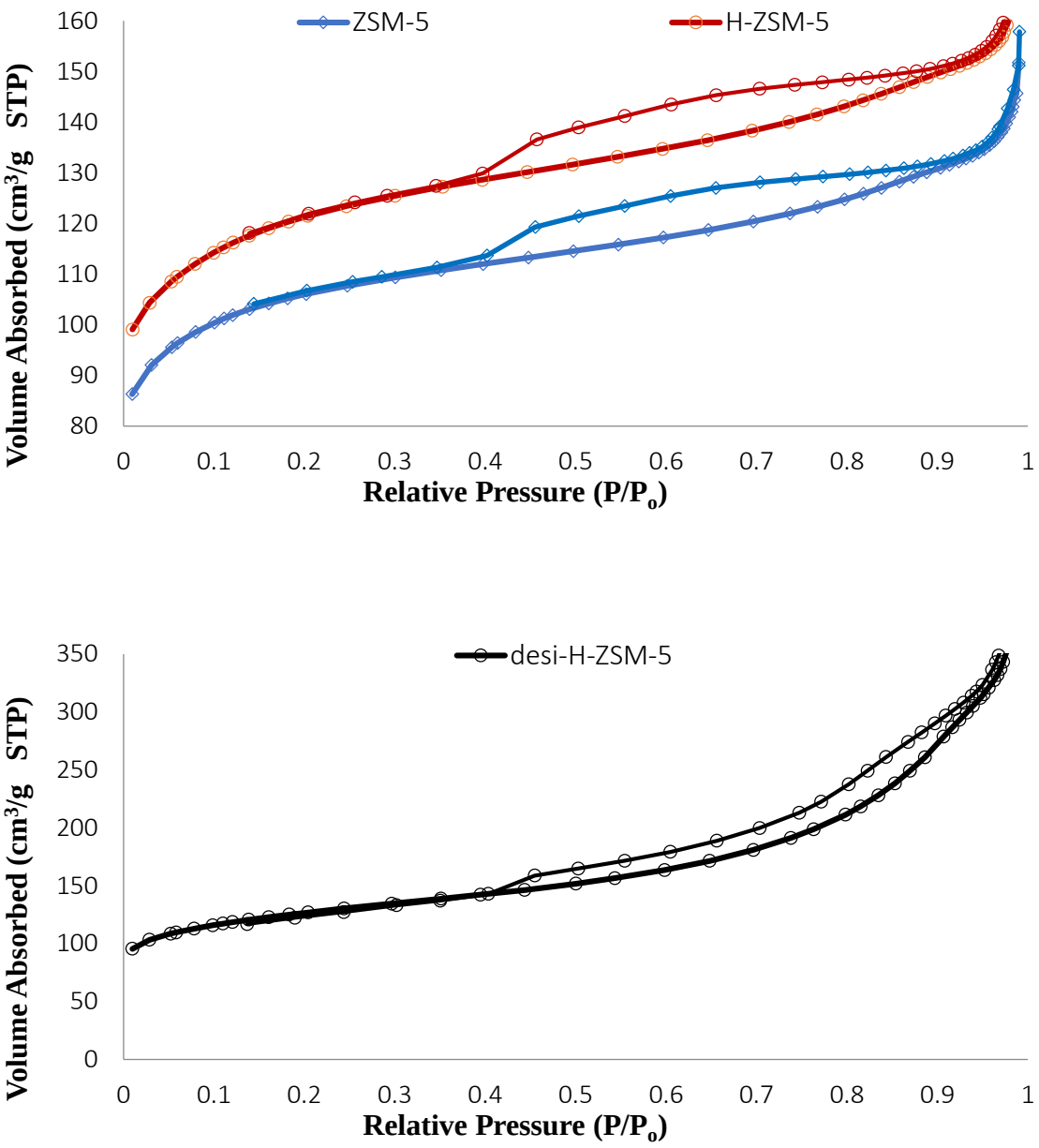


Figure 3-3: N_2 adsorption-desorption isotherm

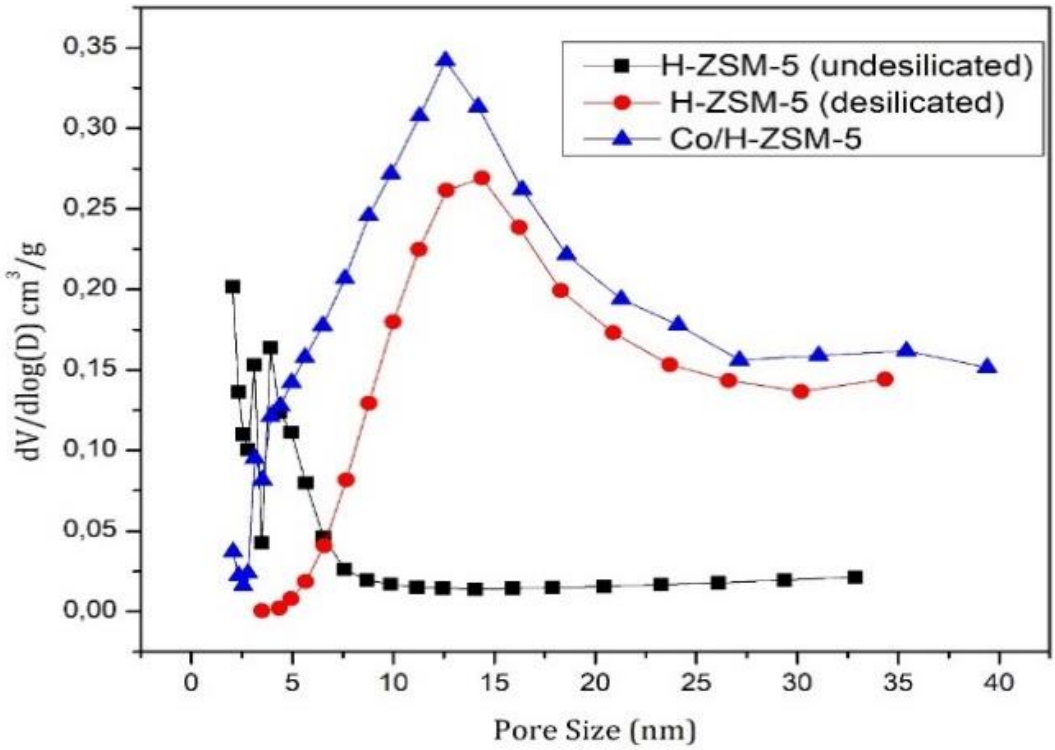


Figure 3-4: BJH pore size distribution of H-ZSM-5 support and Co/H-ZSM-5 catalyst

Figure 3-3 depicts the Nitrogen adsorption and desorption isotherms at 77 K for ZSM-5, H-ZSM-5 and desilicated-H-ZSM-5. The parent ZSM-5 isotherm with a horizontal plateau shape at low relative pressures revealed hysteresis loop and is considered to be of microporous characteristics (Perry et al., 1997). Upon calcination of parent ZSM-5, the similar isotherm and hysteresis loop was observed with a very steep slope from pressure range $P/P_O = 0.96 – 0.99$. After removal of silicon from zeolite via NaOH solution, the N_2 isotherm of the desilicated H-ZSM-5 increased intermediate pressures (P/P_O) between 0.4 - 0.5. The Nitrogen adsorption isotherm of this desilicated H-ZSM-5 in Figure 3-3 is classified type IV according to Perry et al. (1997) This type IV isotherm combined with hysteresis loop is an indication of meso-porosity of the sample, Wang et al. (2013) reported similar work. The presence of meso-porosity in desilicated is also witnessed by an increase in mesopore surface area and decrease in micropore volume given in Table 3-2.

The meso-porosity of desilicated-H-ZSM-5 was further confirmed by BJH pore size distribution in Figure 3-4. Prior to desilication process, H-ZSM-5 showed a narrow BJH pore size distribution of H-ZSM-5. The silicon removal with the 0.2M NaOH aqueous solution altered the size of the mesopores. As shown by BJH pore size distribution, a desilicated-H-ZMS-5 zeolite formed mesopores centred at about 14.3 nm. Abelló et al., (2009) reported the

formation of smaller pores (10 nm) in H-ZSM-5 zeolite subjected in NaOH (0.2M, 338K and 30 mins). This BJH pore size distribution of desilicated-HZSM-5 are in the range of 2 - 50 nm indicating the meso-porosity of this sample. Che & Vedrine, (2012) reported that the range of meso-porous solids samples is between 2 – 50 nm whereas that of micropores is between 0.4 – 2 nm. However, incipient wetness impregnation (IWI) of cobalt shifted the curve slightly to the left. In other words, the pore size of Co/desilicated-H-ZSM-5 decreased to 12.5 nm as a result of pores clogged up by introduced cobalt materials to desilicated H-ZSM-5. Note, the filling of cobalt particles reduced the pore sizes. Interestingly, the pore size distribution curves of both desilicated-H-ZSM-5 and Cobalt on desilicated-H-ZSM-5 have the same shapes.

3.4.2 SEM Results

The Scanning Electron Microscopy images of ZSM-5, calcined H-ZSM-5, desilicated H-ZSM-5 and Co/H-ZSM-5 are shown in Figure 3-5. Looking at Figure 3-5A which is ZSM-5 before calcination and B which is H-ZSM-5 after calcination, there was no change in morphology. In both Figure 3-5A and Figure 3-5B, zeolite particles appeared to be sphere-like. However, the difference between Figure 3-5A and Figure 3-5B is the formation of hydrogen ions (H^+) to be H-form ZSM-5 zeolite B which can be explained by the brightness of Figure 3-5B. The surface of both Figure 3-5A and Figure 3-5B images is observed to be little rough. Once the H-ZSM-5 zeolite undergone desilication process, it was observed that there was porosity developed depicted by Figure 3-5C. These pores observation is in support with the results obtained from nitrogen adsorption-desorption, which confirms the presence of porosity in H-ZSM-5 zeolite. After adding cobalt particles, the surface Figure 3-5D which is Co/H-ZSM-5 catalyst is observed to be rougher compared to Figure 3-5A, Figure 3-5B and Figure 3-5C. Again, through observation, the pores developed in during desilication in Figure 3-5C were then covered by cobalt particles. Looking at Figure 3-5D, it can be concluded that cobalt was successfully deposited on H-ZSM-5 zeolite surface represented by the whitish particles agglomerated.

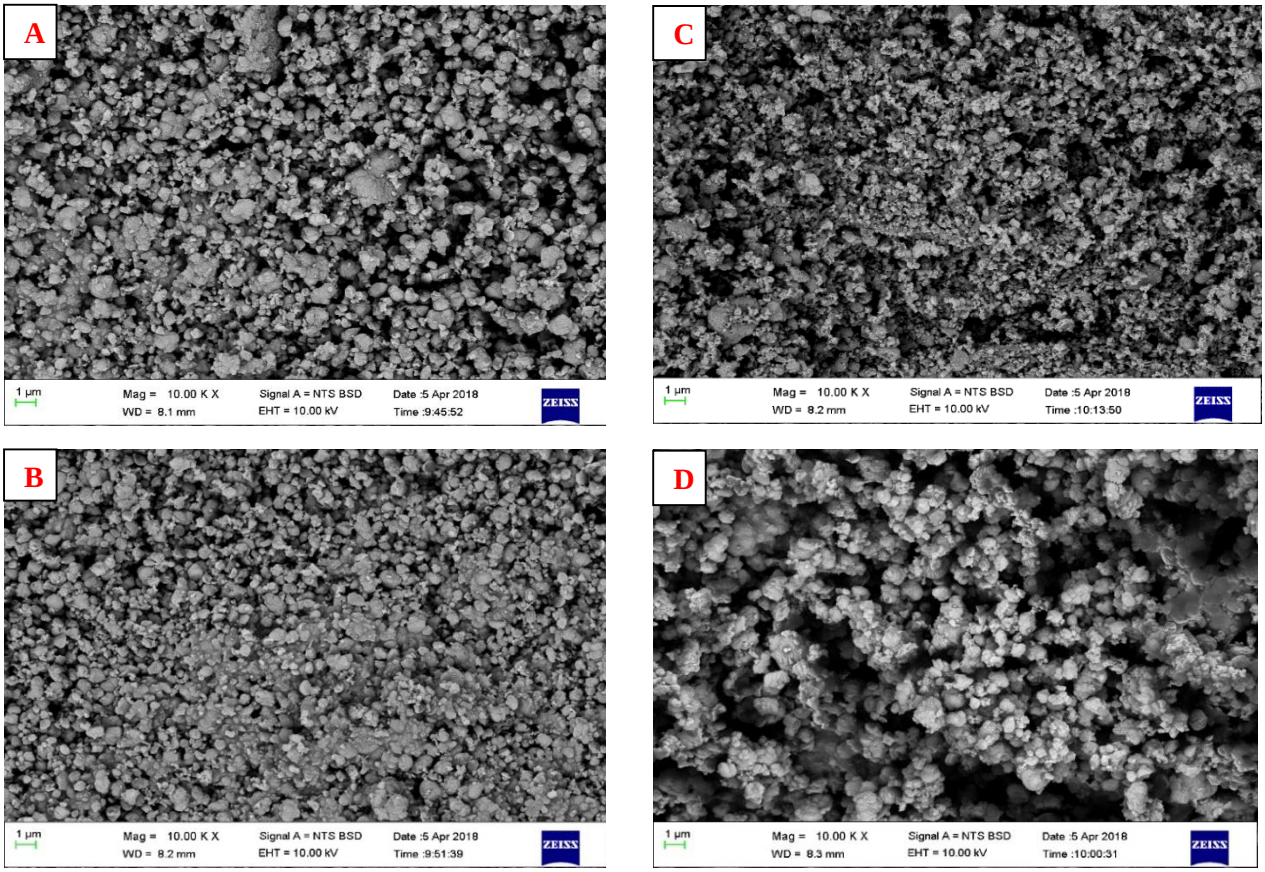


Figure 3-5: SEM images of [A] parent ZSM-5, [B] calcined H-ZSM-5, [C] desilicated-H-ZSM-5 and [D] Co/H-ZSM-5, all in 10 000 X magnification

3.4.3 XRD Results

Figure 3-6 illustrates XRD patterns of Co/H-ZSM-5 catalyst, desilicated and un-desilicated H-ZSM-5 as well as the standard H-ZSM-5. The standard H-ZSM-5 was obtained from IZA database and was used as the reference for comparing the crystalline structure with that of a synthesised H-ZSM-5. The diffraction patterns of synthesized H-ZSM-5 seem to match perfectly with that of standard H-ZSM-5. The high intensity peaks observed at a range of 2θ = 7 - 9° and 22 - 25° represent the crystallinity of H-ZSM-5 zeolite and the MFI morphology zeolite with a high presence of silicon and aluminium elements (Xing et al., 2016a; Xing et al., 2014) . No structural changes in H-ZSM-5 after desilication took place, the desilicated H-ZSM-5 retained the same diffraction patterns. However, making comparison between synthesized-H-ZSM-5 and desilicated-H-ZSM-5 patterns, the intensity of their peaks particularly at 2θ = 22 - 25° were reduced in size as a result of silicon removal. Upon incipient wetness impregnation of cobalt on H-ZSM-5 zeolite support, diffraction peaks emerged at 31.3°, 36.8°, 59.3° and 65.2° representing the successfully impregnated of cobalt (González et al., 2010). In addition, the cobalt peaks at the stated 2θ degrees above correspond with the crystal planes

Co_3O_4 from the American Mineralogists Crystal Structure database (Downs & Hall-Wallace, 2003). The Co_3O_4 size was calculated according to Scherrer formula [3.1] based on diffraction peak at $2\theta = 36.8°$ and results given in Table 5-1. The size of Co_3O_4 particles in Co/H-ZSM-5 was found to be 18.2 nm (Appendix A.1). The Co_3O_4 crystallite size of Co/H-ZSM-5 catalyst (18.2 nm) of this study is close and between results found by Wang et al. (2013) (18 nm) and Xing et al. (2016) (18. 6 nm). The size of Co^0 on Co/H-ZSM-5 catalyst based on equation [3.2] was 13.7 nm.

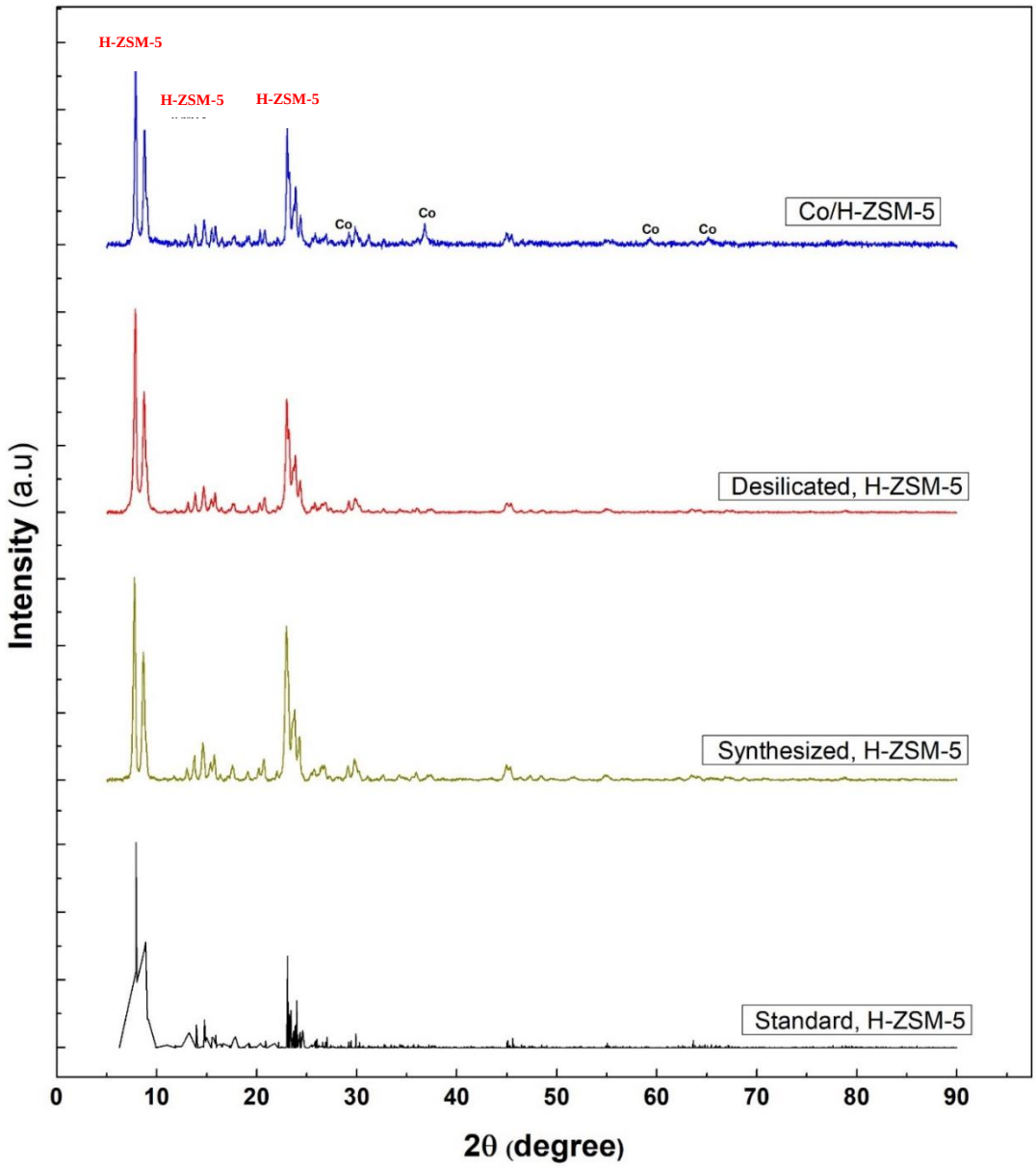


Figure 3-6: XRD patterns of standard H-ZSM-5, synthesized H-ZSM-5, desilicated H-ZSM-5 and Co/H-ZSM-5 catalyst.

3.4.4 FT-IR (in ATR) results

FT-IR in Figure 3-7 & Figure 3-8 were conducted to study the nature of acidity over ZSM-5 zeolites. Figure 3-7 gives the analysis comparison between desilicated & undesilicated-H-ZSM-5 zeolites spectra. These spectra present the group of organic compounds within zeolite by looking at functional group and group frequencies. It has already been mentioned and known that zeolite exists as alumino-silicate sample. The band observed at frequency wavelength of 1076 cm^{-1} is associated with silicate. An interpretation of infrared spectra by John Coates (2006) stated that organic silicone (functional group of –Si-O-Si-) is located within the frequency ranges 1095 – 1075 cm^{-1}. Both desilicated and undesilicated-H-ZSM-5 provide similar spectra however the existence of functional group (-Si-O-Si-) at 1076 cm^{-1} decreased in size which could be the result of silicon removal. H-ZSM-5 zeolite contains hydroxyl (OH^-) group at wavelength range of 3570-3200 cm^{-1}. This hydroxyl group is observed before calcination in Figure 3-8 at band 3409 and 3506 cm^{-1} for Co/undesilicated-H-ZSM-5 and Co/desilicated-H-ZSM-5 respectively. According to literature (Coates, 2006), the hydroxide anion alters the structure of zeolite from Si-O-Si to silanol group Si-OH-Al. The IR band located at 3506 cm^{-1} signifies a strong BrØnsted acid or acidic hydroxyls Si-OH-Al sites which is closely similar to 3610 cm^{-1} obtained by Holm et al. (2009). The IR band located at 3506 cm^{-1} signifies a strong BrØnsted acid or acidic hydroxyl Si-OH-Al sites which is closely similar to 3610 cm^{-1} obtained by Holm et al. (2009). Upon desilication in diluted 0.2M NaOH, the band of Si-OH-Al group decreased and narrowed as represented in Figure 3-8. Sadowska et al. (2013) reported a complete disappearance of Si-OH-Al band in 1M NaOH. NaOH solution is believed to have reduced the acidity of zeolite regardless of the ion exchanged with NH_4^+.

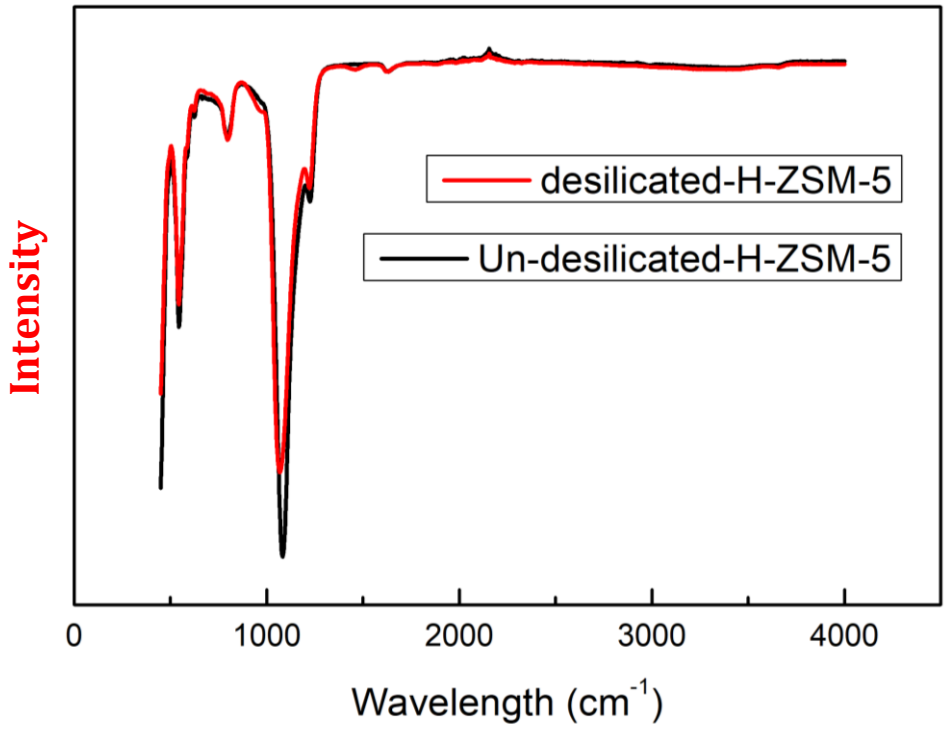


Figure 3-7: FT-IR spectra desilicated and undesilicated-H-ZSM-5 zeolite catalysts.

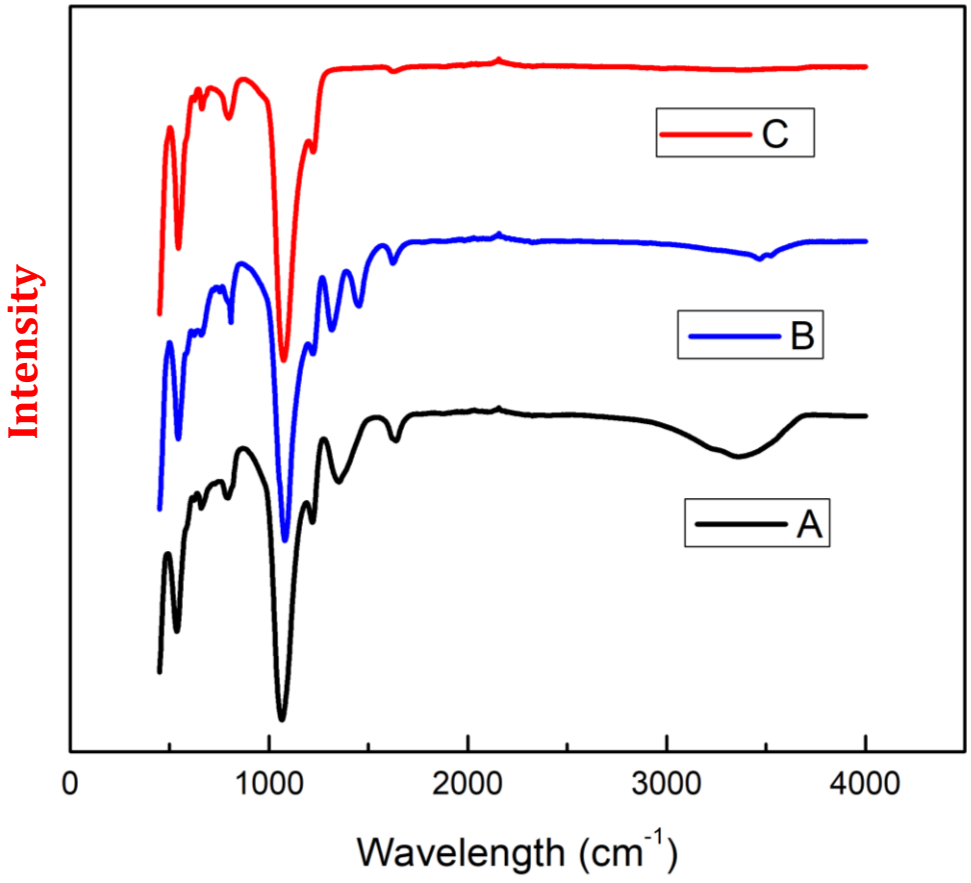


Figure 3-8: The FT-IR spectra [A]: Co/undesilicated H-ZSM-5 before calcination, [B]: Co/desilicated-H-ZSM-5 before calcination, [C]: Co/desilicated-H-ZSM-5 catalyst

3.4.5 EDS Results

The Energy Dispersive Electroscopy (EDS) in Figure 3-9 shows the elemental compositions presence in zeolite support and bifunctional catalyst. Looking at Figure 3-9A, initially before desilication of zeolite, calcined ZSM-5 zeolite detected 48.14% O, 1.08% Al and 50.78% Si of elemental weight percentages. Since zeolite is mainly defined as alumno-silicate materials, it is essential to specify its silicon to aluminium molar ratio. From Figure 3-9A, the ratio of Si/Al was found to be 48% (as presented in Table 3-1) which is almost the same as that of ammonium form of zeolite (~40%). Same spectrum was detected for desilicated-H-ZSM-5 depicted by Figure 3-9B, but with an additional element of sodium (Na) appeared. The detected Na element comes from the NaOH aqueous solution used for desilication process, meaning not all Na^+ ions were removed during filtration and washing stage. However, other explanation is that zeolite itself also contain small composition of sodium. The Si signal intensity of the desilicated-H-ZSM-5 (Fig 3-8B) reduced as a result of silicon extraction during desilication process. Very interestingly, the Si/A*l* molar ratio dramatically decreased from 48 to 26 confirming the success of silicon extraction.

The EDS results in Figure 3-9C and Figure 3-9D detected element of cobalt which was impregnated into zeolite support. During incipient wetness impregnation method, zeolite support was loaded unto 10% weight of cobalt (analogous to that Sartipi et al., 2013) but only 7. 98 wt.% of Co was detected in the final Co/H-ZSM-5. It is very arguable that the possible reason of 7.98% Co instead of 10%, could be that EDS only analysed one area of the sample. Perhaps, the Co weight percentage of the whole sample could average to 10 %. (Matamela & Daramola, 2014) reported a 25% weight of Co after following the same IWI method. Sartipi et al. (2014) obtained a weight percentage of 9.3 % Co in the Co/SiO_2 catalyst. A sudden increase of Cobalt wt.% from 7.98 % to 22.75% was observed in Figure 3-9D, simply because cobalt was deposited in a mesoporous surface of H-ZSM-5 with more active sites.

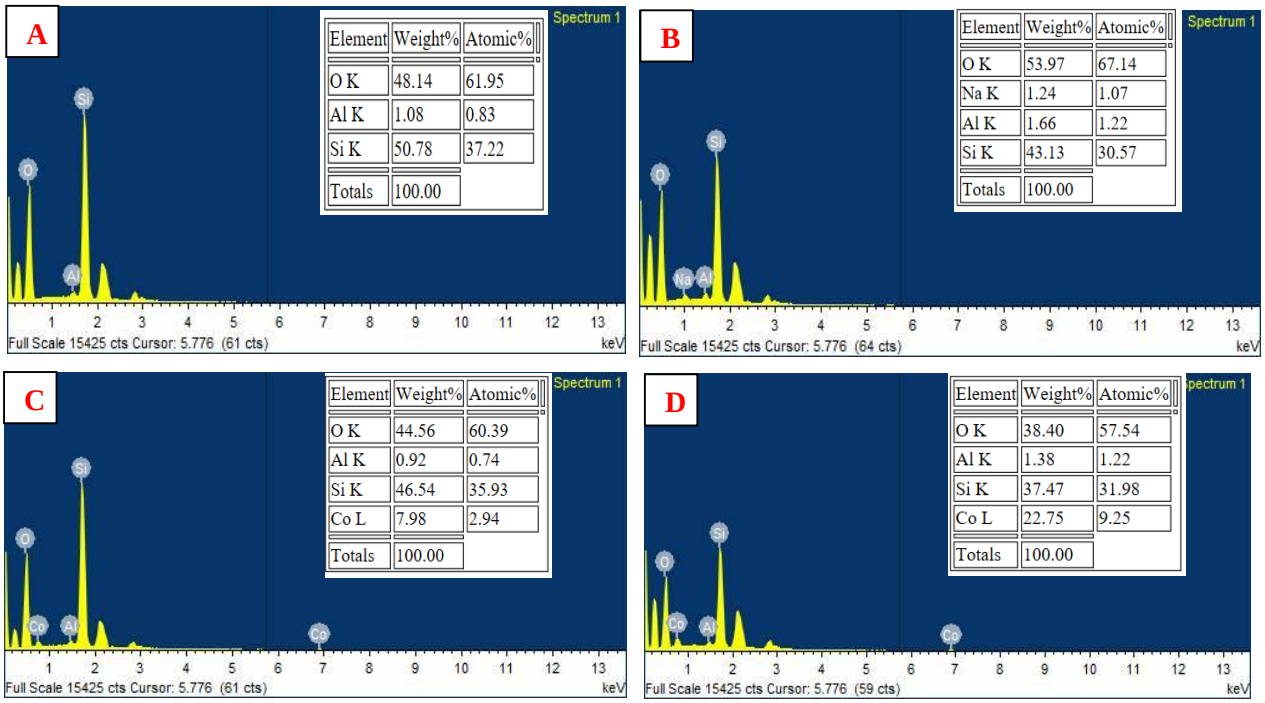


Figure 3-9: The Energy Dispersive Electroscopy (EDS) analysis results of [A] calcined-ZSM-5, [B] desilicated H-ZSM-5, [C] Co/H-ZSM-5 and [D] Co/desilicated-H-ZSM-5 catalysts

3.4.6 Transmission Electron Microscopy (TEM) Results

The morphology and structure of H-ZSM-5 support is clearly visible (Figure 4.10) and embedded with cobalt particles. According to Figure 3-10A, most cobalt particles clustered at the centre of H-ZSM-5 with very few dispersed outwardly. The poor dispersion of cobalt particles from Figure 3-10A is a result of micro-porosity of H-ZSM-5. In Figure 3-10B, the cobalt particles are dispersed outwardly and on the out surface of the H-ZSM-5 due to the presence of increased pore sizes of the support.

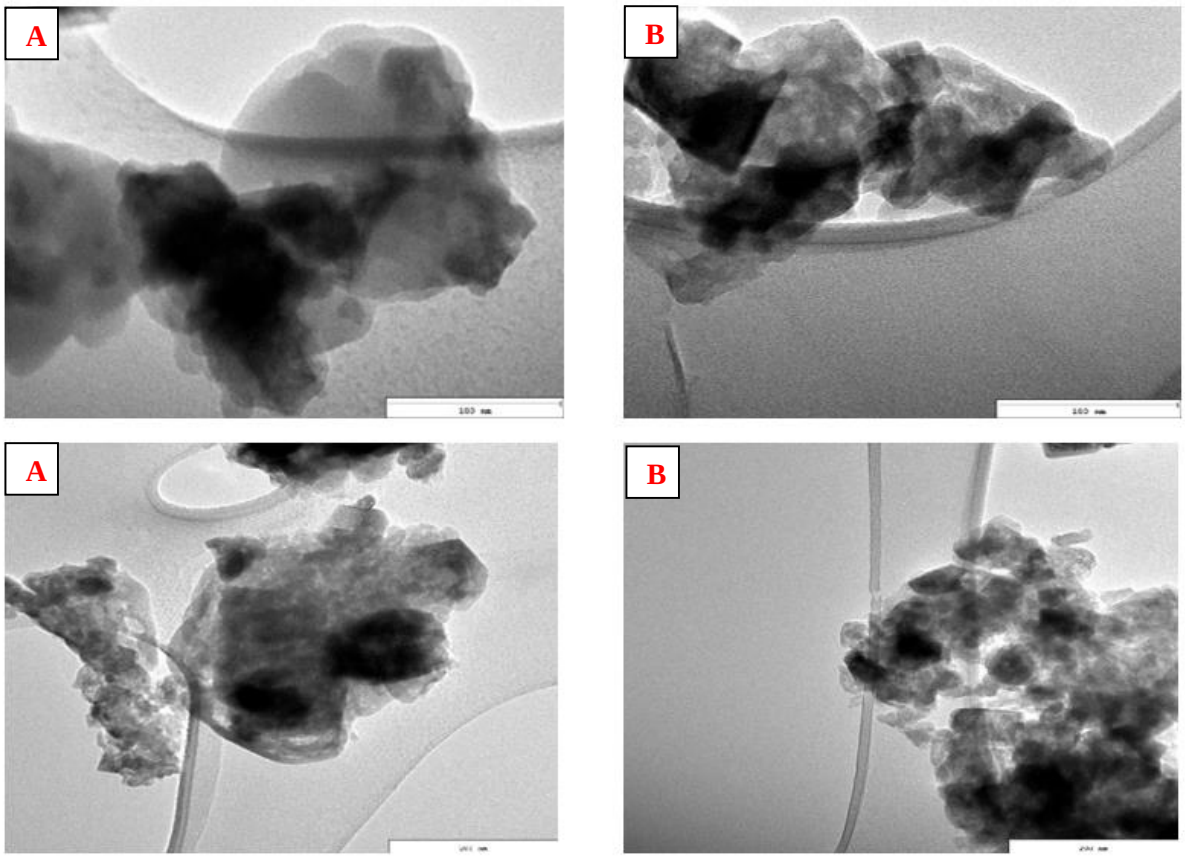


Figure 3-10: TEM images of Cobalt-zeolite and Cobalt mesoporous-zeolite catalysts, magnification (X100 nm and X200 nm)

3.4.7 Temperature Programmed Reduction (TPR) Results

Temperature Programmed Reduction (TPR) profile in Figure 3-11 presents the reduction of unpromoted Co/H-ZSM-5 catalyst in a flow of H_2. TPR was carried out using 5%H_2/Ar from 20 to 900 °C. TPR displayed several peaks with the first two major reduction peaks attributed to the reduction of tetra-Oxide form of Cobalt (Co_3O_4) to Cobalt-Oxide (CoO) to Cobalt metal (Co). Khodakov et al. (2007) reported that performances of promoted cobalt catalysts supported on mesoporous alumina for Fischer-Tropsch synthesis that low temperature peaks within 200 °C – 400 °C are commonly attributed to partial reduction of Co_3O_4 to CoO, medium temperature peaks which reportedly occur within the range of 400 °C – 600 °C signified the emergence of Cobalt metal from Cobalt-Oxide (CoO to Co) while high temperature peaks (normally above 600 °C) are usually cobalt metal mixed up with the support.

In this study, the first and second reduction peaks appeared within 210 °C – 290 °C centred at about 275 °C and broad range of 300 °C – 465 °C centred at 320 °C, respectively. Therefore,

it can be concluded that the first peak in Figure 3-9 is attributed to reduction of Co_3O_4 to CoO and second peak to reduction of CoO to Co which could have occurred at an early stage before the range 400 °C – 600 °C. The third peak centred at temperature of 615 °C is considered a maximum calcination temperature to establish fully interaction between cobalt (Co) and zeolite (H-ZSM-5). Temperature peak (615 °C) also indicated the excess reduction temperature of alumina inside zeolite since zeolite is known as alumino-silicate sample. In other, the peak occurred at 615 °C clearly indicate it is very difficult to reduce the catalyst due to the strong interaction between Co metal and H-ZSM-5 support. The steps of reduction for fully conversion from tetra-Oxide of Cobalt (Co_3O_4) to metallic Co can be represented in the following reactions (3.3) and (3.4) to estimate consumption of hydrogen (H_2) stoichiometrically.

$$Co_3O_4(s) + H_2(g) \rightarrow 3CoO(s) + H_2O(g) \qquad \text{(Vosoughi et al., 2017)} \qquad [3.3]$$

$$3CoO(s) + 3H_2(g) \rightarrow 3Co(s) + 3H_2O(g) \qquad \text{(Vosoughi et al., 2017)} \qquad [3.4]$$

The estimated amount of H_2 consumption from TPR analysis could be used in comparison with measured H_2 update during in-situ **reduction** catalyst despite different conditions. H_2 consumption from TPR can be calculated using the degree of reduction (DOR). DOR is defined as the ratio of the amount of H_2 consumed during reduction form TPR analysis over the amount of H_2 required stoichiometrically to convert all Co_3O_4 to metallic Co (Vosoughi et al., 2017).

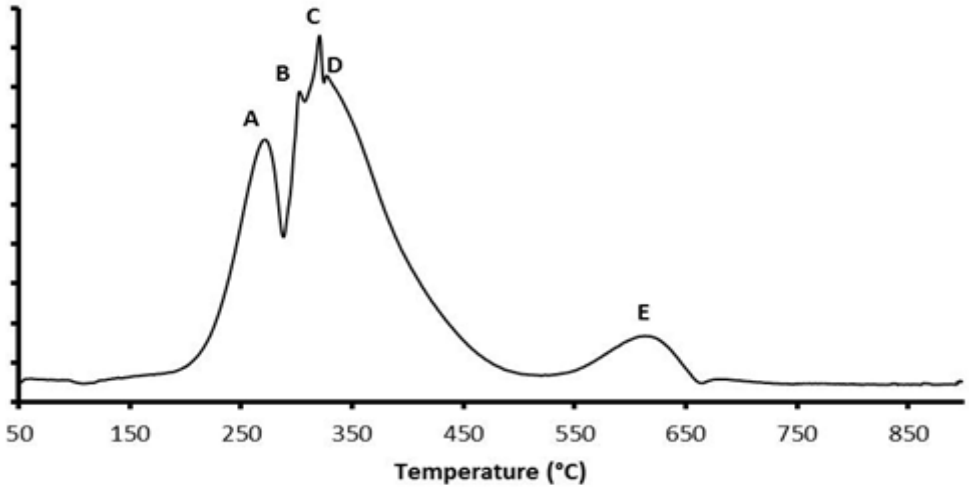


Figure 3-11: TPR profile of bi-functional catalyst (Co/H-ZSM-5).

3.5 Fisher-Tropsch Synthesis (FTS) studies

3.5.1 FTS experimental setup

The catalytic performance was evaluated in a fixed bed reactor operated as PFR, shown schematically in Figure 3-12. All gases were kept, supplied from gas cylinders connected with pressure regulators (V-1) used to manage pressure to the system gas lines. Along the gas lines to the reactor, a two-valve (V-2) was fitted to switch between hydrogen gas for catalyst reduction and synthetic gas for FT reaction. A pressure gauge (P-1) read the pressure of the reactor, with thermocouple on top of the reactor regulating the reactor temperature.

The syngas into the reactor allowed to react for a certain period of time. The reaction products and un-reacted gases entered the two traps from the bottom of the reactor. These traps were designed to collect condensable products, trap-1 (kept heated at 150 °C) was used to collect heavy hydrocarbons (wax) and trap-2 (kept at room temperature) was used to absorb oil and water. All these condensed products were removed after every reaction.

The gaseous products and un-reacted materials passed through the traps were sent through the gas lines/tubes to the online gas chromatography (GC-TCD and GC-FID). Between the traps and GCs, pressure gauge was fitted to along the gas lines to measure the pressure of the GCs and these gas lines were heated to up 100 °C to avoid condensation of the products. The GC was used to analyse reaction products and un-reacted gases, while inorganics and un-reacted materials (H_2, N_2, CO, CO_2) were analysed by Thermal Conductivity Detector (TCD-GC) using argon as a courier gas whilst gaseous hydrocarbons $C_1 - C_{6+}$ were analysed by Flame Ionization Detector (FID-GC) using nitrogen as a courier gas. The FID-GC connected with soap bubble meter to measure volumetric flow rates. The valves and detectors of GC were heated to 100 °C and 220°C respectively. The GCs were programmed to analyse at 200°C oven temperature for an hour and another one to cool down to room temperature. The PC transmission box receives signals from the GC to the computer for analysis using DataApex chromatograph software called Clarity ® (v.2.5). This software helps by integrating the produced products and un-reacted materials showing them as peaks of measured areas. The area of these peaks was the used to calculate the reactants conversion and products selectivity. Examples of the peaks can be seen in appendix B.

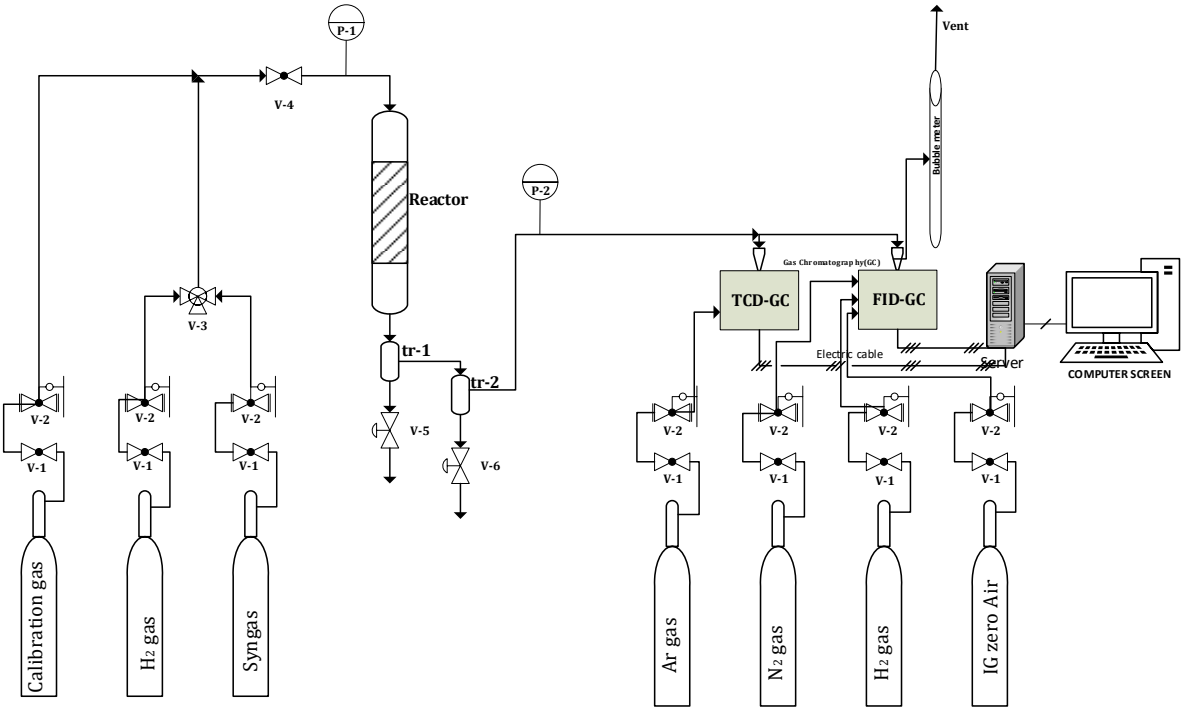


Figure 3-12: Fischer-Tropsch experimental setup

3.5.2 Reactor Design

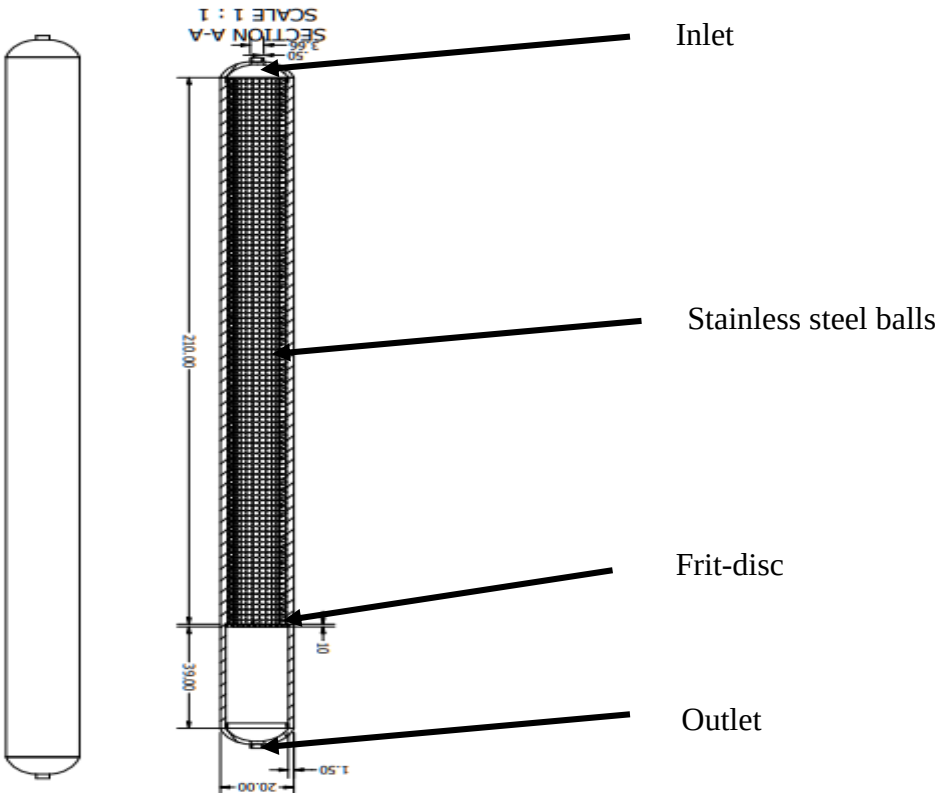


Figure 3-13: A schematic of reactor design

Figure 3-12 shows the design of reactor used in this study. The reactor is made by stainless steel and Swagelok fittings with the following dimensions: length (*l*) of 250 mm, inner diameter (ID) of 16 mm and outer diameter (OD) of 20 mm, with a thermocouple placed from the top to the inside of the reactor to regulate the temperature. This reactor was filled with stainless steel (SS) balls (about 2 mm) which function for pre-heating the gas feed before it gets in contact with the catalyst, keeping and maintaining constant heat temperature of the reactor and evenly distributes the flow of the gas inside the reactor. These SS balls are packed on top of a frit-disc (about 90 mm from the bottom). A frit-disc supports the catalyst. The catalyst is loaded inside the reactor between quartz wool on top of a frit-disc. Quartz wool holds the catalyst since frit-disc made with holes.

3.5.3 Catalyst Loading and reduction

In all experiments conducted, 0.5g of catalyst was loaded inside the reactor and allowed a reaction for about 48 h. Once catalyst is loaded, catalyst was activated at 8 bar pressure for about 17 – 20 h using hydrogen gas flow 30cm^3 STP/min at a reactor temperature of 330°C. The reactor was then allowed to cool down to room temperature at 2°C/min before switching to syngas for FT reaction. This catalyst reduction method was adapted from (Sartipi et al. (2013), Matamela. (2014) and Daramola et al. (2017))

The reaction conditions were temperature of 250°C, syngas ratio (H_2/CO) of 2.5, pressure of 15 bar and flow rate of 1200 gas hourly space velocity (GHSV).

3.5.4 Gas Chromatography & Product analysis

During FTS, the gaseous products from the reactor (Figure 3-12) were analysed by the two online gas chromatography, thermal conductivity detector (TCD) and flame ionization detector (FID). The calibration of GC was done before running the experiment. Syngas with compositions: H_2 (50%), CO (20%), N_2 (30%) and calibration gas with compositions: H_2, N_2, CO, CH_4, C_2H_4, C_2H_6, CO_2. The syngas components were allowed to pass through TCD while calibration gas through FID. The produced traces from both TCD and FID were recorded and used for CO conversion and product selectivity. The traces were recorded in terms of peak areas, where peak area of a component was equivalent to number of moles of that component. The calibration results from both TCD and FID were tabulated in Appendix B, Table B.1.1 AND Table B.2.1 respectively. Figure 3-13 displayed an example of the peaks from TCD syngas calibration.

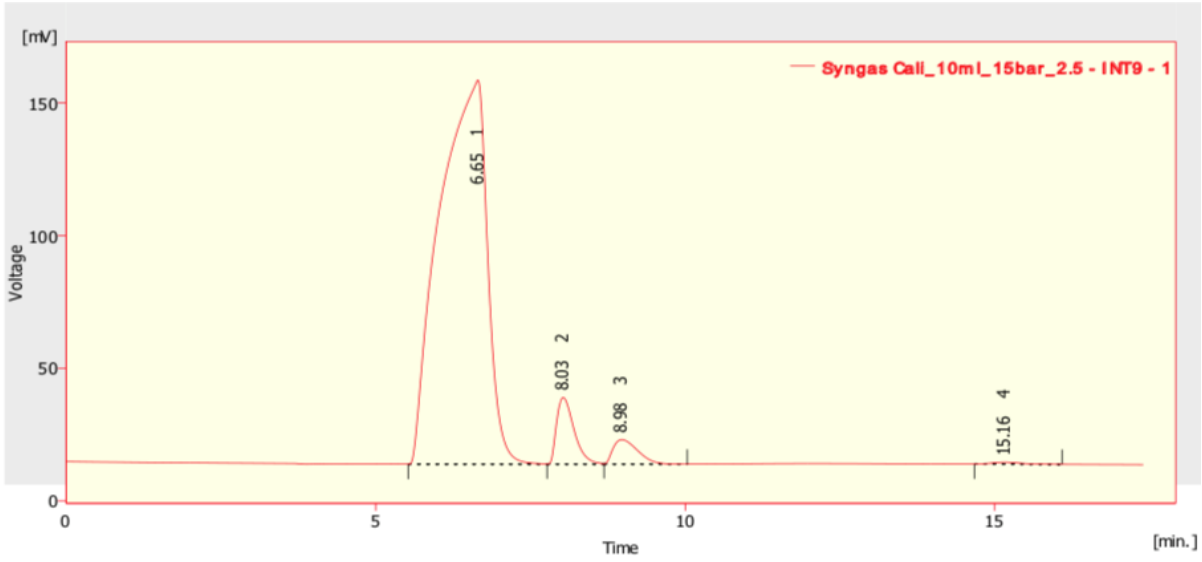


Figure 3-13: Syngas calibration peaks from TCD

The identification of the names of the peaks:

The GC analyses the substances of the gases from lowest atomic weight substance to the highest atomic weight substance. Clarity Data apex software displayed the peaks according to their weight.

- For instance, in Figure 3-13 the arrangements of the peaks are as follows: H_2 peak, N_2 peak, CO peak and Ar peak. Argon which acts as a carrier gas was also detected by the GC-TCD.
- The order of peaks for calibration gas from the FID were as follows: H_2 peak, N_2 peak, CO peak, CH_4 peak, C_2H_4 peak, C_2H_6 peak and CO_2 peak. Results tabulated in Appendix B, Table C.2.5.

Table 3-3: Characteristics and operating conditions of GC

On-line GC	
Detector	Flame Ionized Detector (FID)
Model	Packard-Bell, GC model 433
Column Specification	Packed, stainless steel, 2 m x 1/8 inches
Carrier gas	Nitrogen gas
Detector Temperature (°C)	220
Oven initial temperature (°C)	Room temperature
Oven final temperature (°C)	200
Hold time (mins)	60
Injector Temperature (°C)	100
Stationary Phase	Parapaq Q, 80 – 100 mesh
Product analysis	Hydrocarbons – $C_1 – C_{6+}$
Detector	Thermal Conductivity Detector (TCD)
Model	HP, Hewlett-Packard 5890
Column Specification	Packed, stainless steel, 11.5mX 1/8 inches
Carrier gas	Argon gas
Detector Temperature (°C)	220
Oven initial temperature (°C)	Room temperature
Oven final temperature (°C)	200
Hold time (mins)	60
Injector Temperature (°C)	100
Stationary Phase	Carboxen – 1000, 60/80 mesh
Product analysis	Inorganics – N_2, H_2, CO, CH_4, CO_2
Offline GC	
Detector	Flame Ionized Detector (FID)
Model	Varian 3700
Column Specification	30m x 0.53 x 5 micrometers
Stationary Phase	Zebron, ZB-1
Product analysis	Oil and Wax

3.5.5 Data analysis & calculations

3.5.5.1 Conversion calculations

The reaction products from syngas were analysed by both TCD and FID detectors. The results of these products were obtained in the form of area under detected peaks displayed in a computer using Clarity Software. Areas of the products were converted into mole compositions of each component using the calibration results from syngas (CO, H_2 & N_2) and calibration gas (H_2, N_2, CO, CH_4, C_2H_4, C_2H_6, CO_2). Area to mole ratio before reaction of each component in a syngas was calculated and used with area of each component after reaction to determine the flow rate of each component in a syngas after reaction. N_2 was considered less reactive or either an inert during reaction, however it was used during CO conversion calculation indicated by equation [3.5]

The percentages of CO conversion and hydrocarbon selectivity calculated similarly to those described by Matamela, (2014), Moyo, (2012) & Xiong et al. (2011).

$$\%\ CO\ Conversion = \frac{\left[X_{CO,in} - X_{CO,out}\left(\frac{X_{N_2,in}}{X_{N_2,out}}\right)\right]}{X_{CO,in}} \times 100 \qquad [3.5]$$

Where $\left(\frac{X_{N_2,in}}{X_{N_2,out}}\right)$ is a gas contraction factor:

$X_{N_2,in}$ = molar fraction of nitrogen in the reactor feed;

$X_{N_2,out}$ = molar fraction of nitrogen in the reactor outlet;

$X_{CO,in}$ = molar fraction of carbon monoxide in the reactor feed;

$X_{CO,out}$ = molar fraction of carbon monoxide in the reactor outlet.

Since nitrogen does not react during the reaction, its amount in the feed stream is equal to that in the outlet stream. The molar fraction of nitrogen in the reactor outlet ($X_{N_2,out}$) can calculated from nitrogen balance equation [3.6] around the reactor:

$$F_{in} \cdot X_{N_2,in} = F_{out} \cdot X_{N_2,out} \quad [3.6]$$

Where:

F_{in} = total molar flow rate (mol/min) of the reactor;

F_{out} = total molar flow rate (mol/min) of the outlet gas stream, calculated from measured volumetric flowrate using standard volume flow of a gas.

The total outlet volumetric flow rate was measured using a bubble meter method and a stopwatch.

3.5.5.2 Selectivity calculations

The calibration results from calibration gas recorded in appendix were used to calculate selectivity of the hydrocarbons. However, the calibration data only contain the hydrocarbons of C_1 and C_2. Therefore, the selectivity of C_{3+} hydrocarbon products was calculated using reference hydrocarbon compounds (from calibration data) and relative molar response factors. The reference hydrocarbons were C_2H_6 for paraffins and C_2H_4 for olefins. The molar response factors for hydrocarbons are given in Table 3-4.

Table 3-4: Molar response for hydrocarbon products (Adapted from Swinnerton. (1967))

Carbon Number	Olefin	Paraffin
1	-	1
2	1	1
3	0.7	0.74
4	0.78	0.55
5	0.47	0.47
6	0.4	0.4
7	0.35	0.35
8	0.32	0.32
9	0.28	0.28
10	0.24	0.24
11	0.21	0.21
12	0.19	0.19
13	0.18	0.18
14	0.17	0.17
15	0.15	0.15

In order to perform product selectivity, the amount of product for each hydrocarbon component in the outlet stream was calculated as follows:

$$N_{HC,i} = X_{c_2,cal} \cdot \quad F_{tot,out} \cdot t_{rxn} \cdot \left(\frac{A_{HC,i}}{A_{C_2,cal}}\right) \qquad [3.7]$$

Where :

$N_{HC,i}$ = the number of moles of product for each component in a gas;

$X_{C_2,cal}$ = the average mole fraction of C_2 hydrocarbons in the calibration gas;

t_{rxn} = total time reaction;

$F_{tot,out}$= total outlet gas flow rate;

$A_{HC,i}$ = integrated peak area of produced hydrocarbon component;

$A_{C_2,cal}$ = integrated peak area C_2 hydrocarbons in the calibration gas.

$$X_{HC,i} = \frac{A_{HC,i} \cdot Rf_{,i}}{A_{C_2,cal}} \cdot X_{C_2,cal} \qquad [3.8]$$

Where :

$X_{HC,i}$ = the mole fraction of product for each component in a gas;

$Rf_{,i}$ = the response factor for carbon number i;

$A_{C_2,cal}$ = integrated peak area C_2 hydrocarbons in the calibration gas;

$X_{C_2,cal}$ = the average mole fraction of C_2 hydrocarbons in the calibration gas;

$A_{HC,i}$ = integrated peak area of produced hydrocarbon component.

$$Selectivity\ (S_{HC,i}) = \left(\frac{N_{HC,i}}{\Delta W}\right)\left(\frac{t_{rxn}}{-r_{co}}\right) \qquad [3.9]$$

$N_{HC,i}$ = the number of moles of product for each component in a gas;

ΔW = weight of a catalyst;

t_{rxn} = total reaction time;

r_{co} = rate of CO conversion

$$\%\, Selectivity = \frac{S_{HC,i}}{\sum S_{HC,i}} \times 100 \qquad [3.10]$$

$S_{HC,i} =$ moles produced of paraffin i;

$\sum S_{HC,i} =$ sum of all moles produced paraffin i;

The intrinsic CO consumption rate was calculated using the following equation [3.11]

$$-r_{CO} = \frac{F_{CO,i}(X_{CO,out} - X_{CO,in})}{\Delta W} \quad \text{(Zohdi-Fasaei et al.,2016)} \qquad [3.11]$$

Where ΔW and $F_{CO,i}$ are catalyst weight (g) and CO molar flow rate (mol/min) (before and after reaction) respectively

The rate of FTS reaction was calculated using the following equation [3.12]

$$r_{FTS} = k_{FT} \frac{P_{CO}\, P_{H_2}}{(1 + k_{CO} P_{CO})^2} \quad \text{(Zohdi-Fasaei et al.,2016)} \qquad [3.12]$$

r_{FTS} is the rate of FT reaction, k_{FT} is the reaction constant at a given temperature, k_{CO} is the rate of CO constant, P_{CO} is the partial pressure of carbon monoxide gas and P_{H_2} is the partial pressure of hydrogen gas.

In order to determine whether product distribution was more selective olefin or paraffin, olefin ratio was calculated. Olefin ratio was calculated using equation [3.13]

$$Olefin\ Ratio = \frac{Olefin}{Olefin + Paraffin} \quad (De\ \ La\ Osa\ et\ al., 2011) \qquad [3.13]$$

3.6 Concluding Remarks

The characterization of ZSM-5 (Si/A*l* = 40) was found to contain micropore characteristics. Mesoporous H-ZSM-5 zeolites were successfully synthesized from H-ZSM-5 (Si/A*l* = 40) by desilication method in 0.2M NaOH aqueous solution at various treatment temperature (40 °C, 55 °C & 70 °C). The meso-porosity of H-ZSM-5 was obtained by a further ion-exchanging with 1M NH_4NO_3 aqueous solution followed by calcination. Upon desilication, a sudden

increase in the size and volume of mesopores was observed as explained by the BJH pore size distribution. Note-worthily, the changes in desilicated-H-ZSM-5 was not just on porosity but also in chemical composition of zeolite. This can be explained by a dropped in Si/A*l* ratio due to selective extraction of silicon.

CHAPTER 4

Performance of bi-functional Co/undesilicated-H-ZSM-5 and Co/desilicated-HZSM-5 catalysts during Fischer-Tropsch Synthesis

4.1 Introduction

This chapter focused on the use of desilication method. Desilication is the selective extraction of silicon from zeolite by treatment in alkaline solutions to prepare hierarchical zeolites as established by Groen et al. (2004); Ogura et al. (2001); Suzuki & Okuhara, (2001).

In previous studies on the ZSM-5 porosity improvement by desilication, Groen et al. (2004) reported the investigation of optimization of ZSM-5 by varying treatment time and temperature but no evidence on the activity and performance of FTS catalyst on desilicated-ZSM-5 supports. There are several studies on ZSM-5 zeolites upon alkaline treatment in NaOH solutions (Ogura et al., 2001; Suzuki & Okuhara., 2001). Ogura et al. (2001) investigated ZSM-5 treated under various time conditions but tested the catalytic activity for cumene cracking. Suzuki & Okuhara. (2001) reported ZSM-5 treated under various temperature with no further investigation on the catalyst activity and performance during FTS. A recent performance and activity of desilicated-ZSM-5 on cobalt catalyst has been reported by Sartipi et al. (2013) although no further investigation on the optimization of ZSM-5.This chapter focused on the effect of desilication method under the optimization of ZSM-5 porosity by varying treatment temperature and investigate the influence on the activity and performance of Co/desilicated-H-ZSM-5 during FT reaction. Temperatures treatment used are 40 °C, 55 °C and 70 °C at constant time treatment.

The FTS results are discussed in terms of carbon monoxide conversion and selectivity of hydrocarbons products and its comparison with that of desilicated H-ZSM-5 supported cobalt catalyst as well as other findings. In this study, the hydrocarbons discussed are mainly two organic compounds known as olefins and paraffins. Olefins are unsaturated hydrocarbons with one double bond between two carbons atoms and paraffins are saturated hydrocarbons with only single bonds between carbon atoms. The percentages of CO conversion and hydrocarbon selectivity were calculated based on Matamela & Daramola. (2014)(Michael Olawale

Daramola et al., 2017); Moyo (2012); Xiong et al. (2011)(calculation method given in chapter 3, section 3.5.5).

4.2 Experimental Operating Conditions

The CO conversions given in both Table 4-2 and Table 5-1 were obtained under the following conditions

Table 4-1: Summary of experimental conditions for FT synthesis

Reactor	**Fixed-bed reactor operated as PFR**
Catalyst	Co (10%)/H-ZSM-5
Catalyst weight (g)	0.5
Syngas composition	H_2 (50%), CO (20%), N_2 (30%)
Flow rate (ml/min or GHSV)	20 or 1200
Temperature (°C)	250
Pressure (bar)	15

4.3 Results and discussion

Under the process conditions mentioned in chapter 3.2, the CO conversion over Co/H-ZSM-5 (un-desilicated) obtained was 49.7 %. Matamela & Daramola. (2014) reported CO conversion of 53.77 % under similar conditions and Sartipi et al. (2013) reported CO conversion of 62% under different process conditions of temperature (240 °C) and H_2/CO = 2 (see Table 4-3). The slight difference in CO conversion of Matamela & Daramola. (2014) and conversion of this study could be the amount of reaction time. In this study, CO conversion was recorded every 2 hours for 48 hours after attaining stability for 25 hours (as represented in Figure 4-1) which average to 49.7% while Matamela & Daramola. (2014) recorded CO conversion every 2 hours for about 4 days which then average to 53.77%. The CO conversion variations between Sartipi et al. (2014) and this study varied due to process conditions. Figure 4-1 shows CO conversion under un-desilicated H-ZSM-5 supported cobalt fluctuates more compared to desilicated H-ZSM-5 supported catalysts which stabilize the conversion. For Co/H-ZSM-5 (un-desilicated) catalyst, the CO conversion became steady after 58 hours. Co/H-ZSM-5 (55) catalyst was found to have the highest stability throughout the process. Calleja et al. (1995) reported that a high H_2/CO ratio results in high conversion as proved by comparing Sartipi et al. (2013)

conversion of 32% and 49.7% conversion of this study under the use of $H_2/CO = 2$ and $H_2/CO = 2.5$ respectively.

Table 4-2: CO conversions over Co-based catalyst on desilicated H-ZSM-5 supports during FT synthesis

Catalyst	Average Conversion (%)
Co/H-ZSM-5	49.7
Co/H-ZSM-5 (desilicated at 40°C)	76.9
Co/H-ZSM-5 (desilicated at 55°C)	84.2
Co/H-ZSM-5 (desilicated at 70°C)	79.8

Upon the introduction of mesoporous H-ZSM-5 supported Co-catalyst, the CO conversion dramatically increase to above 75%. The rise in CO conversion is the result of an increase in Cobalt dispersion or Co loading due to an increase of surface area from H-ZSM-5 (un-desilicated) to H-ZSM-5 (desilicated). The CO conversion increases from 49.7% to 76.9%, 84.2% and 79.9% over Co/H-ZSM-5 (desilicated) catalysts prepared with NaOH solutions of treatment temperatures; 40 °C, 55 °C and 70 °C, respectively. Sartipi et al. (2014) reported 75% CO conversion on Co/meso-H-ZSM-5 catalyst prepared with NaOH at 70 °C treatment temperature under process conditions; temperature 240 °C and $H_2/CO = 2$ (see Table 4-3). According to Calleja et al. (1995), increasing H_2/CO ratio increases CO conversion. The CO conversion over Co/H-ZSM-5 (un-desilicated) is low since it is prevented by diffusion limitations of reactants caused by micropore sizes of H-ZSM-5 and poor metal dispersion over H-ZSM-5 support. The highest CO conversion obtained for this research over Cobalt supported by H-ZSM-5 (desilicated at 55 °C) is 84.2%. The H-ZSM-5 treatment temperature in 0.2M NaOH of 55 °C can be regarded as optimal among 40 °C and 70 °C. Groen et al. (2004) reported an optimal temperature of 338K (65 °C) for treatment of ZSM-5 in 0.2 NaOH aqueous solution for 30 minutes.

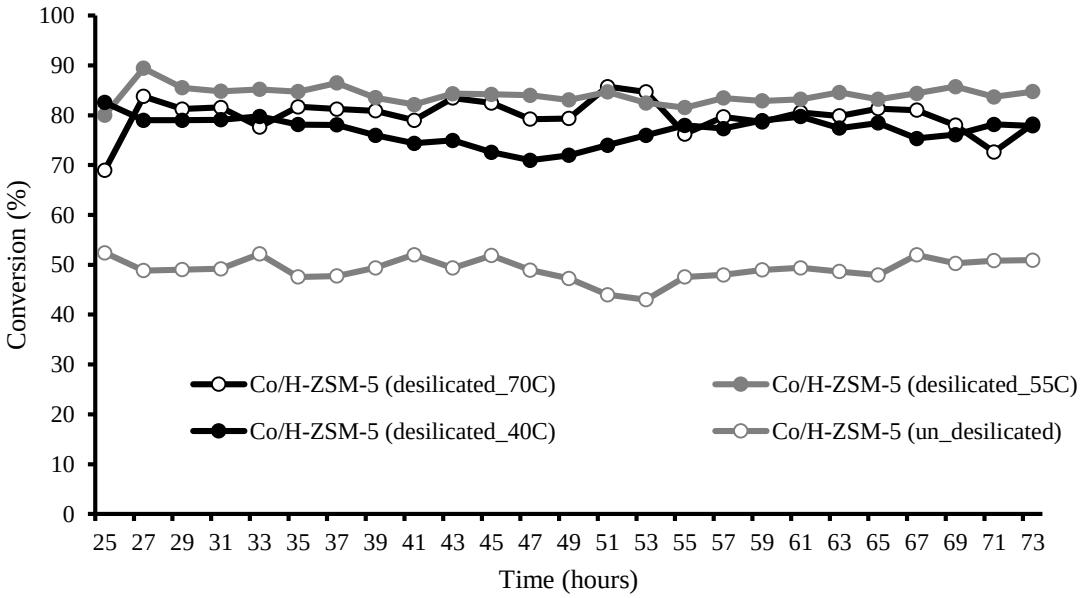
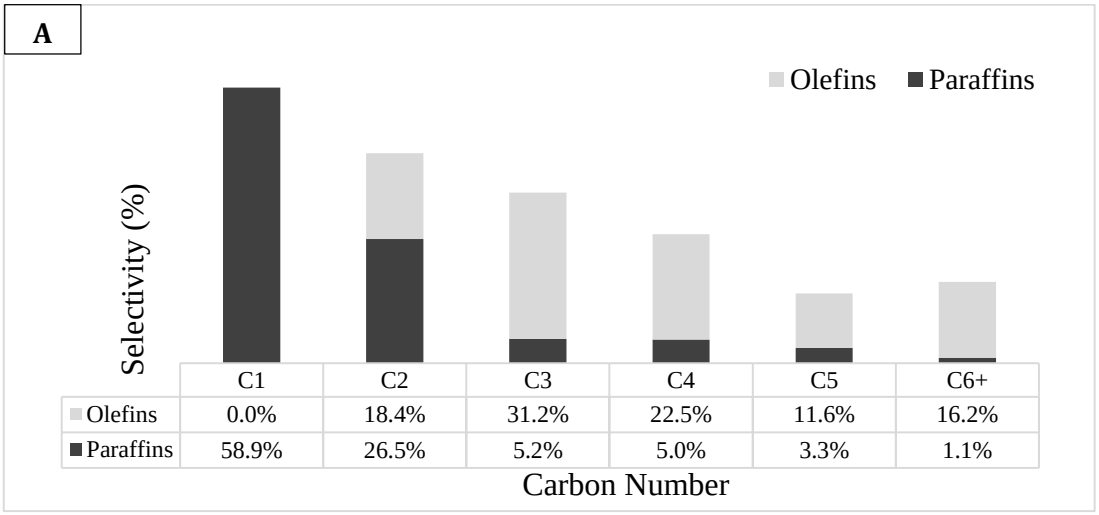


Figure 4-1: A change of CO conversion with time every two hours for 48 hours (2 days) over Co/H-ZSM-5 catalysts on FT synthesis

The development of bi-functional Co/H-ZSM-5 catalyst in this study is expected to break or challenge the Anderson-Schulz-Flory (ASF) product distribution which states that in most conventional FT catalysts, the products follow the ASF distribution yielding maximum selectivity of gasoline (C_5 – C_{11}) and diesel (C_{12} – C_{20}) hydrocarbons 45% and 30 % respectively. Literature reveals that zeolite, which is acidic, acts as a determining factor for product distribution since its function is hydrocracking and isomerization once hydrocarbons are formed by FT catalyst. This study tested whether the meso-porosity of H-ZSM-5 zeolite supported on Co catalyst increase the higher hydrocarbons (C_5 – C_{6+}).

Figure 4-2A shows the performance of bi-functional catalyst (Co/H-ZSM-5) during FTS. Under the process conditions given in Table 4-1, the comparison in performance of cobalt metal supported loaded on H-ZSM-5 (un-desilicated) and H-ZSM-5 (desilicated) zeolites were studied. The hydrocarbon distribution was given in terms of both olefins and paraffins selectivity. The bi-functional catalyst (Co/H-ZSM-5) whether on desilicated zeolite or not, was more selective to olefins over paraffins which agreed with Linghu et al. (2006). The highest selectivity to methane (C_1) was 58.9% with only 8.8 % C_{5+} selectivity over Co/H-ZSM-5 (un-desilicated) where methane selectivity is closely analogous to 53% reported by Matamela. (2014) under the same process conditions (given in Table 4-1). Sartipi et al. (2014) reported the methane (C_1) and C_{5+} selectivity of 21 % and 50% respectively (see Table 4-3). Methane selectivity of this study almost three higher than that of Sartipi et al (2014); due to a higher H_2

diffusion rate in the zeolite surface than CO diffusion. This was evidenced by Vervloet et al. (2012) that higher H_2/CO ratio yield higher methane production. Co/H-ZSM-5 catalyst (see Fig. 4-1A) proved to be favourable towards lower hydrocarbons ($C_2 – C_4$). Selectivity to paraffin C_2 was 26.5% and to olefin C_3 was 31.2%. Thereafter, selectivity decreased from C_3 to C_4 due to over cracking of HCs in zeolite which further resulted to a poor selectivity to desired products ($C_5 – C_{6+}$) with C_5 and C_{6+} paraffin of 3.3% and 1.1% respectively together with C_5 and C_{6+} olefins of 11.6 % and 16.2%. Matamela. (2014) obtained C_5 paraffin and C_5 olefins of 4% and 8% respectively. However, the overall (both paraffins & olefins) $C_5 – C_{6+}$ selectivity on this study was calculated to be 16,1 % which is closely equal to 15% reported by Matamela and Daramola. (2014). In summary, presence of micropores of zeolite acidic sites causes over-cracking of primary hydrocarbons because of slow transportation of products inside zeolite (Kang et al., 2011). Apart from the ~50% CO conversion of syngas to liquid fuels, the gasoline-range or higher HCs were poorly produced. However, the introduction of meso-porosity unto H-ZSM-5 zeolite enhanced the selectivity of these higher hydrocarbons, see Figure 4-2B, Figure 4-2C and Figure 4-2D.

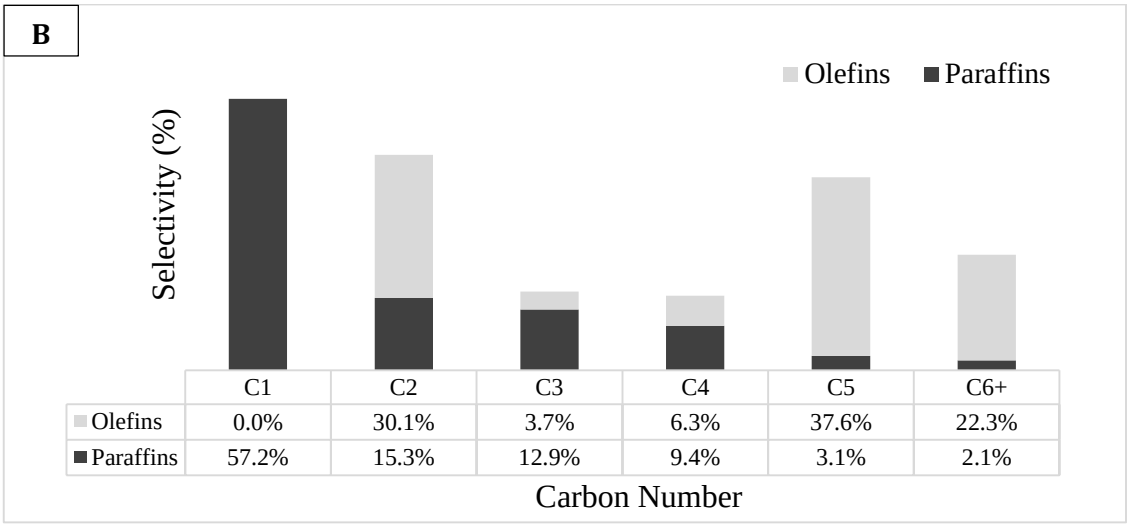


	C1	C2	C3	C4	C5	C6+
Olefins	0.0%	18.4%	31.2%	22.5%	11.6%	16.2%
Paraffins	58.9%	26.5%	5.2%	5.0%	3.3%	1.1%

Figure 4-2A: Product distribution of both paraffins and olefins over a Co/H-ZSM-5 (un-desilicated)

The product selectivity depended on the temperature treatment of NaOH used for mesoporous ZSM-5 preparation. For the meso-H-ZMS-5 prepared using 40°C treatment temperature which is denoted as Co/H-ZSM-5(40), the methane (C_1) and $C_2 – C_4$ selectivity decreased to 57.2% and 37.9% respectively, while $C_5 – C_{6+}$ selectivity increased from 8.8 % to 12.3%. In more detail (see Figure 4-2A and Figure 4-2B), the selectivity to C_2 paraffin decreased from 26.5% to 15.3% and the selectivity to C_3 and C_4 olefin decreased from 31.2% to 3.7% and 22.5% to

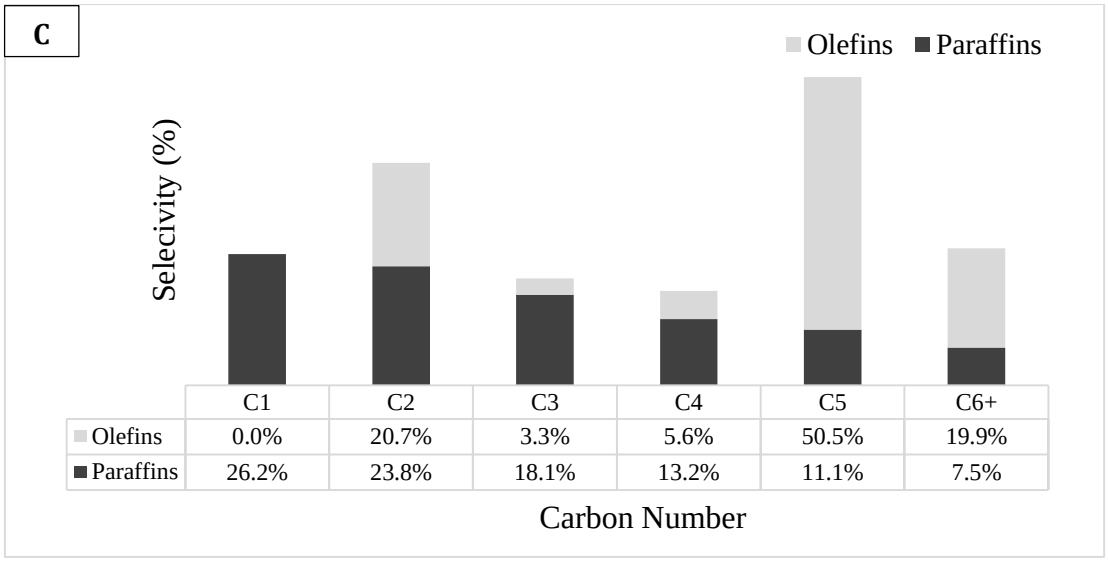
6.3% respectively. The performance of Co/H-ZSM-5(40) catalyst significantly increased the selectivity to C_5 and C_{6+} olefin hydrocarbons from 11.6% to 37.6% and 16.2% to 22.3% respectively. Through results observation, the desilicated-H-ZSM-5 prepared using 0.2M NaOH aqueous solution at 40°C had no major influence on paraffin higher hydrocarbons.



	C1	C2	C3	C4	C5	C6+
Olefins	0.0%	30.1%	3.7%	6.3%	37.6%	22.3%
Paraffins	57.2%	15.3%	12.9%	9.4%	3.1%	2.1%

Figure 4-2B: Product distribution of both paraffins and olefins over a Co/H-ZSM-5 (desilicated at 40°C)

Further increases in NaOH temperature treatment to 55°C for mesoporous ZSM-5 preparation increased the $C_5 - C_{6+}$ selectivity to 47. 9% and dramatically decreased C_1 selectivity to 26.2 %. Figure 5-2C depicts the product distribution results of desilicated-H-ZSM-5 prepared under 55°C of 0.2M NaOH aqueous solution supported on cobalt metal which can denoted as Co/H-ZSM-5(55). Comparing Figure 4-2B and Figure 4-2C, the selectivity to C_3 & C_4 paraffin and olefins remains unchanged. Interestingly, about 50% significant drop towards C_1 and C_2 selectivity. For instance, selectivity to C_2 hydrocarbons decreased from paraffin (15.3%) and olefin (30.1%) to 11.2% and 6.7% respectively. It is important to mention the increase in C_5 hydrocarbons (from 37.6% to 56.5% C_5 olefin). It can be concluded that the performance of desilicated-Co/H-ZSM-5(55) catalyst (Figure 4-2C) was highly mesoporous and had bigger pore sizes which allowed an easier and faster access of higher hydrocarbons compared to the performance of Co/H-ZSM-5(40) catalyst (Figure 4-2B). Groen et al. (2004) reported increase of BET surface area to 550 m^2/g of ZSM-5 prepared at about 65°C in 0.2M NaOH aqueous solution, however the performance this support on cobalt metal during FTS was not studied.



	C1	C2	C3	C4	C5	C6+
Olefins	0.0%	20.7%	3.3%	5.6%	50.5%	19.9%
Paraffins	26.2%	23.8%	18.1%	13.2%	11.1%	7.5%

Figure 4-2C: Product distribution of both paraffins and olefins over a Co/H-ZSM-5 (desilicated at 55 °C)

Unexpectedly, the performance of desilicated-Co/H-ZSM-5(70) catalyst on FTS brought about no better results (Figure 4-2D) compared to Figure 4-2C. This can be justified by more undesirable methane (40.5 %) and $C_2 - C_4$ selectivity (49.5 %) with a drop in $C_5 - C_{6+}$ selectivity (29.0 %). However, the use of Co/H-ZSM-5(70) catalyst maintained high selectivity to some HCs. For instance, selectivity to C_5 olefins slightly increased to 39.5 %. The production of higher ($C_5 - C_{6+}$) selectivity can be results of weak acidity of catalysts. In other words, desilication increased the catalytic activity resulting from treatment with NaOH caused a loss in the acidity of zeolite thus improved the selectivity of HCs. A clear observation between Figure 4-2B and Figure 4-2D was that although desilicated Co/H-ZSM-5(70) catalyst outperformed desilicated Co/H-ZSM-5(40) in terms of gasoline-range ($C_5 - C_{6+}$) hydrocarbons, it cannot be recommended due to its hydrocracking characteristics. In terms of overall performance, the best results were achieved over desilicated-Co/H-ZSM-5(40).

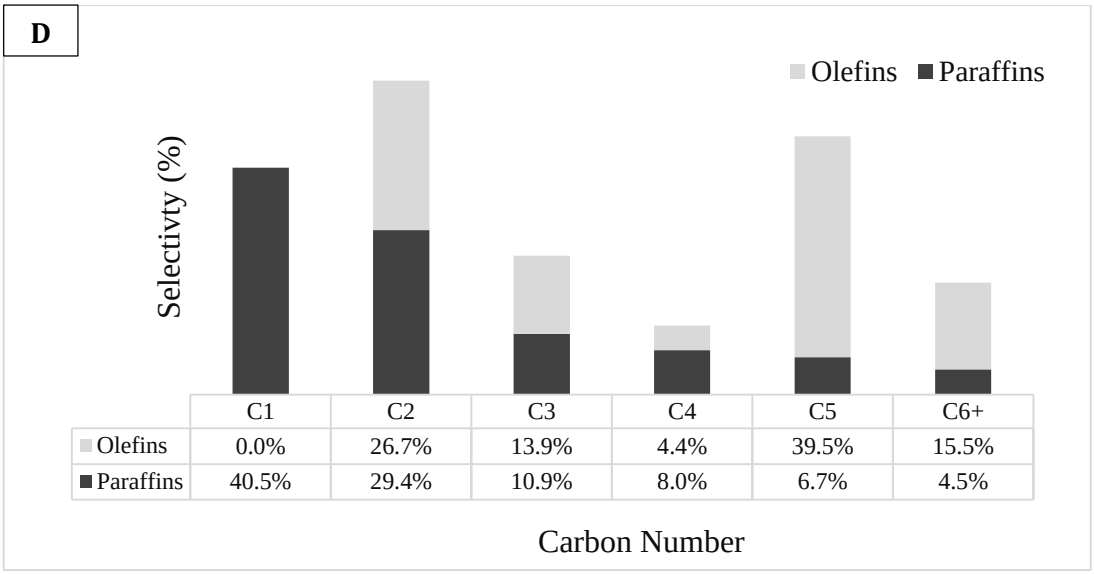


Figure 4-2D: Product distribution of both paraffins and olefins over a Co/H-ZSM-5 (desilicated at 70 °C).

Table 4-3: Comparison of CO conversion and average products selectivity between (Sartipi et al., 2014), (Matamela, 2014)) and this study

Process conditions	**Catalyst**	**%X_{CO}**	**C_1**	**$C_2 - C_4$**	**C_{5+}**
1200 ml/gcat.hr,15 bar, 250 °C, H_2/CO = 2.5 (from this study)	Co/H-ZSM-5	49.7	47.8	43.4	8.8
	Co/H-ZSM-5(40)	76.9	49.8	39.7	12.3
	Co/H-ZSM-5(55)	84.2	21.7	30.4	47.9
	Co/H-ZSM-5(70)	79.8	21.5	49.5	29.0
2400 ml/gcat.hr,15 bar, 240 °C, H_2/CO = 2 (from Sartipi et al. (2014))	Co/H-ZSM-5	62	21	16	50
	Co/meso-H-ZSM-5(70)	75	16	14	55
1200 ml/gcat.hr,15 bar, 250 °C, H_2/CO =2.5 (from Daramola et al. (2017))	Co/H-ZSM-5	53.7	34.6	50.4%	15%

Table 4-4 shows the performance of the catalyst in terms of their product distributions, whether it was more selective to olefins or paraffins. This was determined by calculating olefin ratio for each hydrocarbon except methane. Olefin ratio was calculated using the equation [3.13]. A decrease in olefin ratio signified the increase in paraffin. If the olefin ratio was found to be less than 0.5, therefore it meant there more paraffin hydrocarbons produced than olefins and vice versa.

C_{6+} olefin ratio slightly decreased from 0.93 over Co/H-ZSM-5 catalyst to 0.91 over Ca-Co/H-ZSM-5(40) catalyst. C_5 olefin ratio decreased from 0.92 over Co/H-ZSM-5(40) to 0.77 over Ca-Co/H-ZSM-5(55) while C_{6+} olefin ratio dropped from 0.91 to 0.48. Note worthily, through observation of these results, as the CO conversion increases the olefin ratio decrease. Ngantsoue-Hoc et al. (2002) and De la Osa et al. (2011) reported that the fraction of alkene (olefin ratio) decreased as CO conversion increased for both unpromoted and calcium promoted catalysts. In all the tested cobalt catalysts, hydrocarbon distributions were found to be more favourable to olefins (olefin ratio > 0.5) than paraffins. This agrees with the literature (Bezemer et al., 2006), cobalt based catalyst is more selective to olefins than paraffins. Meanwhile, C_3 selectivity was only an exception with more paraffin than olefin. The rate of CO consumption depended on the CO conversion and calculated via equation [3.11] and rate of Fischer-Trospch synthesis via equation [3.12].

Table 4-4: Olefin ratio, rate of CO consumption and rate of Fischer-Tropsch reaction.

			Olefin ratio				
Catalyst	**r_{CO} (mol/gcat.min)**	**r_{FTS} (mol/gcat.min)**	**C_2**	**C_3**	**C_4**	**C_5**	**C_{6+}**
Co/H-ZSM-5	2.22×10^{-4}	1.06×10^{-2}	0.41	0.86	0.82	0.78	0.93
Co/H-ZSM-5(40)	3.38×10^{-4}	1.06×10^{-2}	0.66	0.22	0.40	0.92	0.91
Co/H-ZSM-5(55)	3.76×10^{-4}	1.06×10^{-2}	0.63	0.23	0.32	0.77	0.48
Co/H-ZSM-5(70)	3.55×10^{-4}	1.06×10^{-2}	0.34	0.24	0.76	0.68	0.62

4.4 Concluding remark

Chapter 5 discussed the catalytic performance of four synthesized Co-based catalysts; Co/H-ZSM-5, Co/H-ZSM-5(40), Co/H-ZSM-5(55) and Co/H-ZSM-5(70). It detailed the effect of desilication of H-ZSM-5 at different temperatures on the Co-based catalyst during FTS. The discussion of the FT results was based on the CO conversion and hydrocarbon selectivity. In addition, the obtained results were in the form of alkanes and alkenes but discussed as paraffins and olefins. The correlation between olefins and paraffins were calculated as olefin ratio. The rate of CO consumptions during FT reaction was also calculated and discussed. The conclusion of catalytic performance of the four named catalysts in terms of their CO conversions and product selectivity were outlined in chapter 7.

CHAPTER 5

Effect of the promoted catalysts during Fischer-Tropsch Synthesis

5.1 Introduction

The previous chapter, chapter 4, focused on the performance and comparison between Co based catalysts supported on un-desilicated and desilicated zeolite (H-ZSM-5). It was concluded that the mesoporous H-ZSM-5 improved cobalt catalyst activity as well as increased selectivity towards C_{5+} hydrocarbons. Nonetheless, the best performing catalyst, Co/H-ZSM-5(55), produced a slight high number of light hydrocarbons ($C_2 – C_4$) and methane products.

This chapter focused on the promotion of both Co/H-ZSM-5 and Co/H-ZSM-5(55) catalysts by calcium, to reduce the formation of light hydrocarbons whilst enhancing the C_{5+} hydrocarbons. De La Osa et al. (2011), Schulz & Claeys. (1999) and Van Der Laan & Beenackers. (1999) had reported that calcium promoted on cobalt based catalyst has a tendency of introducing a secondary reaction for the re-adsorption of reactive light hydrocarbons (ethene and propene) into a growing C_{5+} hydrocarbons. This is because it has been widely demonstrated that the addition of metal promoters to FTS catalysts improve the FTS performances (including activity, stability and selectivity) (Tao et al., 2006), as well as increasing cobalt dispersion and its reducibility (Bao et al., 2009). For Co/H-ZSM-5, transition metals such ruthenium and nickel have been recently used as promoters to increase the reducibility and activity of the catalyst. Wang et al. (2013) studied the influence of Ru and Ni promoters over Co/H-ZSM-5 catalysts on gasoline-range production. Studies by these authors showed that Ru-Co/H-ZSM-5 catalyst had the highest activity, stability and reduction degree whereas Ni-Co/H-ZSM-5 catalyst with maximum CO conversion and GRH ($C_5 – C_{11}$) selectivity. However, the cost of these transition metals is quite high.

The addition of calcium promoter over cobalt-based catalyst has been studied by Bao et al. (2009) and De La Osa et al. (2011). In both studies, calcium was promoted to Co/Al_2O_3 catalyst. Bao et al., (2009) studied the effect of calcium oxide on the Fischer-Tropsch synthesis activity and selectivity. These authors reported that reducibility, activity, cobalt particle size and C_{5+} selectivity increased with increasing calcium oxide content. De La Osa et al. (2011) results agreed with those previously reported by Bao et al. (2009) in terms of added alkali-earth metal promoter increasing C_{5+} hydrocarbons. However, De La Osa (2011) and his co-workers noted the hindrance of $–CH_2–$ monomer into growing chain influenced by increasing reaction temperature. There is no report in research studies for calcium promotion to Co/H-ZSM-5

catalyst. Sartipi et al. (2014) reported the influence of desilication (mesoporosity) on Co/H-ZSM-5 catalyst and Matamela. (2014) studied the effects of FTS process conditions on Co/H-ZSM-5. This study aims to evaluate and report the effects of calcium-promoted mesoporous Co/H-ZSM-5 catalyst on the catalytic performance (FTS activity and product selectivity). The Ca-Co/desilicated-H-ZSM-5 catalyst was prepared (section 3.2.2), characterized by XRD, EDS and evaluated on FTS for CO conversion and product selectivity. The results were compared with calcium-promoted Co/H-ZSM-5, unpromoted Co/H-ZSM-5 and various research studies.

5.2 Results and Discussion

5.2.1 Characterization of promoted catalyst

Following the XRD patterns in Figure 3-6, a further XRD analysis was conducted to study the effect of calcium promotion on the crystalline structure of the Co/H-ZSM-5 catalyst. The XRD patterns of Co/H-ZSM-5, Ca-Co/undesilicated-H-ZSM-5 and Ca-Co/desilicated-H-ZSM-5 catalysts are displayed in Figure 5-1. The highest peaks at 2θ values of 7.5° and 23.8° represent the characteristic of the ZSM-5 zeolite (Xing et al., 2016b). The three catalysts in Figure 5-1 have the identical XRD patterns but with different intensity sizes of diffraction peaks. The detected diffraction peaks at 2θ = 31.3°, 36.8°, 59.3° and 65.2° indicate the presence of Co_3O_4 in all the catalysts (González et al., 2010).The intensity of Co_3O_4 peaks in Ca-Co/desilicated-H-ZSM-5 catalyst are more intense than that of the Co/H-ZSM-5 catalyst, suggesting that the cobalt crystalline size became bigger (Table 5-1) after desilication and calcium promotion. It was observed the size of Co_3O_4 crystallite increased due calcium loading (see Table 5-1), which agreed with Bao et al. (2009), that promoting catalyst by alkali-earth oxides/nitrate increases the Co_3O_4 crystallite size. It is worth noting that no peaks of calcium nitrate were detected on the XRD patterns indicating an evenly dispersion of calcium nitrate over the H-ZSM-5 support. The size of Co_3O_4 crystallite with 18.3 nm on Co/H-ZSM-5 catalyst slightly increased to 19.1 nm on Ca-Co/undesilicated-H-ZSM-5 catalyst after calcium addition. The size of Co_3O_4 particle significantly increased to 22.7 nm Ca-Co/desilicated-H-ZSM-5 catalyst. De la Osa et al. (2011) reported an increase in Co_3O_4 crystallite size from 9.6 nm on Co/Al_2O_3 to 13.1 nm on Ca-Co/Al_2O_3 catalysts. The Ru and Ni promotion on Co/H-ZSM-5 catalyst had an opposite influence on the Co_3O_4 crystallite size by decreasing the Co_3O_4 crystallite size of 18 nm to 16 nm and 12 nm respectively (Wang et al., 2013). The results given in Table 5-1 were obtained using Scherrer formula [3.1] and [3.2].

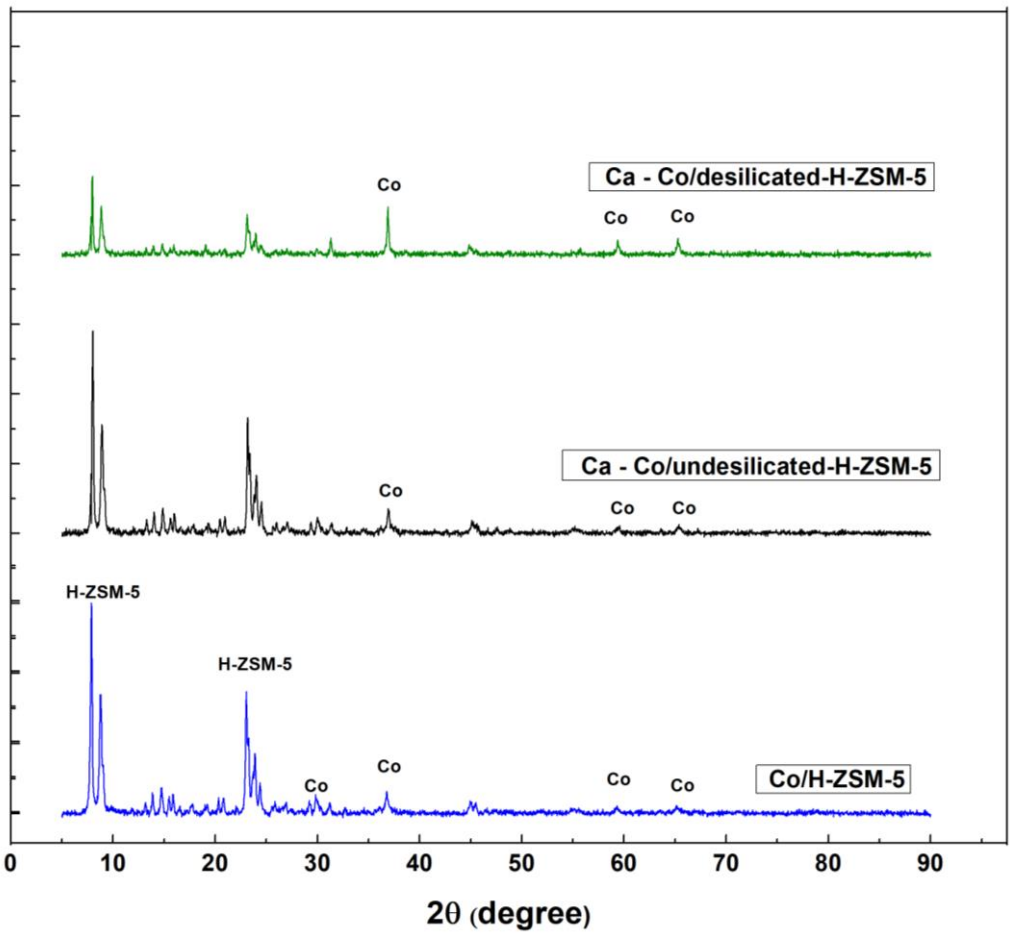


Figure 5-1: XRD patterns of unpromoted Co/H-ZSM-5 catalyst and calcium promoted Co/H-ZSM-5 catalysts.

Table 5-1: Summary of cobalt crystallite sizes based on XRD

Catalyst	Co_3O_4 (nm)	Co^0 (nm)
Co/H-ZSM-5	18.3	13.7
Ca-Co/undesilicated-H-ZSM-5	19.1	14.3
Ca-Co/undesilicated-H-ZSM-5	22.7	17.0

Figure 5-2 shows the elemental compositions in calcium-promoted cobalt-zeolite catalysts. As discussed in chapter 3, Figure 5-2A represents the elemental contents of Co/H-ZSM-5 before desilication with 7.98 wt.% of Co which increased to 22.75 % over mesoporous-H-ZSM-5 (Figure 4-7D). The addition of calcium promoter on Co/undesilicated-H-ZSM-5 catalyst (depicted by Figure 5-2B) brought some alteration on composition of elements. 2.0 % weight of calcium was added into cobalt-zeolite catalyst, but 1.64 wt. % of Ca was detected. Out of

10.0 wt. % of Co loaded unto zeolite, only 5.95 wt.% compared to 7.98 wt.% was detectable due to the occupied active sites of zeolite by the new element of calcium.

When calcium was loaded unto cobalt supported on mesoporous H-ZSM-5 with more active sites, its weight percentage failed to be detected (Figure 5-2C). But the weight percentage of Co examined, increased from 5.98 wt.% to 16.28 wt.% because of more active sites. Another component to take note of was silicon. In Figure 5-2C, 36.45 wt.% of Si was detected as compared to 40.63 wt.% (Figure 5-2B). This drop in Si wt. % indicated the success of silicon removal during desilication method on NaOH aqueous solution discussed in chapter 4 (section 3.2.2).

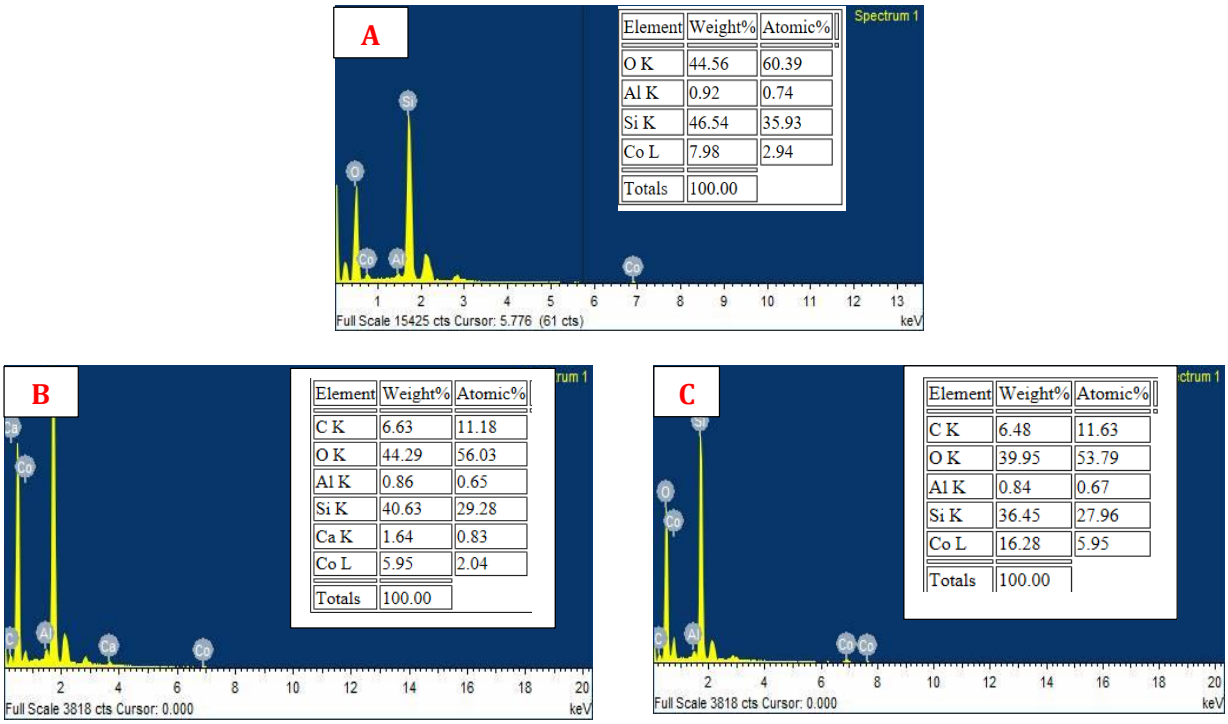


Figure 5-2: The Energy Dispersive Electroscopy (EDS) analysis results of [A] Co/H-ZSM-5 and [B] Ca-Co/undesilicated-H-ZSM-5 catalysts and [C] Ca-Co/desilicated-H-ZSM-5 catalysts

5.2.2 Performance of Ca-Co/H-ZSM-5 catalysts

Table 5-2: CO conversions over calcium promoted Co/H-ZSM-5 catalyst during FT synthesis

Catalyst	CO Conversion (%)
Ca-Co/H-ZSM-5	50.2
Ca-Co/H-ZSM-5(55)	90.9

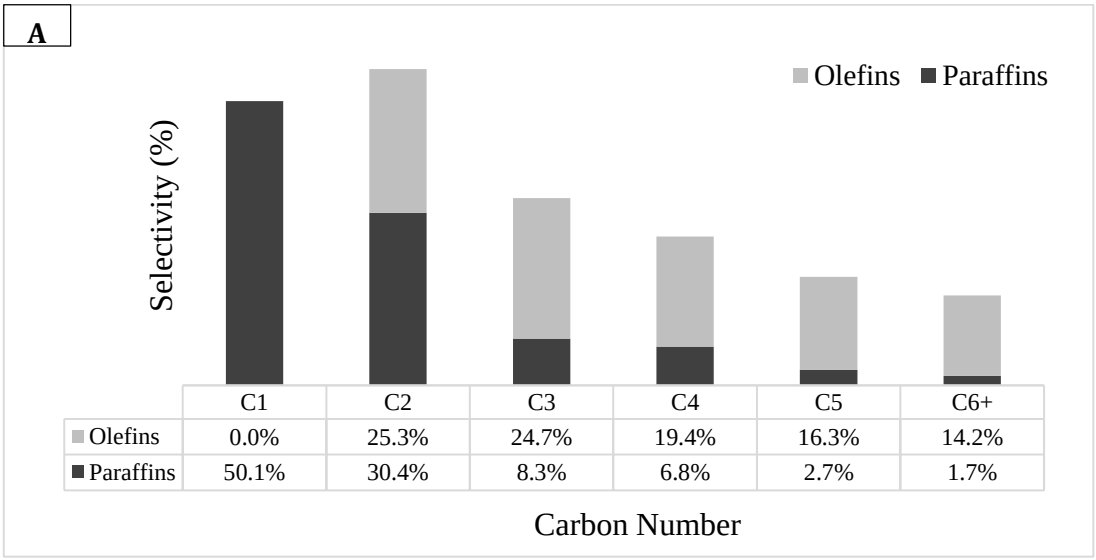
Since a higher conversion was obtained from Co/H-ZSM-5(55) catalyst as reported in Table 6-2, the study was proceeded by promoting both un-desilicated Co/H-ZSM-5 and Co/H-ZSM-5(55) catalysts. Calcium promoted catalysts of both Co/H-ZSM-5 and Co/H-ZSM-5(55) are denoted as Co/H-ZSM-5 and Ca-Co/H-ZSM-5(55) respectively. The addition of Ca to Co/H-ZSM-5 improved the activity of the catalysts. By adding calcium, CO conversions increased to 50.2 % and 90.9 % over Ca-Co/H-ZSM-5 and Ca-Co/H-ZSM-5(55) respectively (Table 5-2). This CO conversion increase can be supported by the study of Tao et al. (2006) that calcium is known to favour dissociative adsorption of CO but suppress H_2 adsorption during FTS reaction.

Figure 5-3A and Figure 5-3B show the selectivity of all produced hydrocarbons using calcium promoted Co/un-desilicated-H-ZSM-5 and Co/H-ZSM-5 catalysts. Comparing the performance of the two calcium promoted catalysts, one supported on microporous H-ZSM-5 and the other on mesoporous H-ZSM-5, gives the effect of the calcium promotion during FTS. The first observation was that the effect of calcium promotion enhanced the selectivity of higher hydrocarbons ($C_5 – C_{6+}$). For instance, on the unpromoted, un-desilicated catalyst (Fig. 4-2A), selective to C_5 olefin was 11.6% which increased to 16.3% over promoted catalyst (Fig. 5-3A). And when Co/H-ZSM-5(55) was promoted, selective to C_5 paraffin increased from 11.0% (Figure 4-3B) to 22.8% (Figure 5-3B). Bao et al. (2009) reported the increased selectivity of C_{5+} hydrocarbons from 77.75 % over Co/Al_2O_3 catalyst to 83.54 % over Ca-Co/Al_2O_3 catalyst. The results of Bao et al. (2009) and of this study are in agreement to the results reported by De La Osa et al. (2011). Hydrocarbon distribution obtained with calcium promoted on cobalt-based alumina catalyst also showed an increase to C_{5+} selectivity from 95.76% to 97.91% using H_2/CO of 2, temperature of 220 °C, pressure of 20 bars and flow rate of 4000 h^{-1} (De la Osa et al., 2011). However, the contrast between results of this study, Bao et al. (2009) and De La Osa et al., (2011) was that there was increase in ($C_1 – C_4$) hydrocarbons with calcium promoted as well as a depletion of C_{5+} hydrocarbon selectivity when reaction temperature was increased, all reported by De La Osa et al. (2011).

From the comparison of the two promoted catalyst in this study, it was quite siginficant to note that the addition of alkali-earth metal promoter (Ca) to the mesoporous zeolite (desilicated-H-ZSM-5) Co-catalyst favoured C_{6+} paraffins over olefins. In Figure 5-3B, selectivity of C_{6+} paraffins was 34.5% , almost four times more than of C_{6+} olefins (8.6%). Calcium promotion on cobalt-mesoporous zeolite improved the $C_5 – C_{6+}$ selectivity. Selective to C_5 olefin hydrocarbon tripled from 16.3% to 48.3% whereas C_5 paraffin hydrocarbon dramatically increased to 22.8 % from 2.7 %. According to Ngantsoue-Hoc et al. (2002) increased in CO

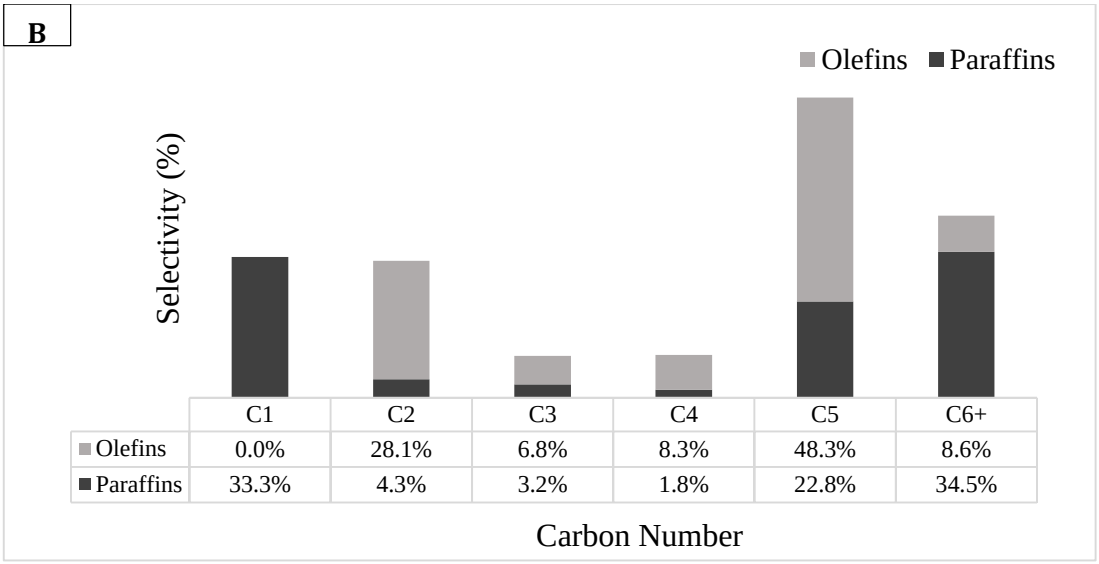
conversion means a drop in olefin ratio, it was therefore proved in this study the increase in CO conversion from 84.2 % to 90.9 % resuluted in C_5 olefin ratio decreased from 0.77 over Co/H-ZSM-5(55) to 0.68 over Ca-Co/H-ZSM-5(55) while C_{6+} olefin ratio dropped from 0.48 to 0.20.

In general, the $C_5 – C_{6+}$ selectivity continued to increase after promotion of the catalysts due to the re-adsorption of smaller olefin hydrocarbons in the presence of calcium metal ((De La Osa et al. (2011), Schulz & Claeys. (1999) and Van Der Laan & Beenackers. (1999)). Another important reason for the shift to higher hydrocarbon distributions ($C_5 – C_{6+}$) was because of cobalt particle sizes. Cobalt particle sizes serve to signify that larger cobalt particles lead to higher ($C_5 – C_{6+}$) production while smaller particles lead to higher methane (C_1) and ($C_2 – C_4$) hydrocarbon distributions (Tavasoli et al., 2007). In the Ca-Co/H-ZSM-5(55) catalyst, which had the highest cobalt particles size of 17.0 nm (Table 5-1) produced the highest C_{5+} selectivity. Bezemer et al. (2006) and Bao et al. (2009) and also reported the same trend that C_{5+} selectivity increased when cobalt particle size was increased.



	C1	C2	C3	C4	C5	C6+
Olefins	0.0%	25.3%	24.7%	19.4%	16.3%	14.2%
Paraffins	50.1%	30.4%	8.3%	6.8%	2.7%	1.7%

Figure 5-3A: Product distribution (olefins and paraffins) on Ca-Co/HZSM-5 catalyst at pressure of 15 bar.



	C1	C2	C3	C4	C5	C6+
Olefins	0.0%	28.1%	6.8%	8.3%	48.3%	8.6%
Paraffins	33.3%	4.3%	3.2%	1.8%	22.8%	34.5%

Figure 5-3B: Product distribution (olefins and paraffins) on Ca-Co/HZSM-5(55) catalyst at pressure of 15 bar.

Table 5-3 represents the catalytic performances of various promoted catalysts applied at different process conditions during FTS. From the results found in this study, calcium promoted catalyst observed to be more favourable to C_{5+} hydrocarbons (57.3%) over C_1 (28.1%) and (C_2 - C_4) lower hydrocarbons (14.1%). To better understand the effect of calcium promoter, results from other research studies (Table 5-3) were compared to the findings of this study. Although the supports to cobalt catalysts were different, promoted cobalt catalyst from literature recorded higher selectivity to C_{5+} hydrocarbons. In addition, the calcium promoted Co-catalyst on alumina support showed the highest gasoline-range hydrocarbon (GRHs) selectivity as represented in Table 5-3. On the other side, calcium promoted on Iron catalyst had the least selectivity towards GRHs.

Table 5-3: Comparison of % CO conversion and hydrocarbon selectivity of the calcium promoted cobalt-based catalyst in this study with other promoted catalysts in the literature.

					% Hydrocarbon Selectivity			
Catalyst	**Support**	**Promoter**	**Conditions**	**% X_{CO}**	**C_1**	**C_2 - C_4**	**C_{5+}**	**References**
Cobalt	H-ZSM-5 desilicated	Ca	H_2/CO = 2.5, 15 bars, 250 °C, 1200 GHSV	90.9	28.6	14.1	57.3	This study
Cobalt	Al_2O_3	Ca	H_2/CO = 2, 10 bars, 230 °C, 1500 GHSV	39.7	8.61	7.85	83.5	Bao et al., (2009)
Cobalt	H-ZSM-5	Ni	H_2/CO = 2, 20 bars, 251 °C, 1500 GHSV	60.0	-	25.1 ($C_1 - C_4$)	72.5	Wang et al. (2012)
Cobalt	H-ZSM-5	Ru	H_2/CO = 2, 20 bars, 251 °C, 1500 GHSV	58.2	-	36.3 ($C_1 - C_4$)	60.3	Wang et al. (2012)
Iron	Manganese	Ca	H_2/CO = 0.67, 15 bars, 250 °C, 2000 GHSV	51.0	8.3	25.2	43.2	Tao et al. (2006)
Cobalt	Al_2O_3	Ca	H_2/CO = 2, 20 bars, 220 °C, 4000 GHSV	55.7	-	1.97	97.6	de la Ola (2011)

5.3 Concluding remark

Chapter 5 focused on the performance of the calcium promoted cobalt-zeolite catalysts carried out in the fixed bed reactor (operated as PFR) under the same process conditions of temperature of 250°C, pressure of 15 bar, syngas ratio of 2.5, flow rate of 1200 gas hourly space velocity and catalyst weight of 0.5g. Prior to catalytic performances, the synthesized promoted catalysts were characterized using XRD and EDS scientific techniques. One Ca promoted cobalt catalyst was supported on the un-desilicated zeolite (H-ZSM-5) while the other supported on mesoporous (desilicated zeolite. The effect of calcium promotion on the Fischer-Tropsch synthesis catalysts was discussed in terms of activity, CO conversion and hydrocarbon selectivity. The FTS results from the two-calcium promoted Co-based catalysts were compared to determine which of the two catalysts was preferable for a group of desired products. The chapter also covered the discussion of these results with other research studies. The conclusion based on the results discussion in this chapter is outlined in chapter 7.

CHAPTER 6

Performance evaluation of the promoted Co/H-ZSM-5 catalyst at low pressure during Fischer-Tropsch Synthesis

6.1 Introduction

Fischer-Trospch synthesis is a chemical process that is strongly influenced by its process conditions, including reaction temperature, pressure, flow rate, syngas ratio and time on stream. Researchers have studied the effects of these process parameters in terms of FTS activity, CO conversion and hydrocarbon selectivity of hydrocarbons. In this study, the effect of decreasing pressure during FTS was investigated, while maintaining reaction temperature, flow rate, syngas ratio, time on stream and weight catalyst.

In chapter 5, the results of the best performing calcium-promoted catalyst, Ca-Co/H-ZSM-5(55), were determined at the pressure of 15 bars. This chapter reported the CO conversion and hydrocarbon selectivity of Ca-Co/H-ZSM-5(55) catalyst performance at low pressure under experimental conditions described in Table 6-1. Therefore, the experimental results data obtained were discussed and compared with the previous findings in chapter 4 & 5 and with literature.

6.2 Experimental Conditions

The FT experiments were carried out as described in chapter 3, except that pressure was changed to 2 and 8 bar.

5.3 Results and Discussion

The best performing catalyst (Ca-Co/H-ZSM-5(55)) was further tested on FTS at pressure under 15 bars but at the same temperature (250 °C), flow rate (1200 GHSV), syngas ratio (H_2/CO =2.5) and catalyst weight (0.5g). Adding calcium promter (2.0 %) to Co/desilicated-H-ZSM-5 increased the % CO conversion to 90.9% from 50.2 % Co/un-desilicated-H-ZSM-5 as indicated in the chapter 5. Therefore, Table 6-2 shows that % CO conversion generally decreased with a decrease in pressure on Ca-Co/HZSM-5(55) catalyst. When the pressure was decreased to 8 bar and 2 bar from 15 bars, the % CO conversion decreased to 47.7% and 17.4% respectively. A drop in % CO conversion by decreasing pressure was expected because the partial pressures of the reactants (CO and H_2) decreased. Matamela & Daramola. (2014) studied the effect of low pressure at similar process conditions (Table 6-1) except that their catalyst was not promoted nor desilicated. They obtained % CO conversion of 4.48% and 4.18 % at

pressures 8 bars and 2 bars respectively. In this study, it can be concluded that the effect calcium promotion of Co/H-ZSM-5 and desilication of H-ZSM-5 enhanced the activity of the catalyst as well as FTS performance. Figures 6-1 discussed the product selectivity based on the effect of changing pressure but keeping other conditions constant (given in Table 6-1).

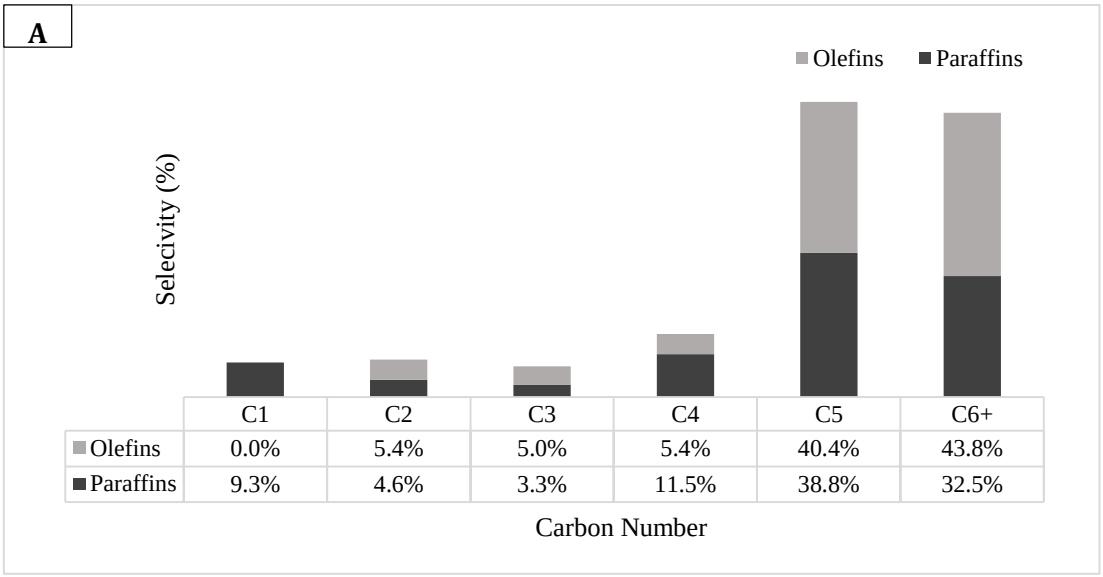
Table 6-1: Effect of low pressure on CO conversion

Catalyst	Pressure (bar)	CO Conversion (%)
Ca-Co/H-ZSM-5 (55)	8	47.7
Ca-Co/H-ZSM-5 (55)	2	17.4

As to the hydrocarbon distribution over Ca-Co/H-ZSM-5(55) catalyst, Figure 6-1A and Figure 6-1B show the product selectivity at a pressure of 8 bars and pressure of 2 bars respectively. Following the results in Figure 5-3B obtained at pressure of 15 bars, the Ca-Co/H-ZSM-5(55) catalyst at 8 bar displayed a drastic decrease in selectivity of the methane from 33.3 % (Fig. 5-3B) to 9.3 % and was more favourable to higher hydrocarbons. From Figure 6-1A, the same characteristics was observed similar to Figures in chapter 4.2, Figures in chapter 5.3, Daramola et al. (2017) Sartipi et al. (2013) and Bao et al. (2009), the promoted cobalt-based catalyst was still more selective to olefins than paraffins. Nonetheless being more selective to olefins, its selectivity to C_4 paraffin was more than C_4 olefin, with 11.5 % C_4 paraffin and 5.4 % olefin. For comparison Ca-Co/H-ZSM-5(55) catalyst at 8 bars (Figure 6-1A) was highly selective to C_{6+} olefins (43.8 %), when compared to its selectivity at 15 bar of pressure, which is 8.6 % selective to C_{6+} olefins as shown in Figure 5-3B. Selectivity to C_5 olefin remained above 40.0 %, with 40.4 % at 8 bars (Figure 5-1A) and 48.3 % at 15 bar (Figure 5-3B). The retained high selectivity to higher hydrocarbons (C_5 – C_{6+}) manifests the advantage of the presence of calcium in cobalt based catalyst which is known for its re-adsorption of smaller reactive products (such as ethene and propene) into increasing, adding to (C_{5+}) longer hydrocarbons (Van Der Laan & Beenackers. (1999), Schulz & Claeys. (1999) and De La Osa et al. (2011)).

For lower hydrocarbons, Ca-Co/H-ZSM-5(55) catalyst at 8 bars decreased the selectivity of C_2 olefin significantly to 5.4 % from 28.1 % shown in Figure 5-3B whereas the selectivity of C_2 paraffin remained almost constant (~4.3 %). At 8 bars, Ca-Co/H-ZSM-5(55) kept the selectivity of C_3 paraffin at about 3.3 % which was the same as 3.2 % from Fig. 5-3B. Again, the selective to lower hydrocarbons of olefins kept decreasing, C_3 olefin from 6.8 % to 5.0 % and C_4 olefin from 8.4 % to 5.4 %. The significant decrease in lower hydrocarbons of olefins

while selectivity of lower hydrocarbons of paraffin remained minimal, can be explained by the fact that C_2 and C_3 olefins are much unsaturated, reactive and subject to re-adsorb in the presence of calcium promoted catalyst. As a result, the growth of longer hydrocarbons began to be observed at C_4 paraffins. Selective to C_4 paraffin increased from 1.8 % (Figure 5-3B) to 11.5 % (Figure 6-1A). As a summary, the performance of Ca-Co/H-ZSM-5(55) catalyst on FTS was more favourable to higher HCs at lower pressure operation but high CO conversion was achieved at higher pressure operation.

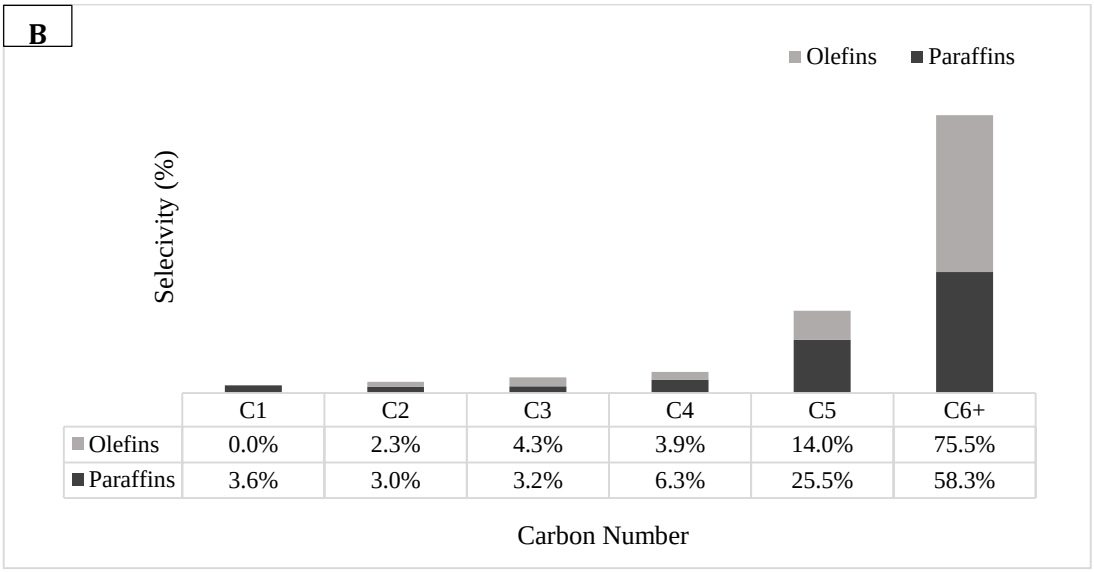


	C1	C2	C3	C4	C5	C6+
Olefins	0.0%	5.4%	5.0%	5.4%	40.4%	43.8%
Paraffins	9.3%	4.6%	3.3%	11.5%	38.8%	32.5%

Figure 6-1A: Product distribution (olefins and paraffins) on Ca-Co/HZSM-5(55) catalyst at pressure of 8 bar.

In case of performance of Ca-Co/H-ZSM-5(55) catalyst on FTS at 2 bars of pressure, 17.4 % CO conversion was obtained (see Table 6-2) and the product selectivity results associated with this CO conversion were reported in Figure 6-1B. Similarly, to Figure 6-1A, the Ca-Co/H-ZSM-5(55) catalyst performance at 2 bars displayed a continued increasing trend of product selectivity (for olefins and paraffins) from C_2 olefin (2.3 %) to C_{6+} olefin (75.5 %) and C_1 paraffin (3.6 %) to C_{6+} paraffin (58.3 %). From FTS operation at 8 bars to 2 bars, the promoted bi-functional catalyst resulted in further decrease of selectivity to both methane and lower hydrocarbons (C_2 - C_4). The effect of decreasing pressure from 15 bars, 8 bars to 2 bars had a great effect to methane selectivity since it decreased from 33. 3 %, 9.3 % to 3.6 % respectively. Daramola et al. (2017) obtained methane selectivity of 1 %, 6 % and 3 % under the operation at 15 bars, 8 bars and 2 bars respectively. However, their findings were based on the use of H_2/CO syngas ratio of 1.5 and unpromoted/not-desilicated Co/H-ZSM-5 catalyst. Notably, selectivity to C_2, C_3 and C_4 olefins decreased from 5.4 %, 5.0 % and 5.4 % (Figure 6-1A) to

2.3 %, 4.3 % and 3.9 % (Figure 6-1B) respectively while boosted the C_{6+} olefin from 43.8 % to 75.5 %. These results of decreased smaller olefin products increased longer hydrocarbons (C_{5+}) on calcium promoted catalyst is agreement with literature (De La Osa et al., 2011). Unlike in Figure 6-1A, selective to C_5 paraffin exceeded C_5 olefin at 2 bars FT operation.



	C1	C2	C3	C4	C5	C6+
Olefins	0.0%	2.3%	4.3%	3.9%	14.0%	75.5%
Paraffins	3.6%	3.0%	3.2%	6.3%	25.5%	58.3%

Figure 6-1B: Product distribution (olefins and paraffins) on Ca-Co/HZSM-5(55) catalyst at pressure of 2 bar.

Figures 6-2 shows whether product distributions were more selective to olefins or paraffins using calcium promoted catalyst on FTS. As it was mentioned in chapter 4, olefin ratio was determined by calculating for each hydrocarbon using equation [3.13]. Figure 6-2 illustrates the influence the pressure olefin selectivity of Fischer-Trospch synthesis products for the calcium promoted cobalt-zeolite catalysts. A behaviour with decreasing pressure was observed reducing the olefin ratio. Olefin ratios obtained at pressure of 15 bars were more than 0.65 except C_{6+} olefins for Ca-Co/H-ZSM-5(55) catalyst which was about 0.2. In other words, Ca-Co/H-ZSM-5(55) catalyst produced 80 % of C_{6+} paraffins as compared to its corresponding olefins.

It was previously reported by Ngantsoue-Hoc et al., (2002) and De La Osa et al., (2011), that as CO conversion increases, olefin ratio decreases. Conversely, in this case it is not so. Meanwhile, it was proved (Table 6-2) that a decreased of the pressure, decreased CO conversion. At low pressure, hydrocarbons distribution shifted to paraffin products. For instance, for Ca-Co/H-ZSM-5(55) catalyst, it resulted with about 0.82 of C_3 olefin ratio at 15 bars as opposed to 0.38 C_3 olefin ratio at 2 bars. Comparison of promoted catalysts (from Figure 6-2) graphically represented that pressure of 8 bars and 2 bars, reduced the olefin ratio because

olefin ratio for each hydrocarbon was found to be below 0.60 as opposed to olefin ratio greater than 0.65 at 15 bars of pressure. Therefore, it can be concluded that the olefin ratio was found to be influenced by the pressure of FT reaction.

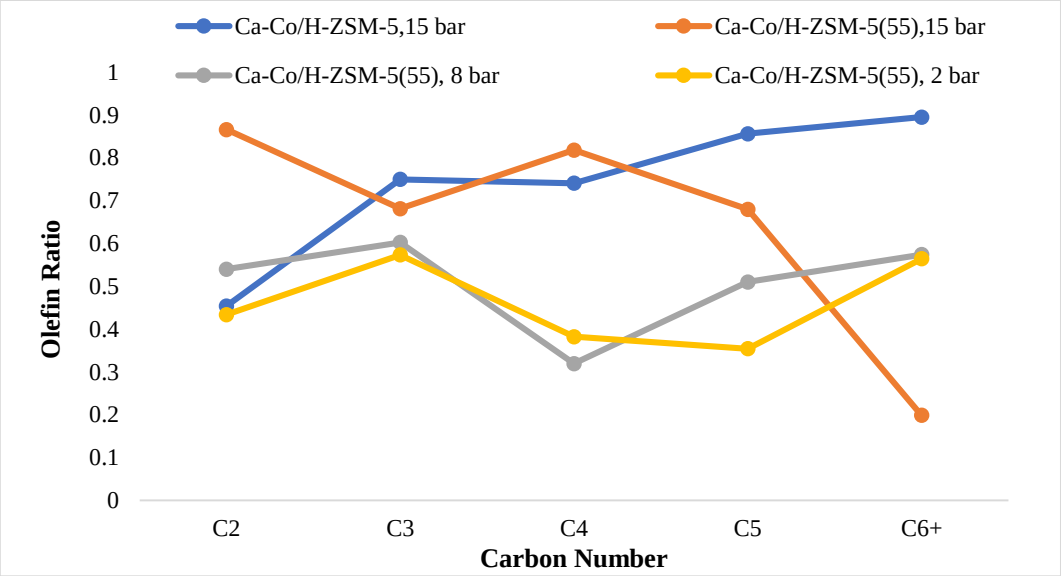


Figure 6-2: Olefin ratio on calcium promoted catalysts at different pressure

6.4 Concluding remark

From chapter 5, the preferred catalyst in terms of its activity, CO conversion and product distribution was found to be (Ca-Co/H-ZSM-5(55)) catalyst. Therefore, this chapter proceeded from chapter 5 where the preferred catalyst was further tested on FTS at lower pressure conditions of 8 bars and 2 bars but keeping other process conditions the same. The results from this chapter were also discussed in terms of CO conversion and product selectivity. This chapter covered the comparison with chapter 4, chapter 5 and other relevant previous research studies. It included the effect of lowering pressure on the olefins and paraffins based on their olefin ratios. The conclusion for this chapter is also reported in chapter 7.

CHAPTER 7

Conclusion and Recommendations

7.1 Conclusions

Fischer-Tropsch synthesis can be a beneficial process for waste management processes, due to its possible use of waste carbonaceous materials as feedstocks. Carbonaceous materials such as waste tyres can undergo gasification to produce synthetic gases. This syngas can then be used to produce liquid fuel (hydrocarbons) via Fischer-Tropsch synthesis (FTS) process. One of the major challenges in FTS is the choice of effective catalyst to produce the desired products while considering energy usage. Cobalt-based FT catalyst combined with zeolite considered the best option due to its use in low temperature Fischer-Trospch, high activity, stability and lifespan. This study aimed to optimize bi-functional Co/H-ZSM-5 catalyst via incipient wetness impregnation method and then evaluated during FTS process. Prior to that, desilication of H-ZSM-5 via NaOH aqueous solution was done to create mesoporous H-ZSM-5. In later stages, Co/H-ZSM-5 catalysts were promoted by alkaline-earth metal (calcium) to improve its catalytic performance during FTS.

Objective 1

Mesoporous H-ZSM-5 and Co/H-ZMS-5 were prepared via desilication and incipient wetness impregnation methods, respectively. H-ZSM-5 and Co/H-ZSM-5 were characterized by XRD (for crystallinity), SEM-EDS (for surface morphology and elemental compositions), N_2 physisorption (for surface area, pore sizes and pore volumes) and FTIR (for chemistry).

The characterization of ZSM-5 (Si/A*l* = 40) was found to contain micropore characteristics. Mesoporous H-ZSM-5 zeolites were successfully synthesized from H-ZSM-5 (Si/A*l* = 40) by desilication method in 0.2M NaOH aqueous solution at various treatment temperature (40 °C, 55 °C & 70 °C). The meso-porosity of H-ZSM-5 was obtained by a further ion-exchanging with 1M NH_4NO_3 aqueous solution followed by calcination. Upon desilication, a sudden increase in the size and volume of mesopores was observed as explained by the BJH pore size distribution (from N_2 physisorption). From N_2 physisorption results, surface area increased from 391 m^2/g to 419 m^2/g after desilication. Note-worthily, the changes in desilicated-H-ZSM-5 was not just on porosity but also in chemical composition of zeolite. EDS recorded the aluminium and silicon contents. From this EDS results, Si/A*l* ratio dropped to 26, due to a successfully selective extraction of silicon. 10 % of Co (from Cobalt (II) nitrate hexa-hydrate ($Co(NO_3)_2.6H_2O$) was then impregnated into H-ZSM-5 and desilicated-H-ZSM-5 zeolites

supports. According to XRD and EDS results, active cobalt metal was successfully impregnated.

A total of four synthesized Co-based catalysts (Co/H-ZSM-5, Co/H-ZSM-5(40), Co/H-ZSM-5(55) and Co/H-ZSM-5(70)) were evaluated during FTS under the same process conditions of temperature (250 °C), pressure (15 bar), flow rate (1200 GHSV), H_2/CO ratio of 2.5 and weight catalyst of 5 g. The FT results were recorded in terms of CO conversion and hydrocarbon selectivity. The use of mesoporous-H-ZSM-5 support on Co-based catalyst increased the CO conversion from about 50% to above 75%. Meaning, the meso-porosity in desilicated-H-ZSM-5 increased the catalytic activity and performance. On the hand, the mesoporous-H-ZSM-5 zeolites on Cobalt were found to be efficient catalysts to produce gasoline-range (C_5 – C_{6+}) hydrocarbons from syngas in FTS. Based on the optimum catalyst (Co/H-ZSM-5(55), the CO conversion increased to a maximum of 84.2 % and selectivity to C_{5+} of 47.9%. In addition, it was more selective to olefins than paraffins with the highest C_5 and C_{6+} olefin selectivity of 50.5 % and 19.9 % respectively.

Objective 2

Out of the four evaluated catalysts from objective 1, two Co-based catalysts were promoted by alkaline-earth metal (calcium). Co/H-ZSM-5(55) was calcium-promoted based on its best FT results and Co/H-ZSM-5 was also calcium promoted for comparison purpose. XRD and EDS showed the successfully calcium promoted in Co/H-ZSM-5 catalysts. Based on XRD results, calcium promotion increased the cobalt particle sizes from 13.7 nm to a maximum of 17.0 nm

Therefore, the two promoted catalysts, namely Ca-Co/H-ZSM-5 and Ca-Co/H-ZSM-5(55), were evaluated on FTS under the same process conditions used in objective 1. The first observation after catalyst promotion, based hydrocarbon selectivity was paraffins were more selective than olefins (> C_4). For instance, based on Ca-Co/HZ-SM-5(55), selectivity to C_{6+} were 8.6% olefins and 34.5% paraffins as compared to 19.9% olefins and 7.5% paraffins of Co/H-ZSM-5(55). Secondly, promotion of Co/H-ZSM-5 catalyst by calcium reduced the hydrogenation which suppressed methane formation. Lastly, the calcium-promoted co-based catalysts enhanced CO conversion (90.9%) and selectivity to gasoline-range hydrocarbons.

Objective 3

The two calcium-promoted catalysts (Ca-Co/H-ZSM-5 and Ca-Co/H-ZSM-5(55)) were further evaluated on FTS under low pressure of 8 bar and 2 bar while keeping other process conditions. Lowering pressure condition decreased the CO partial pressures which led to lower conversion of CO. However, promoted catalysts operated at low FT pressure enhanced the C_{5+} hydrocarbon selectivity. For instance, the highest selectivity to hydrocarbons more than ($> C_4$) was selective to C_{6+} (75.5 %) obtained at the lowest pressure of 2 bars.

7.2 Recommendations

Based on the findings of this research study, the following ideas may be recommended for the future studies:

- Varying the concentration of the NaOH alkaline solution during desilication to determine the optimum concentration for the development of zeolite mesoporosity.
- The laboratory experimental setup uses control valves to manually gas flow but making use of electronic control can maintain the stability of the flow and result in few errors of results.
- For further evaluation of the promoted Ca-Co/desilicated-H-ZSM-5 catalyst, varying operating conditions (reaction temperature, syngas ratio, flow rate, catalyst weight) can be necessary to determine the effect of catalyst promotion in terms of CO conversion and hydrocarbons selectivity.

References

Abelló, S., Bonilla, A., & Pérez-Ramírez, J. (2009). Mesoporous ZSM-5 zeolite catalysts prepared by desilication with organic hydroxides and comparison with NaOH leaching. *Applied Catalysis A: General*, *364*(1–2), 191–198.

Atashi, H., Siami, F., Mirzaei, A. A., & Sarkari, M. (2010). Kinetic study of Fischer-Tropsch process on titania-supported cobalt-manganese catalyst. *Journal of Industrial and Engineering Chemistry*, *16*(6), 952–961.

Bao, A., Liew, K., & Li, J. (2009). Fischer-Tropsch synthesis on CaO-promoted Co/Al2O3 catalysts. *Journal of Molecular Catalysis A: Chemical*, *304*(1–2), 47–51.

Barrett, E. P., Joyner, L. G., & Halenda, P. P. (1951). The Determination of Pore Volume and Area Distributions in Porous Substances. I. Computations from Nitrogen Isotherms. *Journal of the American Chemical Society*, *73*(1), 373–380.

Bezemer, G. L., Bitter, J. H., Kuipers, H. P. C. E., Oosterbeek, H., Holewijn, J. E., Xu, X., Kapteijn, F., Van Diilen, A. J., & De Jong, K. P. (2006). Cobalt particle size effects in the Fischer-Tropsch reaction studied with carbon nanofiber supported catalysts. *Journal of the American Chemical Society*, *128*(12), 3956–3964.

Biloen, P., & Sachtler, W. M. H. (1981). Mechanism of hydrocarbon synthesis over Fischer-Tropsch catalysts. *Advances in Catalysis*, *30*, 165-216.

Bowen, T. C., Noble, R. D., & Falconer, J. L. (2004). Fundamentals and applications of pervaporation through zeolite membranes. In *Journal of Membrane Science*.

Bukur, D. B., Ma, W. P., & Carreto-Vazquez, V. (2005). Attrition studies with precipitated iron Fischer-Tropsch catalysts under reaction conditions. *Topics in Catalysis*, *32*(3–4), 135–141.

Calleja, G., de Lucas, A., & van Grieken, R. (1995). Co/HZSM-5 catalyst for syngas conversion: influence of process variables. *Fuel*, *74*(3), 445–451.

Caro, J., & Noack, M. (2008). Zeolite membranes - Recent developments and progress. In *Microporous and Mesoporous Materials*.

Chiou, Y. H., Tsai, T. G., Sung, S. L., Shih, H. C., Wu, C. N., & Chao, K. J. (1996). Synthesis and characterization of zeolite (MFI) membrane on anodic alumina. *Journal of the Chemical Society - Faraday Transactions*, *92*(6), 1061–1066.

Coates, J. (2006). Interpretation of Infrared Spectra, A practical approach. In *Interpretation of Infrared Spectra, A practical approach*.

Corma, A., Rey, F., Valencia, S., Jordá, J. L., & Rius, J. (2003). A zeolite with interconnected 8-, 10- and 12-ring pores and its unique catalytic selectivity. *Nature Materials*, *2*(7), 493–497.

Dagle, R. A., Lizarazo-Adarme, J. A., Lebarbier Dagle, V., Gray, M. J., White, J. F., King, D. L., & Palo, D. R. (2014). Syngas conversion to gasoline-range hydrocarbons over Pd/ZnO/Al 2 O 3 and ZSM-5 composite catalyst system. *Fuel Processing Technology*, *123*, 65–74.

Dalai, A. K., & Davis, B. H. (2008). Fischer–Tropsch synthesis: a review of water effects on the performances of unsupported and supported Co catalysts. Applied Catalysis A: General, 348(1), 1-15.

Dancuart, L. P., & Steynberg, A. P. (2007). Fischer-Tropsch based GTL technology: a new process? In *Studies in Surface Science and Catalysis* (Vol. 163). Elsevier B.V.

Daniell, J., Köpke, M., & Simpson, S. D. (2012). Commercial biomass syngas fermentation. In *Energies* (Vol. 5, Issue 12).

Daramola, M. O., Burger, A. J., Giroir-Fendler, A., Miachon, S., & Lorenzen, L. (2010). Extractor-type catalytic membrane reactor with nanocomposite MFI-alumina membrane tube as separation unit: Prospect for ultra-pure para-Xylene production from m-Xylene isomerization over Pt-HZSM-5 catalyst. *Applied Catalysis A: General*.

Daramola, Michael O., Aransiola, E. F., & Ojumu, T. V. (2012). Potential applications of zeolite membranes in reaction coupling separation processes. *Materials*, *5*(11), 2101–2136.

Daramola, Michael Olawale, Matamela, K., & Sadare, O. O. (2017). Effect of CO2 co-feeding on the conversion of syngas derived from waste to liquid fuel over a bi-functional Co/H-ZSM-5 catalyst. *Journal of Environmental Chemical Engineering*, *5*(1), 54–62.

De Klerk & Furimsky, D. K. & F. (2010). *Catalysis in the Refining of Fischer-Trospch Syncrude*. *1970*.

De La Osa, A. R., De Lucas, A., Romero, A., Valverde, J. L., & Sánchez, P. (2011). Fischer-Tropsch diesel production over calcium-promoted Co/alumina catalyst: Effect of reaction conditions. *Fuel*, *90*(5), 1935–1945.

Dias, J. A. C., & Assaf, J. M. (2003). Influence of calcium content in Ni/CaO/γ-Al2O3 catalysts for CO2-reforming of methane. *Catalysis Today*, *85*(1), 59–68.

Dong, J., & Lin, Y. S. (1998). In situ synthesis of P-type zeolite membranes on porous α-alumina supports. *Industrial and Engineering Chemistry Research*, *37*(6), 2404–2409.

Downs, R. T., & Hall-Wallace, M. (2003). *The American Mineralogists Crystal Structure database*. 88(1) :247-250.

Dry, M. E. (2002). High quality diesel via the Fischer-Tropsch process - A review. *Journal of Chemical Technology and Biotechnology*, *77*(1), 43–50.

Eschemann, T. O., Bitter, J. H., & De Jong, K. P. (2014). Effects of loading and synthesis method of titania-supported cobalt catalysts for Fischer-Tropsch synthesis. *Catalysis*

Today, *228*, 89–95.

Gayubo, A. G., Vicente, J., Ereña, J., Oar-Arteta, L., Azkoiti, M. J., Olazar, M., & Bilbao, J. (2014). Causes of deactivation of bifunctional catalysts made up of CuO-ZnO-Al 2O3 and desilicated HZSM-5 zeolite in DME steam reforming. *Applied Catalysis A: General*, *483*, 76–84.

Gil, B., Mokrzycki, Ł., Sulikowski, B., Olejniczak, Z., & Walas, S. (2010). Desilication of ZSM-5 and ZSM-12 zeolites: Impact on textural, acidic and catalytic properties. *Catalysis Today*, *152*(1–4), 24–32.

González, O., Pérez, H., Navarro, P., Almeida, L. C., Pacheco, J. G., & Montes, M. (2010). Use of different mesostructured materials based on silica as cobalt supports for the Fischer-Tropsch synthesis. *Catalysis Today*.

Groen, J. C., Peffer, L. A. A., Moulijn, J. A., & Pérez-Ramírez, J. (2004). Mesoporosity development in ZSM-5 zeolite upon optimized desilication conditions in alkaline medium. *Colloids and Surfaces A: Physicochemical and Engineering Aspects*, *241*(1–3), 53–58.

Guo, C., Wu, Y., & Zhan, J. (2013). Study on bimodal mesoporous Co/SiO2 catalysts for the Fischer-Tropsch synthesis. *Reaction Kinetics, Mechanisms and Catalysis*, *109*(2), 497–508.

Hedlund, J., Schoeman, B., & Sterte, J. (1997). Ultrathin oriented zeolite LTA films. *Chemical Communications*, *13*, 1193–1194.

Hedlund, J., Sterte, J., Anthonis, M., Bons, A. J., Carstensen, B., Corcoran, N., Cox, D., Deckman, H., De Gijnst, W., De Moor, P. P., Lai, F., McHenry, J., Mortier, W., Reinoso, J., & Peters, J. (2002). High-flux MFI membranes. *Microporous and Mesoporous Materials*, *52*(3), 179–189.

Holm, M. S., Hansen, M. K. ., & Christensen, C. H. . (2009). "One-pot" Ion-exchange and mesopore formation during desilication. *European Journal of Inorganic Chemistry*, *9*, 1194–1198.

Hu, J., Yu, F., & Lu, Y. (2012). Application of fischer-tropsch synthesis in biomass to liquid conversion. *Catalysts*, *2*(2), 303–326.

Janssen, A. H., Schmidt, I., Jacobsen, C. J. H., Koster, A. J., & de Jong, K. P. (2003). Exploratory study of mesopore templating with carbon during zeolite synthesis. *Microporous and Mesoporous Materials*, *65*(1), 59–75.

Kalipcilar, H., Bowen, T. C., Noble, R. D., & Falconer, J. L. (2002). Synthesis and separation performance of SSZ-13 zeolite membranes on tubular supports. *Chemistry of Materials*, *14*(8), 3458–3464.

Kang, J., Cheng, K., Zhang, L., Zhang, Q., Ding, J., Hua, W., Lou, Y., Zhai, Q., & Wang, Y. (2011). Mesoporous zeolite-supported ruthenium nanoparticles as highly selective fischer-tropsch catalysts for the production of C5-C11 isoparaffins. *Angewandte Chemie*

- *International Edition*, *50*(22), 5200–5203.

Khodakov, A. Y., Chu, W., & Fongarland, P. (2007). Advances in the development of novel cobalt Fischer-Tropsch catalysts for synthesis of long-chain hydrocarbons and clean fuels. *Chemical Reviews*, *107*(5), 1692–1744.

Kim, K., Kim, Y., Yang, C., Moon, J., Kim, B., Lee, J., Lee, U., Lee, S., Kim, J., Eom, W., Lee, S., Kang, M., & Lee, Y. (2013). Long-term operation of biomass-to-liquid systems coupled to gasification and Fischer-Tropsch processes for biofuel production. *Bioresource Technology*, *127*, 391–399.

Li, S., Tuan, V. A., Falconer, J. L., & Noble, R. D. (2002). X-type zeolite membranes: Preparation, characterization, and pervaporation performance. *Microporous and Mesoporous Materials*, *53*(1–3), 59–70.

Linghu, W., Liu, X., Li, X., & Fujimoto, K. (2006). Selective synthesis of higher linear α-olefins over cobalt Fischer-Tropsch catalyst. *Catalysis Letters*, *108*(1–2), 11–13.

Lögdberg, S. (2007). *Development of Fischer-Tropsch catalysis for gasified biomass*.

Lu, X. (2011). Synthesis : Towards Understanding. *Dissertation*.

Lualdi, M. (2012). Fischer-Tropsch Synthesis over Cobalt-based Catalysts for BTL Applications. In *Chemical Engineering Stockholm*.

Luo, M., Bao, S., Keogh, R. S., Sarkar, A., Jacobs, G., & Davis, B. H. (2006). Fischer Tropsch synthesis: A comparison of iron and cobalt catalysts. *AIChE Annual Meeting, Conference Proceedings*.

Maghsoudi, H. (2016). Defects of Zeolite Membranes: Characterization, Modification and Post-treatment Techniques. *Separation and Purification Reviews*, *45*(3), 169–192.

Martínez, A., López, C., Márquez, F., & Díaz, I. (2003). Fischer-Tropsch synthesis of hydrocarbons over mesoporous Co/SBA-15 catalysts: The influence of metal loading, cobalt precursor, and promoters. *Journal of Catalysis*, *220*(2), 486–499.

Matamela, K. (2014). Synthesis and Performance Evaluation of Co / H-ZSM-5 Bi- functional Catalyst for Fischer-Tropsch Synthesis. *University of Witwatersrand*, *351237*.

Matamela, K., & Daramola, M. O. (n.d.). *CONVERSION OF SYNGAS DERVIED FROM WASTE TYRES TO LIQUID FUEL OVER A BI-FUNCTIONAL Co / H-ZSM-5 CATALYST : EFFECT OF OPERATING VARIABLES*. *November 2016*, 14–17.

Mirzaei, A. A., Habibpour, R., Faizi, M., & Kashi, E. (2006). Characterization of iron-cobalt oxide catalysts: Effect of different supports and promoters upon the structure and morphology of precursors and catalysts. *Applied Catalysis A: General*, *301*(2), 272–283.

Moyo, M. (2012). *Cobalt and Iron Supported on Carbon Spheres Catalysts for Fischer-Tropsch Synthesis*. 219.

Müller, M., Harvey, G., & Prins, R. (2000). Comparison of the dealumination of zeolites

beta, mordenite, ZSM-5 and ferrierite by thermal treatment, leaching with oxalic acid and treatment with SiCl 4 by 1 H, 29 Si and 27 A1 MAS NMR. *Microporous and Mesoporous Materials*, *34*(2), 135–147.

Muñoz, T., & Balkus, K. J. (1999). Preparation of oriented zeolite UTD-1 membranes via pulsed laser ablation. *Journal of the American Chemical Society*, *121*(1), 139–146.

Nada. (2011). *TRANSPORT MANAGERS BOOK : HELPING YOU REACH YOUR REAL DESTINATION*.

Navajas, A., Mallada, R., Téllez, C., Coronas, J., Menéndez, M., & Santamaría, J. (2002). Preparation of mordenite membranes for pervaporation of water-ethanol mixtures. *Desalination*, *148*(1–3), 25–29.

Ngantsoue-Hoc, W., Zhang, Y., O'Brien, R. J., Luo, M., & Davis, B. H. (2002). Fischer-Tropsch synthesis: Activity and selectivity for Group I alkali promoted iron-based catalysts. *Applied Catalysis A: General*, *236*(1–2), 77–89.

Nishiyama, N., Ueyama, K., & Matsukata, M. (1996). Synthesis of defect-free zeolite-alumina composite membranes by a vapor-phase transport method. *Microporous Materials*, *7*(6), 299–308.

Ogura, M., Shinomiya, S. Y., Tateno, J., Nara, Y., Nomura, M., Kikuchi, E., & Matsukata, M. (2001). Alkali-treatment technique - New method for modification of structural and acid-catalytic properties of ZSM-5 zeolites. *Applied Catalysis A: General*, *219*(1–2), 33–43.

Perry, R. ., Perry, S., Green, D. ., & Maloney, J. . (1997). Gasification, in: R. H. Perry, (Ed.), Perry's Chemical Engineers' Handbook, 7th ed. In *McGraw-Hill New York*.

Sadowska, K., Wach, A., Olejniczak, Z., Kuśtrowski, P., & Datka, J. (2013). Hierarchic zeolites: Zeolite ZSM-5 desilicated with NaOH and NaOH/tetrabutylamine hydroxide. *Microporous and Mesoporous Materials*, *167*, 82–88.

Sartipi, S., Alberts, M., Santos, V. P., Nasalevich, M., Gascon, J., & Kapteijn, F. (2014). Insights into the catalytic performance of mesoporous h-zsm-5-supported cobalt in fischer-tropsch synthesis. *ChemCatChem*, *6*(1), 142–151.

Sartipi, S., Parashar, K., Makkee, M., Gascon, J., & Kapteijn, F. (2013). Breaking the Fischer-Tropsch synthesis selectivity: Direct conversion of syngas to gasoline over hierarchical Co/H-ZSM-5 catalysts. *Catalysis Science and Technology*, *3*(3), 572–575.

Sartipi, S., Parashar, K., Valero-Romero, M. J., Santos, V. P., Van Der Linden, B., Makkee, M., Kapteijn, F., & Gascon, J. (2013). Hierarchical H-ZSM-5-supported cobalt for the direct synthesis of gasoline-range hydrocarbons from syngas: Advantages, limitations, and mechanistic insight. *Journal of Catalysis*, *305*, 179–190.

Sartipi, S., Van Dijk, J. E., Gascon, J., & Kapteijn, F. (2013). Toward bifunctional catalysts for the direct conversion of syngas to gasoline range hydrocarbons: H-ZSM-5 coated Co versus H-ZSM-5 supported Co. *Applied Catalysis A: General*, *456*, 11–22.

Satterfield, C. N., Huff, G. A., & Longwell, J. P. (1982). Product Distribution from Iron Catalysts in Fischer-Tropsch Slurry Reactors. *Industrial and Engineering Chemistry Process Design and Development*, *21*(3), 465–470.

Schmidt, F., Lohe, M. R., Büchner, B., Giordanino, F., Bonino, F., & Kaskel, S. (2013). Improved catalytic performance of hierarchical ZSM-5 synthesized by desilication with surfactants. *Microporous and Mesoporous Materials*, *165*, 148–157

Schulz, H., & Claeys, M. (1999). Kinetic modelling of Fischer-Tropsch product distributions. *Applied Catalysis A: General*, *186*(1–2), 91–107.

Society, A. C., Loeb, S., Barrer, R. M., Sieves, Z. M., Breck, D. W., Wiley, J., & Breck, D. M. (1987). *United States Patent 19*. *4*, 45–50.

Sun, B., Qiao, M., Fan, K., Ulrich, J., & Tao, F. F. (2011). Fischer-Tropsch synthesis over molecular sieve supported catalysts. *ChemCatChem*, *3*(3), 542–550.

Sun, J., Chen, Y., & Chen, J. (2017). Towards stable Fe-based catalysts with suitable active phase for Fischer-Tropsch synthesis to lower olefins. *Catalysis Communications*, *91*, 34–37.

Suzuki, T., & Okuhara, T. (2001). Change in pore structure of MFI zeolite by treatment with NaOH aqueous solution. *Microporous and Mesoporous Materials*, *43*(1), 83–89.

Tanaka, K., Yoshikawa, R., Ying, C., Kita, H., & Okamoto, K. I. (2001). Application of zeolite membranes to esterification reactions. *Catalysis Today*, *67*(1–3), 121–125.

Tao, Z., Yang, Y., Zhang, C., Li, T., Wang, J., Wan, H., Xiang, H., & Li, Y. (2006). Effect of calcium promoter on a precipitated iron-manganese catalyst for Fischer-Tropsch synthesis. *Catalysis Communications*, *7*(12), 1061–1066.

Tavasoli, A., Sadaghiani, K., Khodadadi, A. A., & Mortazavi, Y. (2007). Raising distillate selectivity and catalyst life time in Fischer-Tropsch synthesis by using a novel dual-bed reactor. *Iranian Journal of Chemistry and Chemical Engineering*, *26*(2), 109–117.

Tuan, V. A., Li, S., Noble, R. D., & Falconer, J. L. (2001). Preparation and pervaporation properties of a MEL-type zeolite membrane. *Chemical Communications*, *6*, 583–584.

Tuan, Vu A., Li, S., Falconer, J. L., & Noble, R. D. (2002). In situ crystallization of beta zeolite membranes and their permeation and separation properties. *Chemistry of Materials*, *14*(2), 489–492.

Udaya, V., Rao, S., & Gormley, R. J. (1990). Bifunctional catalysis in syngas conversions. *Catalysis Today*, *6*(3), 207–234.

Van Der Laan, G. P., & Beenackers, A. A. C. M. (1999). Kinetics and Selectivity of the Fischer-Tropsch Synthesis: A Literature Review. *Catalysis Reviews - Science and Engineering*, *41*(3–4), 255–318.

van Koningsveld, H., Jansen, J. C., & van Bekkum, H. (1990). The monoclinic framework structure of zeolite H-ZSM-5. Comparison with the orthorhombic framework of as-

synthesized ZSM-5. *Zeolites*, *10*(4), 235–242.

van Wechem, V. M. H., & Senden, M. M. G. (1994). Conversion of natural gas to transportation fuels via the shell middle distillate synthesis process(smds). *Studies in Surface Science and Catalysis*, *81*(C), 43–71.

Vervloet, D., Kapteijn, F., Nijenhuis, J., & Van Ommen, J. R. (2012). Fischer-Tropsch reaction-diffusion in a cobalt catalyst particle: Aspects of activity and selectivity for a variable chain growth probability. *Catalysis Science and Technology*, *2*(6), 1221–1233.

Vosoughi, V., Dalai, A. K., Abatzoglou, N., & Hu, Y. (2017). Performances of promoted cobalt catalysts supported on mesoporous alumina for Fischer-Tropsch synthesis. *Applied Catalysis A: General*, *547*(August), 155–163.

Wang, S., Yin, Q., Guo, J., Ru, B., & Zhu, L. (2013). Improved Fischer-Tropsch synthesis for gasoline over Ru, Ni promoted Co/HZSM-5 catalysts. *Fuel*, *108*, 597–603.

Wang, X., Chen, H. Y., & Sachtler, W. M. H. (2000). Catalytic reduction of NO(x) by hydrocarbons over Co/ZSM-5 catalysts prepared with different methods. *Applied Catalysis B: Environmental*, *26*(4), L227–L239.

Washmon-Kriel, L., & Balkus, K. J. (2000). Preparation and characterization of oriented MAPO-39 membranes. *Microporous and Mesoporous Materials*, *38*(1), 107–121.

Weitkamp, J. (2010). Zeolites and Catalysis. *Zeolites and Catalysis*, *131*, 175–188.

Xing, C., Shen, W., Yang, G., Yang, R., Lu, P., Sun, J., Yoneyama, Y., & Tsubaki, N. (2014). Completed encapsulation of cobalt particles in mesoporous H-ZSM-5 zeolite catalyst for direct synthesis of middle isoparaffin from syngas. *Catalysis Communications*, *55*, 53–56.

Xing, C., Yang, G., Lu, P., Shen, W., Gai, X., Tan, L., Mao, J., Wang, T., Yang, R., & Tsubaki, N. (2016a). A hierarchically spherical Co-based zeolite catalyst with aggregated nanorods structure for improved Fischer-Tropsch synthesis reaction activity and isoparaffin selectivity. *Microporous and Mesoporous Materials*, *233*, 62–69.

Xing, C., Yang, G., Lu, P., Shen, W., Gai, X., Tan, L., Mao, J., Wang, T., Yang, R., & Tsubaki, N. (2016b). A hierarchically spherical Co-based zeolite catalyst with aggregated nanorods structure for improved Fischer-Tropsch synthesis reaction activity and isoparaffin selectivity. *Microporous and Mesoporous Materials*.

Xiong, H., Motchelaho, M. A. M., Moyo, M., Jewell, L. L., & Coville, N. J. (2011). Correlating the preparation and performance of cobalt catalysts supported on carbon nanotubes and carbon spheres in the Fischer-Tropsch synthesis. *Journal of Catalysis*, *278*(1), 26–40.

Yang, Y., Xiang, H. W., Xu, Y. Y., Bai, L., & Li, Y. W. (2004). Effect of potassium promoter on precipitated iron-manganese catalyst for Fischer-Tropsch synthesis. *Applied Catalysis A: General*, *266*(2), 181–194.

Yoo, W. C., Zhang, X., Tsapatsis, M., & Stein, A. (2012). Synthesis of mesoporous ZSM-5 zeolites through desilication and re-assembly processes. *Microporous and Mesoporous Materials*, *149*(1), 147–157.

Zhou, J., Hua, Z., Liu, Z., Wu, W., Zhu, Y., & Shi, J. (2011). Direct synthetic strategy of mesoporous ZSM-5 zeolites by using conventional block copolymer templates and the improved catalytic properties. *ACS Catalysis*, *1*(4), 287–291.

Zohdi-Fasaei, H., Atashi, H., Farshchi Tabrizi, F., & Mirzaei, A. A. (2016). Effects of mass transfer on Fischer-Tropsch kinetics over mesoporous silica-supported Co-Mn-Ce nano catalysts in a fixed-bed reactor. *Journal of Natural Gas Science and Engineering*, *32*, 262–272.

APPENDICES

Appendix A: Calculations for catalysts

A1-1: N_2 physisorption data of catalysts

							Pore Size (nm)			
Samples	BET Surface Area (m^2/g)	Langmuir Surface Area (m^2/g)	External Surface Area (m^2/g)	Micropore Area (m^2/g)	Single point Surface Area (m^2/g)	Micropore volume (cm^3/g)	Adsoprtion pore diameter	Deportion pore diameter	Adsoprtion - Desorption	
ZSM-5	340.4731 ± 10.3225 m^2/g	445.5042 ± 6.1262 m^2/g	121.5366 m^2/g	218.9364 m^2/g	332.9388 m^2/g	0.110717 cm^3/g STP	5,9217	5,3273	0,5944	
H-ZSM-5	391.0382 ± 11.3713 m^2/g	506.3221 ± 7.1720 m^2/g	152.2810 m^2/g	238.7572 m^2/g	382.2843 m^2/g	0.120918 cm^3/g STP	5,2705	4,755	0,5155	
Co/H-ZSM-5 (not-calcined)	144.6848 ± 3.9577 m^2/g	186.4266 ± 2.0851 m^2/g	56.3200 m^2/g	88.3647 m^2/g	142.0510 m^2/g	0.044698 cm^3/g STP	5,6898	5,3449	0,3449	2.91455 nm
Co/H-ZSM-5 (calcined)	289.6738 ± 7.8198 m^2/g	368.2394 ± 5.6002 m^2/g	123.8308 m^2/g	165.8430 m^2/g	283.2882 m^2/g	0.083906 cm^3/g STP	6,0706	5,8219	0,2487	3.00647 nm
H-ZSM-5 (desilicated)	419.7451 ± 8.5407 m^2/g	516.4033 ± 9.2165 m^2/g	227.1329 m^2/g	192.6122 m^2/g	411.7065 m^2/g	0.096307 cm^3/g STP	8,8087	7,4797	1,329	
Co/H-ZSM-5 (not-desi & not-calcined)	60.2735 ± 1.1315 m^2/g	74.2319 ± 1.2331 m^2/g	35.9998 m^2/g	24.2737 m^2/g	59.1433 m^2/g	0.012160 cm^3/g STP	27,7821	25,1084	2,6737	18.96364 nm
Co/H-ZSM-5 (desilicated- calcined)	209.5149 ± 4.2299 m^2/g	257.9201 ± 4.4743 m^2/g	117.4353 m^2/g	92.0795 m^2/g	205.6622 m^2/g	0.046374 cm^3/g STP	13,3103	11,1547	2,1556	8.17678 nm

A.2: XRD catalyst particles size calculations

Co_3O_4 crystalline size on CO/H-ZSM-5 catalyst

$$d = \frac{k\lambda}{\beta cos\theta} = \frac{(0.9 \times 0.789)}{0.03911 \times \cos(0.3211406)} = 18.157\ nm$$

$$d(Co^0) = 0.75 \times 18.157 = 13.618\ nm$$

Where d is the crystalline size (nm), k is the geometrical coefficient constant which is 0.9, λ is the radiation wavelength X-ray (λ= 0.789 nm), β is the width in radians at the half height diffraction peak (known as FWHM stands for full-width at half minimum) and θ is the half of diffraction angle in radians. FWHM for Co/H-ZSM-5 was found to be 0.03911 from Origin Software. Diffraction peak of 2θ = 36.8° was converted into 0.64 radians.

Appendix B: Calculations for CO conversion and hydrocarbon selectivity

B.1: CO conversion calculation

Table B.1.1: TCD results: Areas of peaks from syngas calibration before reaction

Syngas calibration peaks before reaction			
Peak #	H_2	CO	N_2
1	8179,09	325,937	297,5
2	8731,89	352,189	261,016
3	8972,55	364,438	247,103
4	9136,82	368,8	238,626
5	9246,53	367,879	236,442
6	8871,89	356,969	224,453
7	8692,76	354,188	220,442
8	8942,64	369,559	231,421
9	8802,06	360,599	223,92
10	8747,93	359,571	224,174
11	9049,93	372,822	230,776
12	9078,61	372,967	231,564
Average	**8871,1**	**360,49**	**238,95**

Syngas with the following composition; hydrogen (50%), carbon monoxide (20%) and nitrogen (30%) were calibrated through the system before FT reaction. Therefore, peaks were found with area sizes for each component and average areas, recorded in Table C.1.1.

The area to mole ratio for each component was calculated as follows;

For instance,

$$Area\ to\ mole\ ratio\ (CO) = \frac{Average\ area\ of\ CO\ from\ calibration\ results\ of\ syngas}{\%\ CO\ from\ syngas}$$

$$Area\ to\ mole\ ratio\ (CO) = \frac{360.49}{20}$$

$$Area\ to\ mole\ ratio\ (CO) = 18.0247$$

Table B.1.2: Area to mole ratio for each component

Area to mole ratio of syngas	
H_2	177,421
CO	18,0247
N_2	7,9651

Table B.1.3: TCD results: Areas of peaks from syngas after FT reaction

TCD PEAKS after reaction			
Peak #	H_2	CO	N_2
1	6167,03	217,878	303,554
2	6093,71	224,092	290,331
3	6182,65	232,01	301,784
4	5983,87	225,87	294,658
5	5752,86	213,553	296,008
6	5525,02	226,414	286,277
7	5458,36	229,875	291,714
8	5095,56	217,681	285,077
9	4934,24	202,212	273,609
Average	**5688,1**	**221,07**	**291,45**

	% Mole after rxn			% Conversion	
Time, hours	**H_2**	**CO**	**N_2**	**H_2**	**CO**
1	34,75926	12,08777	38,11049	45,27607	52,42344
3	34,346	12,43252	36,45038	43,46396	48,83788
5	34,84729	12,87181	37,88827	44,81572	49,04039
7	33,72691	12,53117	36,99362	45,29829	49,18921
9	32,42487	11,84783	37,16311	47,64991	52,17909
11	31,14069	12,56135	35,94141	48,01423	47,57573
13	30,76497	12,75336	36,62401	49,59868	47,76639
15	28,72016	12,07684	35,79075	51,85321	49,38562
17	27,81091	11,21863	34,35097	51,42336	51,01172
19					
Average	**32,06012**	**12,26459**	**36,59033**	**47,48816**	**49,71216**

In order to calculate CO conversion, mole percentage of CO before and after must be known. % mole of CO before reaction was known as 20% from the syngas composition. %% mole pf CO after reaction was calculated as follows:

$$\%\, mole\ of\ CO\ after\ reaction = \frac{Area\ of\ CO\ from\ syngas, after\ reaction}{area\ to\ mole\ ratio\ of\ CO}$$

$$\%\, mole\ of\ CO, after\ rxn = \frac{202.121\ (at\ peak\ \#9)}{18.0247}$$

$$\%\, mole\ of\ CO, after\ rxn = 11.21863\ \%$$

% mole for all components at different peaks were calculated using the same method, then averaged. The CO conversion therefore calculated below:

$$\%\, CO\ conversion, at\ each\ peak$$

$$= \frac{\%\, mole\ of\ CO\ before\ reaction - \%\, mole\ of\ CO\ after\ reaction \times \left(\frac{\%\, mole\ of N_2\ before\ raction}{\%\, mole\ of N_2\ after\ raction}\right)}{\%\, mole\ of\ CO\ before\ reaction}$$

$$\%\, CO\ conversion, at\ each\ peak = \frac{20 - 11.21863 \times \left(\frac{30}{34.35097}\right)}{20}$$

$$= 51.01172\ \%$$

Therefore, to determine an actual overall CO conversion. All CO conversion at a specific time were averaged.

B.2: Hydrocarbon Selectivity calculations

Table B.2.1: FID results: Areas of peaks from calibration before reaction

Calibration peaks from calibration gas		
	AREA	**Peak %**
H_2	302,482	55,5496
N_2	52,942	9,722584
CO	144,76	26,58459
CH_4	4,532	0,832283
C_2H_4	6,418	0,58932
C_2H_6	8,472	0,777924
CO_2	32,365	5,943701
TOTAL	**551,971**	**100**

Table B.2.2: FID results: Area of peaks products from syngas after reaction

Carbon#	**Peak Area**	
	Olefin	**Paraffin**
	Area $_{HC,i}$	**Area $_{HC,i}$**
C_1	0	459,399
C_2	41,4914	116,438
C_3	13,7212	216,4856
C_4	23,1372	232,031
C_5	208,617	295,2326
C_6	82,0032	429,6038
TOTAL	**368,97**	**1749,19**

Table B.2.3: Molar response factors for hydrocarbons

Carbon #	Olefin	Paraffin
1	0	1
2	1	1
3	0,7	0,74
4	0,78	0,55
5	0,47	0,47
6	0,4	0,4
7	0,35	0,35
8	0,32	0,32
9	0,28	0,28
10	0,24	0,24
11	0,21	0,21
12	0,19	0,19
13	0,18	0,18
14	0,17	0,17
15	0,15	0,15

The hydrocarbons C_2H_6 (paraffins) and C_2H_4 (olefins) data from calibration results were used with relative molar response factors to determine the selectivity of C_{3+} hydrocarbon products. First, the average area for C_2 peaks then moles of C_2 were calculated as follows

$$Average\ area\ of\ C_2(A_{C_2,cal}) = \frac{6.418 + 8.472}{2} = 7.445$$

$$Average\ moles\ of\ C_2\ in\ calib\ gas(A_{C_2,cal}) = \frac{7.445}{551.971} \times 100 = 1.35\ \%$$

$$X_{HC,i} = Rf,_i \left(\frac{A_{HC,i}}{A_{C_2,cal}}\right) \cdot\ X_{C_2,cal} \qquad [3.6]$$

$$X_{HC,i} = 0.4 \times \frac{82.0032}{7.445} \times 1.367244 =\ 6.023822$$

where :

$X_{HC,i}$ = the mole fraction of product for each component in a gas;

$Rf,_i =$ the response factor for carbon number i;

$A_{C_2,cal} =$ integrated peak area C_2 hydrocarbons in the calibration gas;

$X_{C_2,cal}$ = the average mole fraction of C_2 hydrocarbons in the calibration gas;

$A_{HC,i} =$ integrated peak area of produced hydrocarbon component.

Then the moles of each hydrocarbon were calculated using the below formula (3.6), e.g: C6 olefin

$$N_{HC,i} = X_{c_2,cal} \cdot \quad F_{tot,out} \cdot t_{rxn} \cdot \left(\frac{A_{HC,i}}{A_{C_2,cal}}\right) \qquad [3.5]$$

$$N_{HC,i} = 1.35 \times \ 0.000446 \cdot 60 \times \left(\frac{82.0032}{7.445}\right) = \quad 0.40338$$

where :

$N_{HC,i}$ = the number of moles of product for each component in a gas;

$X_{C_2,cal}$ = the average mole fraction of C_2 hydrocarbons in the calibration gas;

$t_{rxn} =$ total time reaction;

$F_{tot,out}$= total outlet gas flow rate;

$A_{HC,i} =$ integrated peak area of produced hydrocarbon component;

$A_{C_2,cal} =$ integrated peak area C_2 hydrocarbons in the calibration gas.

Then the selectivity (in moles) of each hydrocarbon were calculated using the below formula (3.6), e.g: C6 olefin

$$Selectivity\ (S_{HC,i}) = \left(\frac{N_{HC,i}}{\Delta W}\right)\left(\frac{t_{rxn}}{-r_{co}}\right) \times 100 \qquad [3.7]$$

$$Selectivity\ (S_{HC,i}) = \left(\frac{0.40338}{0.5}\right)\left(\frac{60}{0.000376}\right) \times 100 = 12880411\ moles$$

$N_{HC,i} =$ the number of moles of product for each component in a gas;

$\Delta W =$ weight of a catalyst;

$t_{rxn} =$ total reaction time;

r_{co} = rate of CO conversion

Lastly, the % selectivity for each compound was calculated using total moles selectivity for both paraffins and olefins e.g: C_6 olefin

$$\%\, Selectivity = \frac{S_{HC,i}}{\sum S_{HC,i}} \times 100 \qquad [3.8]$$

$$\%\, Selectivity = \frac{12880411}{57954875.345} \times 100 = 22.2249$$

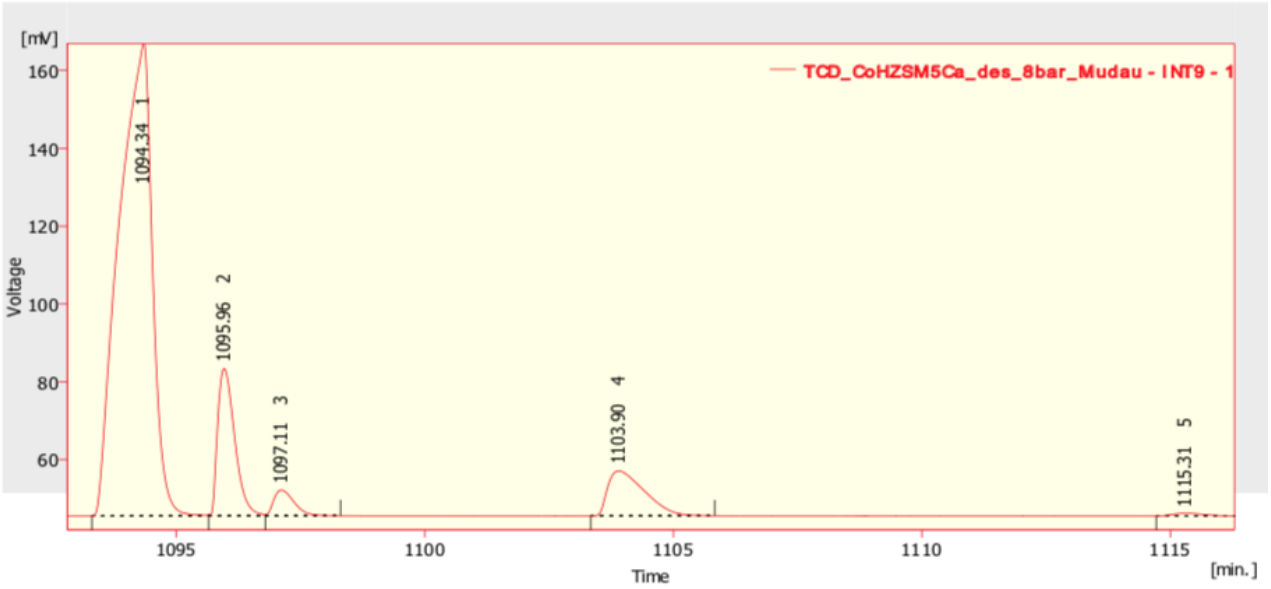
$S_{HC,i}$ = moles produced of paraffin i;

$\sum S_{HC,i}$ = sum of all moles produced paraffin i;

Table B.2.4: % mole, moles and selectivity of hydrocarbons

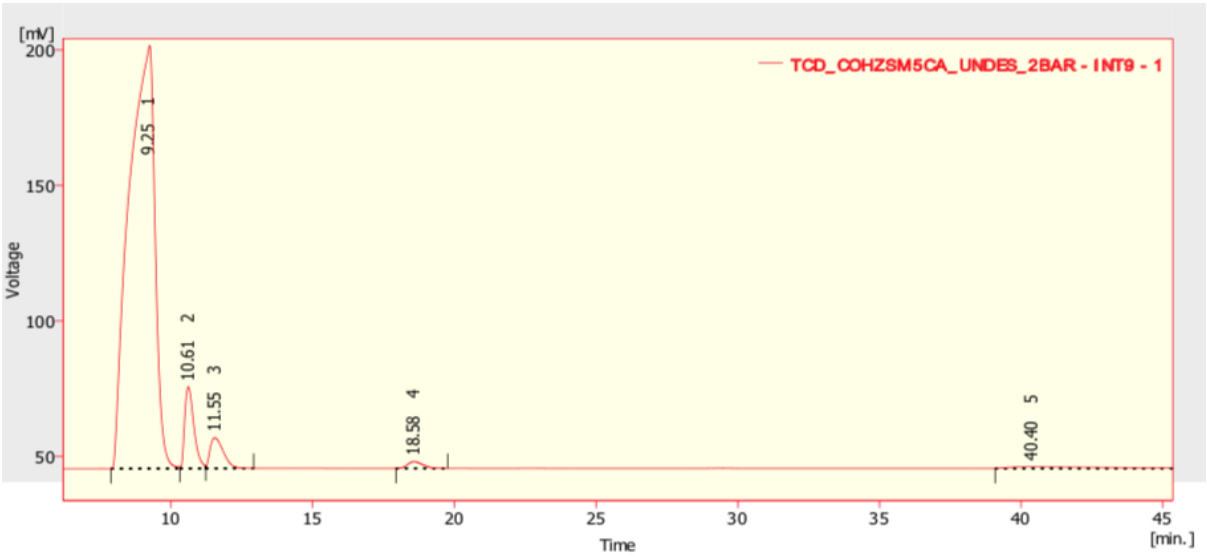
Carbon#	Peak Area	Mole %		Moles (mol)		Selectivity		% Selectivity	
	Paraffin	Olefin	Paraffin	Olefin	Paraffin	Olefin	Paraffin	Olefin	Paraffin
	$A_{HC,i}$	$X_{HC,i}$	$X_{HC,i}$	$N_{HC,i}$	$N_{HC,i}$	$S_{HC,i}$	$S_{\cdot HC,i}$	$S_{HC,i}$	$S_{\cdot HC,i}$
1	459,399	0	84,36677	0	2,259824	0,00000	72158744,815	0	26,26353
2	116,438	7,619727984	21,38337	0,204099857	0,572769	6517139,44654	18289155,894	11,2452	6,656681
3	216,4856	1,763890062	29,41996	0,067495793	1,064912	2155217,07568	34003837,985	3,718785	12,37633
4	232,031	3,314261578	23,43636	0,113813928	1,141381	3634207,54187	36445585,903	6,270754	13,26505
5	295,2326	18,00648454	25,48259	1,026205426	1,452275	32767900,81607	46372791,069	56,54037	16,87825
6	429,6038	6,023822554	31,558	0,403380975	2,113259	12880411,10840	67478743,680	22,2249	24,56015
7									
8									
TOTAL	**1749,19**	**36,72818672**	**215,647**	**1,814995978**	**8,60442**	**57954875,98856**	**274748859,345**	**100**	**100**

Table B.2.5: Some peaks and areas results detected from TCD and FID



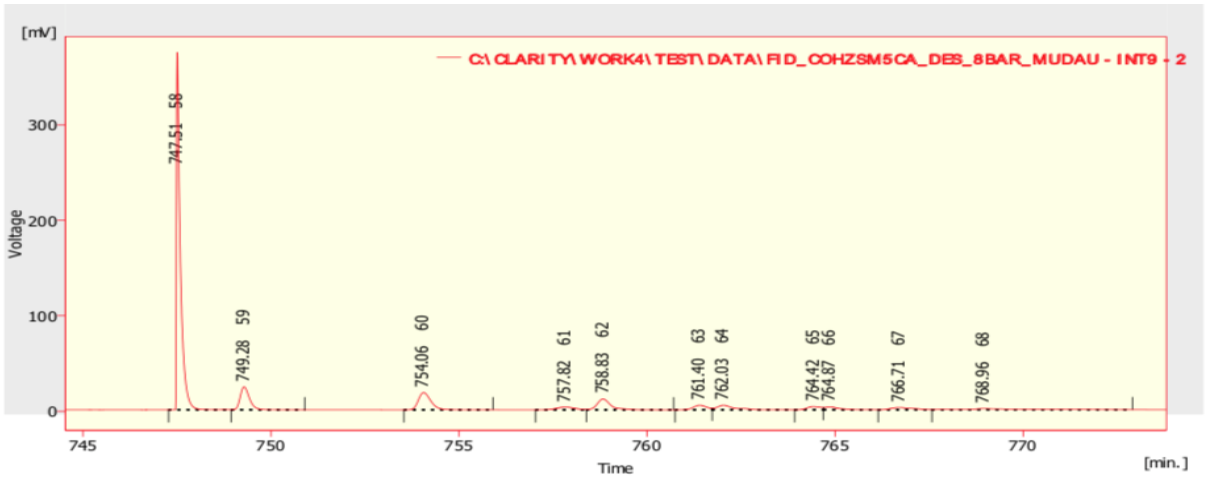
Result Table (Uncal - TCD_CoHZSM5Ca_des_8bar_Mudau - INT9 - 1)

	Reten. Time [min]	Area [mV.s]	Height [mV]	Area [%]	Height [%]	W05 [min]
1	1094.344	5635.981	121.763	76.7	68.2	0.78
2	1095.960	904.318	37.851	12.3	21.2	0.38
3	1097.112	186.540	6.597	2.5	3.7	0.45
4	1103.900	591.045	11.549	8.0	6.5	0.83
5	1115.312	29.653	0.690	0.4	0.4	0.68
	Total	7347.537	178.451	100.0	100.0	

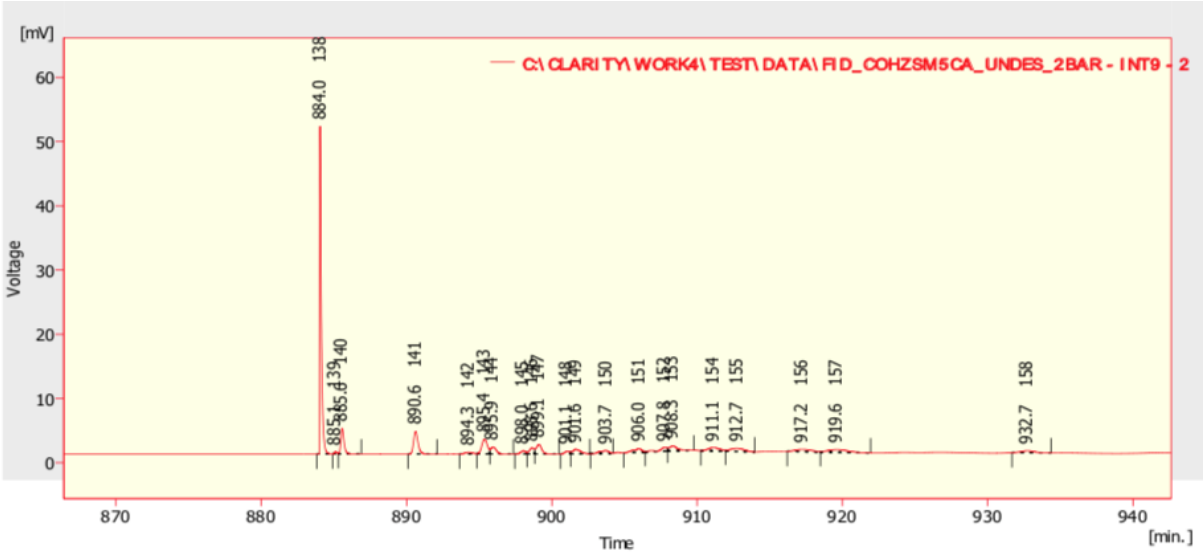


Result Table (Uncal - TCD_COHZSM5CA_UNDES_2BAR - INT9 - 1)

	Reten. Time [min]	Area [mV.s]	Height [mV]	Area [%]	Height [%]	W05 [min]
1	9.248	9915.123	156.099	88.3	77.8	1.11
2	10.612	679.300	30.088	6.1	15.0	0.36
3	11.548	369.735	11.311	3.3	5.6	0.53
4	18.580	93.092	2.486	0.8	1.2	0.59
5	40.396	168.728	0.554	1.5	0.3	4.62
	Total	11225.978	200.537	100.0	100.0	



55	640.224	79.197	2.905	0.3	0.1	0.39
56	642.064	88.850	2.163	0.3	0.1	0.72
57	644.316	101.486	1.070	0.3	0.0	0.80
58	747.508	2658.451	373.709	9.0	12.7	0.10
59	749.284	411.880	24.063	1.4	0.8	0.26
60	754.056	416.507	18.057	1.4	0.6	0.36
61	757.824	96.297	2.828	0.3	0.1	0.54
62	758.828	284.685	11.312	1.0	0.4	0.36



136	788.836	39.044	0.688	0.3	0.1	0.92
137	808.020	22.588	0.350	0.2	0.0	0.98
138	884.048	352.510	50.978	2.6	5.8	0.09
139	885.104	4.281	0.354	0.0	0.0	0.19
140	885.564	60.570	4.019	0.4	0.5	0.22
141	890.616	75.397	3.502	0.6	0.4	0.32
142	894.272	10.237	0.273	0.1	0.0	0.61
143	895.364	62.925	2.316	0.5	0.3	0.44
144	895.948	29.135	1.093	0.2	0.1	0.47
145	898.036	12.193	0.511	0.1	0.1	0.45
146	898.632	21.690	0.957	0.2	0.1	0.39
147	899.108	40.717	1.500	0.3	0.2	0.49
148	901.052	9.812	0.419	0.1	0.0	0.42
149	901.628	27.092	0.726	0.2	0.1	0.62
150	903.704	19.501	0.442	0.1	0.1	0.76
151	905.996	24.462	0.549	0.2	0.1	0.73
152	907.760	23.163	0.585	0.2	0.1	0.46
153	908.324	31.994	0.767	0.2	0.1	0.67
154	911.112	29.951	0.519	0.2	0.1	0.93
155	912.720	33.223	0.491	0.2	0.1	1.18
156	917.224	26.989	0.343	0.2	0.0	1.24
157	919.612	40.945	0.423	0.3	0.0	1.52
158	932.728	19.563	0.312	0.1	0.0	0.96
159	1008.636	339.653	49.141	2.5	5.6	0.09
160	1009.712	4.243	0.347	0.0	0.0	0.20
161	1010.184	57.931	3.800	0.4	0.4	0.23
162	1015.212	72.096	3.360	0.5	0.4	0.32
163	1018.876	9.826	0.265	0.1	0.0	0.60
164	1019.948	60.503	2.257	0.4	0.3	0.44
165	1020.528	28.420	1.078	0.2	0.1	0.46
166	1022.620	11.821	0.492	0.1	0.1	0.45
167	1023.216	20.963	0.915	0.2	0.1	0.39

	Reten. Time [min]	Area [mV.s]	Height [mV]	Area [%]	Height [%]	W05 [min]
30	248,752	450,021	243,757	9,2	13,6	0,12
31	251,832	43,596	18,336	1,6	1	0,3
32	256,604	124,722	17,225	1,9	1	0,38
33	260,368	15,82	0,717	0,1	0	0,34
34	261,156	206,024	14,332	1,4	0,8	0,3
35	264,164	22,908	1,096	0,1	0,1	0,39
36	264,732	201,181	8,659	0,9	0,5	0,34
37	267,344	95,086	3,71	0,4	0,2	0,33
38	269,904	40,683	1,189	0,2	0,1	0,4
39	272,276	92,498	1,252	0,4	0,1	0,58
40	274,9	62,007	0,497	0,1	0	1,15
41	276,088	39,315	0,66	0,2	0	1,02
42	280,928	20,327	0,286	0,1	0	1,27
43	282,784	35,51	0,452	0,2	0	1,23
44	373,004	421,846	241,22	9,1	13,5	0,12
45	376,1	45,156	18,267	1,6	1	0,3
46	380,824	126,276	17,215	1,9	1	0,38
47	384,568	14,91	0,683	0,1	0	0,34
48	385,352	219,886	14,707	1,4	0,8	0,31
49	388,364	24,288	1,177	0,1	0,1	0,38
50	388,92	230,361	9,925	1	0,6	0,33
51	391,52	129,633	5,211	0,6	0,3	0,32
52	394,08	47,239	1,493	0,2	0,1	0,37
53	396,424	84,451	1,065	0,4	0,1	0,94
54	400,092	75,341	0,554	0,2	0	0,98
55	406,708	20,092	0,309	0,1	0	1,02
56	497,24	568,92	229,832	8,6	12,8	0,12
57	500,34	49,213	17,465	1,5	1	0,3
58	505,06	115,748	16,785	1,9	0,9	0,38
59	508,804	13,503	0,616	0,1	0	0,35
60	509,584	218,356	14,548	1,4	0,8	0,3
61	512,592	23,623	1,142	0,1	0,1	0,38
62	513,148	238,046	10,066	1,1	0,6	0,34
63	515,74	147,274	5,984	0,7	0,3	0,32
64	518,3	57,265	1,888	0,3	0,1	0,36
65	520,66	98,465	0,965	0,4	0,1	0,96
66	524,332	48,686	0,487	0,2	0	1
67	530,86	16,679	0,27	0,1	0	0,98
68	621,432	452,47	222,36	8,3	12,4	0,12
69	624,532	38,64	16,938	1,5	0,9	0,3
70	629,276	109,685	16,413	1,8	0,9	0,38
71	632,992	12,536	0,58	0,1	0	0,34
72	633,768	218,76	14,387	1,4	0,8	0,3
73	636,768	22,833	1,114	0,1	0,1	0,38

74	637,32	243,346	10,247	1,1	0,6	0,34
75	639,904	157,064	6,367	0,7	0,4	0,32
76	642,48	67,075	2,218	0,3	0,1	0,35
77	644,84	70,112	0,891	0,3	0	0,6
78	648,496	82,602	0,431	0,2	0	0,98
79	745,616	403,738	217,487	8,1	12,2	0,12
80	748,72	30,852	16,616	1,4	0,9	0,3
81	753,444	105,759	16,274	1,8	0,9	0,38
82	757,168	11,837	0,543	0,1	0	0,34
83	757,948	219,402	14,142	1,4	0,8	0,31
84	760,964	22,034	1,087	0,1	0,1	0,37
85	761,504	247,221	10,444	1,1	0,6	0,34
86	764,072	164,028	6,689	0,7	0,4	0,33
87	766,628	73,892	2,519	0,3	0,1	0,34
88	768,96	105,69	0,887	0,5	0	0,88
	Total	22270,57	1789,051	100	100	